Fakultät für Medizin

Institut/Klinik/Lehrstuhl für Innere Medizin, Schwerpunkt, Gastroenterologie

Role of Autophagy-Related 5 Gene in Pancreatic Cancer and Metastasis

Kivanc Görgülü

Vollständiger Abdruck der von der Fakultät für Medizin der Technischen Universität München zur Erlangung des akademischen Grades eines

Doctor of Philosophy (Ph.D.)

genehmigten Dissertation.

Vorsitzender: Prof. Dr. Jürgen Ruland

Betreuer: Prof. Dr. Hana Algül

Prüfer der Dissertation:

1. Prof. Dr. Roland M. Schmid
2. Prof. Dr. Stephan Herzig
3. Prof. Dr. Julia Mayerle, Ludwig-Maximilians-Universität München

Die Dissertation wurde am 10.12.2018 bei der Fakultät für Medizin der Technischen Universität München eingereicht und durch die Fakultät für Medizin am 05.03.2019 angenommen.

“If one day, my words are against science, choose science."

Mustafa Kemal Atatürk

1 ZUSAMMENFASSUNG

Autophagie ist ein lysosomaler Degradationsprozess, der wesentlich zur zellulären Homöostase über die Eliminierung von Aggregaten und Bereitstellung von Wachstumssubstraten beiträgt. Defekte in der Autophagie wurden mit einer Vielzahl von Tumoren in verschiedenen Organen assoziiert. Eine Rolle in der duktalen Pankreaskarzinogenese (PDAC) wurde ebenfalls beschrieben, wobei detaillierte mechanistische Untersuchungen noch ausstehen.

PDAC wurde in Mäusen durch die konstitutive Aktivierung des *Kras*-Onkogens im Pankreas induziert. Zur Untersuchung der Autophagie während der PDAC Entwicklung wurden *Atg5* homozygot oder heterozygot defiziente Mäuse generiert (*A5;Kras*, *A5+/-;Kras*) und zu verschiedenen Zeitpunkten nach der Geburt mit *Atg5*-kompetenten (*Kras*) Mäusen verglichen. Tumorzellen, isoliert aus den jeweiligen Mausmodellen wurden *in vitro* und *in vivo* (orthotope Transplantation, Schwanzveneninjektion) auf tumorigene und metastatische Fähigkeiten geprüft sowie mechanistisch untersucht. Anhand humaner PDAC Proben aus unabhängigen Patientenkohorten wurde eine Korrelation zwischen ATG5 Proteinlevel und der Metastasierungs-/Überlebensrate untersucht.

Während *Kras* und *A5+/-;Kras* Mäuse alle Schritte von PDAC durchlaufen, entwickeln *A5;Kras* Mäuse nur prämaligne Vorstufen. Interessanterweise ist der Effekt abhängig von der *Atg5*-Gendosis: komplette *Atg5*-Defizienz führt zur Blockade in der Tumorigenese und starke Pankreasdegeneration; heterozygote *Atg5*-Defizienz hingegen erhöht die Tumor-, und Metastasierungsinzidenz. *In vitro* und *in vivo* Analysen erwiesen eine erhöhte Malignität sowie Metastasierungskapazität bei den Zelllinien mit partieller *Atg5*-Defizienz. Mechanistische Analysen deuteten auf reduzierte mitochondriale Funktion und verstärkten Zellstress. Interessanterweise wiesen *A5+/-;Kras*-Zellen ein verändertes Zytokinprofil auf, welches die Differenzierung von pro-tumorigenen Typ 2 Makrophagen förderte. Des weiteren war die extrazelluläre Kathepsinaktivität von *A5+/-;Kras*-Zellen

signifikant erhöht und die Kalziumhomöostase verändert. Dies ermöglicht den *A5+/-;Kras*-Zellen eine verbesserte migratorische Fähigkeit. Untersuchungen humaner PDAC Proben bestätigten, dass niedrige ATG5 Level mit verstärkter Tumormetastasierung und einer kürzeren Überlebensrate einhergehen.
Es konnte gezeigt werden, dass die *Atg5*-Gendosis eine wesentliche Rolle in der PDAC-Entstehung und Metastasierung spielt. Komplette *Atg5*-Defizienz blockiert die PDAC-Entstehung, während partielle *Atg5*-Defizienz die PDAC-Entstehung und Metastasierung signifikant verstärkt.

- Part of this thesis was submitted for publication and the final accepted publication is:

1. **Görgülü, Kivanc**; Diakopoulos, Kalliope N; Ai, Jiaoyu; Schoeps, Benjamin; Kabacaoglu, Derya; Karpathaki, Angeliki-Faidra; Ciecielski, Katrin J; Kaya-Aksoy, Ezgi; Ruess, Dietrich A; Berninger, Alexandra; Kowalska, Marlena; Stevanovic, Marija; Wörmann, Sonja M; Wartmann, Thomas; Zhao, Yue; Halangk, Walter; Voronina, Svetlana; Tepikin, Alexey; Schlitter, Anna Melissa; Steiger, Katja; Artati, Anna; Adamski, Jerzy; Aichler, Michaela; Walch, Axel; Jastroch, Martin; Hartleben, Götz; Mantzoros, Christos S; Weichert, Wilko; Schmid, Roland M; Herzig, Stephan; Krüger, Achim; Sainz, Bruno; Lesina, Marina; Algül, Hana. Levels of the Autophagy Related 5 Protein Affect Progression and Metastasis of Pancreatic Tumors in Mice. Gastroenterology. 2018 Oct 5. pii: S0016-5085(18)35087-X. doi: 10.1053/j.gastro.2018.09.053.

- Additional publications not related to this thesis include:

1. Ruess DA, Heynen GJ, Ciecielski KJ, et al. Mutant KRAS-driven cancers depend on PTPN11/SHP2 phosphatase. *Nat Med*. 2018;24(7):954-960. doi:10.1038/s41591-018-0024-8

2. Ruess DA, Görgülü K, Wörmann SM, Algül H. Pharmacotherapeutic Management of Pancreatic Ductal Adenocarcinoma: Current and Emerging Concepts. *Drugs Aging*. 2017;34(5):331-357. doi:10.1007/s40266-017-0453-y

3. Wörmann SM, Song L, Ai J, et al. Loss of P53 Function Activates JAK2–STAT3 Signaling to Promote Pancreatic Tumor Growth, Stroma Modification, and Gemcitabine Resistance in Mice and Is Associated With Patient Survival. *Gastroenterology*. 2016;151(1):180-193.e12. doi:10.1053/j.gastro.2016.03.010

4. Görgülü K, Diakopoulos KN, Vatansever HS. REVIEW ARTICLE A Star of Connection Between Pancreatic Cancer and Diabetes : Adrenomedullin. 2015;16(5):408-412.

5. Jin Y, Wang L, Qu S, et al. STAMP2 increases oxidative stress and is critical for prostate cancer. *EMBO Mol Med*. 2015;7(3):315-331. doi:10.15252/emmm.201404181

6. Gorgulu K, Gokce B et al. Effect of extremely low frequency electromagnetic fields on a-Lactalbumin and Sulindac treated colon cancer cells: ELF-EMF and colon cancer. *Med Sci* 2014. doi:10.17546/msd.88603

7. Jin Y, Qu S, Tesikova M, et al. Molecular circuit involving KLK4 integrates androgen and mTOR signaling in prostate cancer. 2013. doi:10.1073/pnas.1304318110//DCSupplemental.www.pnas.org/cgi/doi/10.1073/pnas.1304318110

8. Devkota AK, Tavares CDJ, Warthaka M, et al. Investigating the kinetic mechanism of inhibition of elongation factor 2 kinase by NH125: Evidence of a common in vitro artifact. *Biochemistry*. 2012;51(10):2100-2112. doi:10.1021/bi201787p

- Parts of this thesis were presented at the included scientific meetings:

1. Levels of the Autophagy Related 5 Protein Affect Progression and Metastasis of Pancreatic Tumors in Mice.
Kivanc Görgülü, Technical University Munich (Oral Presentation)
(The Frankfurt Cancer Conference, “Turning Molecular Information into Novel Cancer Therapies” - September 25th-27th 2018, Frankfurt, Germany)

2. Levels of the Autophagy Related 5 Protein Affect Progression and Metastasis of Pancreatic Tumors in Mice.
Kivanc Görgülü and Kalliope N. Diakopoulos (Poster Presentation)
(50th European Pancreatic Club - June 13rd- 16th , 2018, Berlin, Germany

2 TABLE OF CONTENT

1 ZUSAMMENFASSUNG 1

2 TABLE OF CONTENT 5

3 INTRODUCTION 9

3.1 Autophagy 9

3.1.1 Mechanism of Autophagy 9

3.1.2 The Role of Autophagy in Cellular Adaptations 11

3.2 Pancreas 13

3.2.1 Pancreatic Morphology and Physiology 13

3.2.2 Pancreatic Pathologies 14

3.2.3 Pancreatic Cancer, Autophagy and Metabolism 15

3.3 Calcium Signaling and Its Role in Tumor Aggressiveness 17

3.4 Tumor Aggressiveness : Metastasis 18

3.5 Aim 19

4 MATERIALS AND METHODS 21

4.1 Mice 21

4.1.1 Mouse models 21

4.1.2 Orthotopic Transplantation 22

4.1.3 Intra-Tail Vein Injections 22

4.1.4 Macrophages Depletion by Liposomal Clodronate 22

4.1.5 Chronic Pancreatitis Model 23

4.2 DNA/RNA studies 24

4.2.1 Mouse genotyping 24

4.2.2 RNA extraction 25

4.2.3 cDNA synthesis 25

4.2.4 Quantitative real time PCR analysis 25

4.2.5 Detection of unspliced and spliced *Xbp1* 26

4.2.6 Agarose gel electrophoresis 27

4.2.7 Microarray analysis 27

4.3 Histology 28

4.3.1 Tissue sections 28

4.3.2 Haematoxylin and eosin (H&E) staining 28

4.3.3 Immunohistochemistry 29

4.3.4 Co-immunofluorescence 30

4.3.5 Detection of GFP-LC3 puncta 30

4.3.6 ADM and PanIN Quantifications 31
4.3.7 Quantification of Macrophage Infiltration (F4/80-Positive) and M2 Polarized Macrophages (CD206-positive) 31
4.3.8 Quantification of Relative Pancreatic Weight, Tumor Incidence, Metastasis Incidence, Tumor and Metastasis Burden 31
4.3.9 Human PDAC Samples 32
4.3.10 Transmission Electron microscopy (TEM) 34
4.4 *In Vitro* Experiments and Proteinbiochemistry 34
4.4.1 Measurement of Serum Amylase and Lipase 34
4.4.2 Tumor Cell Isolation and Cultivation 35
4.4.3 In Vitro Cathepsin Activity Measurements 35
4.4.4 Subcellular Fractination by Isopycnic Percoll Density Centrifugation and Measurement of GLDH Activity 36
4.4.5 Protein Extraction and Quantification 36
4.4.6 SDS-PAGE 37
4.4.7 Western blot 38
4.4.8 Transmission Electron Microscopy (TEM) 39
4.4.9 Measurement of Mitochondrial Metabolism by Seahorse Extracellular Flux 40
4.4.10 Cellular Morphology Analysis and Quantification of Cell Proliferation 41
4.4.11 Autophagic Flux Measurement using Cyto-ID 41
4.4.12 Colony Formation Assay and Cell Treatments 41
4.4.13 Anoikis Assay 42
4.4.14 Boyden Chamber Migration and Invasion Assay 42
4.4.15 Cytokine Array 43
4.4.16 Macrophage Differentiation Assay 43
4.4.17 Measurement of Cytoplasmic Ca^{2+} Response 43
4.4.18 Knockdown of mAtg5 44
4.5 Non-targeted Metabolomics Profiling 45
4.6 Statistics 45
5 RESULTS 47
5.1 Autophagy in the pancreatic cancer 47
5.1.1 Autophagy is induced during pancreatic tumorigenesis. 47
5.1.2 Allelic dosage of Atg5 influences pancreatic tumorigenesis. 48
5.1.3 Allelic dosage of Atg5 do not change chronic pancreatitis induced pancreatic cancer progression. 50

5.1.4 Monoallelic loss of Atg5 alters tumor incidence and metastatic load. 51
5.1.5 Monoallelic loss of Atg5 does not change autophagic flux *in vivo* and *in vitro*. 53
5.1.6 Monoallelic loss of Atg5 does not change basal canonical, non-canonical, selective autophagy regulator pathways in pancreatic cancer cells. 58
5.2 Role of Atg5 in Metastatic Properties of Cancer Cells 60
5.2.1 Monoallelic loss of Atg5 increases metastatic features *in vitro*. 60
5.2.2 Monoallelic loss of Atg5 increases metastatic features *in vivo*. 61
5.2.3 Downregulation of Atg5 increases metastatic features *in vivo* and *in vitro*. 64
5.2.4 Monoallelic loss of Atg5 enhances weight loss of intravenously cancer cells injected mice. 67
5.3 Role of Atg5 in Transcriptional and Metabolic Status of Cancer Cells .. 68
5.3.1 Monoallelic loss of Atg5 induces transcriptional changes. 68
5.3.2 Monoallelic loss of Atg5 induces metabolic changes. 72
5.3.3 Monoallelic loss of Atg5 reduces mitochondrial functionality. 73
5.3.4 P53 status is not altered by monoallelic loss of Atg5 in pancreatic cancer cells. 77
5.4 Role of Atg5 in Cell Autonomous Mechanisms of Mestastasis 78
5.4.1 Atg5 level influences Ca^{2+} flux in the cancer cells. 78
5.4.2 Atg5 level influences extracellular cathepsin activity and filopodia formation in the cancer cells. 80
5.5 Effect of Atg5 levels in Non Cell-Autonomous Mechanisms of Metastasis 85
5.5.1 Atg5 level influences cytokine profile of cancer cells. 85
5.5.2 Atg5 level influences cytokine profile of cancer cells. 86
5.5.3 Depletion of macrophages decreases metastatic capacity of A5+/-;Kras cells. 90
5.6 Levels of Atg5 are correlated to human pancreatic cancer aggressiveness. 91
6 DISCUSSION 102
6.1 Levels of Atg5 determine PDAC-aggressiveness but do not influence canonical autophagy 102
6.2 Monoallelic loss of Atg5 increases aggressiveness of pancreatic cancer. 104
6.3 Loss of one Atg5-allele induces a pro-tumorigenic tumor microenvironment by stimulating M2 macrophages 106
6.4 Decreased levels of Atg5 are correlated to human pancreatic cancer aggressiveness. 107

7 SUMMARY 109
8 REFERENCES 111
9 ABBREVIATIONS 126
10 ACKNOWLEDGEMENTS 128

3 INTRODUCTION

3.1 Autophagy

Autophagy is a mechanism in which, cellular content is transported to lysosomes for degradation, helping to the recycle of cellular structures and providing building blocks for energy production and macromolecules [1]. In the late 1950s, Christian de Duve has discovered this self-eating process by electron microscopy for the first time [2]. From Christian de Duve to Yoshinori Ohsumi, autophagy and lysosomal degradation of engulfed cellular proteins and organelles gained a lot of attention and is awarded with the Nobel Prize for Physiology or Medicine. Mainly, autophagy can be divided into macroautophagy, microautophagy and chaperone-mediated autophagy [3]. In this thesis, elementarily macroautophagy (referred to along this thesis as autophagy) will be analyzed.

3.1.1 Mechanism of Autophagy

Autophagy is a predecessor and notably sheltered cellular catabolic process that comprises the formation of double-membraned vesicles recognized as autophagosomes that envelop unused proteins and damaged organelles for delivery to the lysosome [4,5]. In addition to this main process, there are multiple modes of autophagy, involving several organelles called such as mitophagy for mitochondria, pexophagy for peroxisomes, nucleophagy for nucleus, and ER-phagy for endoplasmic reticulum (ER) [6].

Autophagy occurs in many physiological adaptation processes: production of amino acids throughout starvation, quality check of cellular proteins and organelles, control of expressions of arbitrary substrates, deterioration of pathogens which are mentioned in previous comprehensive reviews [7–15]. The formation and overturn of the autophagosomes include autophagy-related genes (ATGs). The formation process classically divided into several stages named, initiation, nucleation of the autophagosome, expansion and elongation of the autophagosome membrane, closure and fusion with the lysosomes, and the destruction of vesicled contents [5] (Figure 1).

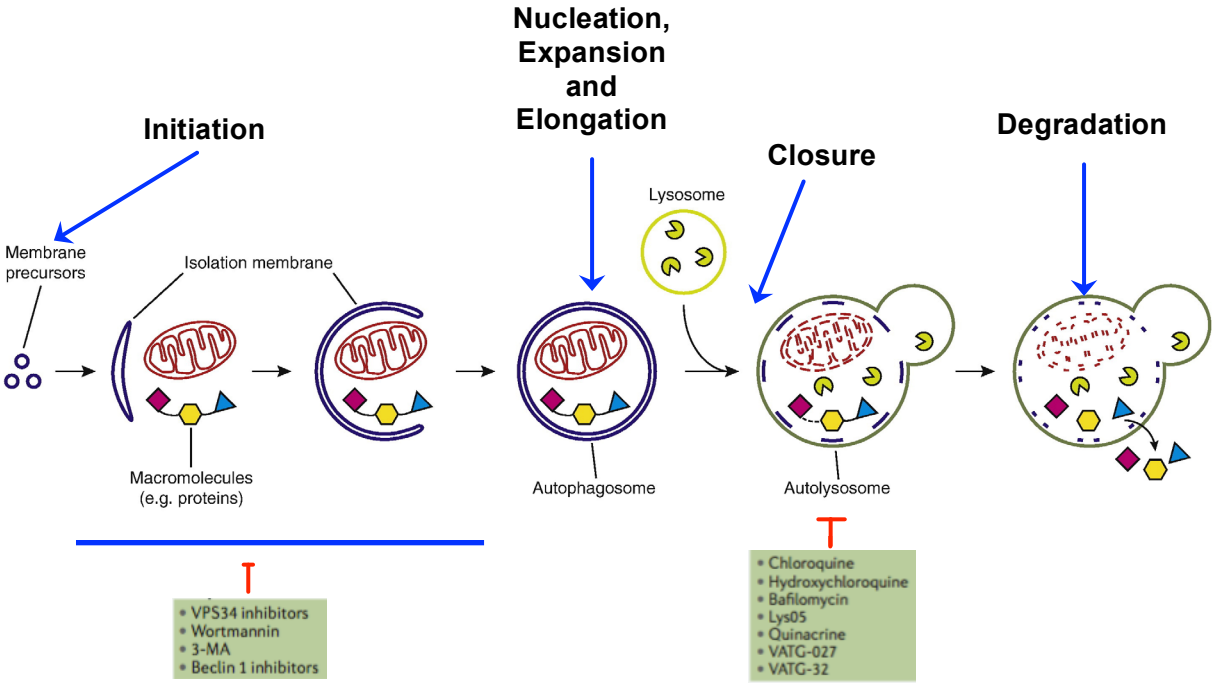

Figure 1: Schematic overview of autophagy and step specific inhibitors of autophagy steps. Adapted from Zaffagnini G. et al 2016 and Mulcahy Levy JM. et al 2017 reviews.

Mammalian autophagic process was characterized after the discovery of the ATG genes and their mammalian homologs. Especially, eighteen ATG proteins and additionally five factors were classified into five functional units composing the autophagic machinery in high eukaryotes [16]. Autophagosomal formation is initated by the UNC-51-like kinase (ULK) complex. It is constructed by ULK1/2 kinase, FIP200, ATG13, and ATG101. The ULK complex is regulated by mammalian target of rapamycin complex 1 (mTORC1) adversely via phosphorylation of ULK1/2 and ATG13 [16]. Deactivation of mTORC1 pioneers the dephosphorylation, displacement, and activation of the ULK complex from the cytoplasm to the phagophore assembly site (PAS), where it assists other factors of the ATG contrivance such as the autophagy-specific class III phosphatidylinositol (PtdIns) 3-kinase (PtdIns3K) complex [16]. This compound is assembled by VPS34, P150, Beclin1/ATG6 and ATG14L and cooperates with several elements such as AMBRA1 and VMP1, which control its activity and allocation. The formation of phosphatidylinositol-3-phosphate (PtdIns3P) at the PAS provoke the engagement of proteins binding this lipid, for instance WIPI and DFCP1 proteins, which besides intercede the generation of phagophore [17]. ATG9 is another essential player for the precursor steps during the genesis of autophagosome[18]. The elongation and closure of the phagophore are

driven by two ubiquitin-like conjugation complexes. First one constitutes the E1-like ATG7 and the E2-like ATG10 enzymes, which regulate the conjugation of the ATG12 to ATG5. ATG5-ATG12 conjugate afterwards unites to ATG16L1 to formate the ATG5-ATG12/ATG16L1 complex [16]. This complex has an inevitable role for autophagosome biogenesis by conducting the other ubiquitin-like conjugation complexes to the PAS and urging the last step of autophagy[16]. The final step engages the conjugation of phosphatidyethanolamine (PE), which are facilliated by the microtubule-associated protein light-chain 3 (LC3) and gamma aminobutyric acid receptor-associated protein (GABARAP) subgroups [19]. ATG4 protease alters these synthesized proteins to generate non-lipidated LC3-I via post-translational modification. Over autophagy occurrence in several conditions, LC3-I evolves into conjugated form through the help of ATG7 and the E2-like enzyme ATG3. This lipidated form of LC3 is called as LC3-II. Lastly, LC3 is incorporated in microtubule-dependent transport of autophagosomes unto lysosomes [20]. Therefore, LC3-II is identified as a whole marker of autophagic induction [21].

It was accepted that ATGs were entirely barged in autophagosome formation. But after a chain of findings, interestingly this group is discovered to have unusual functions independently of autophagy. Atg5 is also one of these ATGs and its unconventional functions distinct from autophagy will be mentioned later.

3.1.2 The Role of Autophagy in Cellular Adaptations

Autophagy is very important cellular process contributing to the balance of cellular homeostasis. Physiological conditions are preserved via microautophagy, chaperone mediated autophagy (CMA) and macroautophagy maintaining normal cellular functions [6,22,23]. Several stimuli such as metabolic, physical, hormonal, nutritional, and chemical can affect the induction of microautophagy, CMA, and macroautophagy [24–28].

Nutrient starvation is the strongest known inducer of autophagy. Most of the cultured mammalian cells have autophagic induction within minutes with highest levels of occurrence under nutrient depletion such as amino acids, glucose, and growth factors (contained in serum) [29]. *In vivo* starvation around 24-48 hours also enables mice to depict higher amount of autophagosomes[30]. mTOR and AMPK have been clearly distinguished as pivotal regulators for starvation-induced autophagy [31,32].

Sirtuins are also recently discovered autophagy regulators under environmental stress and nutrient starvation [33].

In addition to protein synthesis and maturation, ER may also provide a major building blocks for the autophagic isolation membrane [34]. As a cardinal ER stress pathway, the unfolded protein response (UPR), acts also as a strong autophagy inducer [35]. PERK (PKR-like eIF2a kinase, also known as EIF2AK3), ATF6 (activating transcription factor-6), and IRE1 (inositol requiring enzyme 1) are the most important subsidiaries of the UPR. These membrane-associated proteins are normally bound to the chaperone BiP/GRP78 and they are inactivated by this chaperone. The interaction of BiP/GRP78 by misfolded proteins discharge PERK, IRE1, and ATF6 away their detention. Amid these membrane-associated proteins, IRE1 acts as an inhibitor of autophagy, whereas PERK and ATF6 act as an inducers of autophagy [36].

Autophagy can be activated via oxidative stress as a consequence of various mechanisms. Atg4 can be oxidized and activated by exogenous hydrogen peroxide and by the help of hydrogen peroxide it proteolytically matures LC3 [37,38]. Increased reactive oxygen species (ROS) induces autophagy as a cellular response by activating mitogen-activated protein kinases (MAPKs) [39]. At the end, ROS induced DNA damage also triggers the expression of p53 mediated autophagy inducer genes. Stressors for the cells can activate p53 which has a binary effect on autophagy. In the cytoplasm, together with cytoplasmic functions, p53 inhibitis autophagy [40]. On the contrary, along with its nuclear retention and transcriptional activity, p53 increases autophagy [40].

Accumulation of damaged mitochondria causes ROS production. Therefore, damaged mitochondria can be removed by mitophagy, a.k.a. selective autophagic removal of mitochondria, to control mitochondrial quality. This process has very significant functions for balancing homeostasis in the system subsequently, preventing aging, cancer, and neurodegenerative diseases [41,42]. Under normal conditions, functioning mitochondria display an increased mitochondrial trans-membrane potential, which is necessary not only for ATP production, but also for other important mitochondrial functions[43]. In this scenario, PTEN-induced putative kinase 1 (PINK1) is quickly imported and degraded by a protease located on the inner mitochondrial membrane (IMM) [44]. Hypoxia and mitochondrial respiration inhibitors like antimycin A, oligomycin, and rotenone can alter mitochondrial functions

by increasing ROS induced autophagy [38].

3.2 Pancreas

3.2.1 Pancreatic Morphology and Physiology

The pancreas is a retroperitoneally located organ in the abdomen. It contains four regions named as the head, body, tail and uncinate process. Two major arteries, celiac and superior mesenteric arteries, supply its blood and venous drainage occurs by the help of the splenic and superior mesenteric vein draining into portal vein. It can be innervated by the parasympathetic and sympathetic nervous system. Exocrine and endocrine compartments are the main functional anatomic portions [45]. The exocrine pancreas is the main gland responsible for digestion via secreting bicarbonate-rich fluid, called pancreatic juice, into the small intestine [46].

Exocrine compartment covers most of the pancreas volume and contains acinar cells and ducts. Acinar cells secrete three important digestive enzymes, which are proteases, amylase and lipase, into pancreatic juice. The proteases and lipases secreted by pancreas firstly exists as inactive pro-enzymes called zymogens. After secretion into the duodenal lumen, trypsinogen is converted to trypsin by the enterokinase. Then converted trypsin can activate zymogens alongside trypsinogen molecules. Other enzymes like amylase, lipase and ribonucleases are excreted in, an active form. Acinar cells secrete a trypsin inhibitor called pancreatic secretory trypsin inhibitor which protects the pancreatic morphology and physiology from the damage [46].

Digestive enzymes are synthesized via ribosomes of the rough ER in acinar cells. These synthesized proteins (digestive enzymes) can go through some conformational changes in the ER before their transport via vesicles to the Golgi complex. After glycosylation, peptide cleavage, and other posttranslational modifications in the ER, Golgi complex packs secretory proteins as condensed vacuoles that eventually change into zymogen granules. Cholecystokinin (CCK), an intestinal peptide hormone, binds to GPCRs stimulating the protein secretion from acinar cells [46].

In addition to exocrine function of pancreas, endocrine compartment has various vital functions in the body. Endocrine compartment is comprised of Langerhans islets. These islets secrete distinct hormones via alpha, beta, delta, PP, and epsilon cells.

These hormones, insulin, glucagon, amylin, somatostatin, and pancreatic polypeptide, maintain the homeostasis of physiological system [45].

3.2.2 Pancreatic Pathologies

Acute Pancreatitis (AP) is an inflammatory disease of the pancreas mainly linked to mainly gallstones and alcohol misuse risk factors. Smoking might also increase the risk of acute pancreatitis. Upstream obstruction of pancreatic secretion in the pancreatic duct hinders release of zymogen granules from acinar cells. Eventually, zymogen granules fuse with lysosomes and form a mixture of lysosomal and digestion related enzymes. Cathepsin B, as one of the lysosomal enzymes, can enable conversion of trypsinogen to trypsin [47]. Deposition of active trypsin containing vacuoles can start a chain reaction of digestive enzymes causing autodigestion injury in the pancreas [48]. This autodigestion injury evokes infiltration of immune cells. Elementarily, macrophages and neutrophils contribute immune cell population and tumor necrosis factor alpha, interleukin-1,6, and interleukin-8 production [49]. In severe cases, multiorgan failure and sepsis can follow parenchymal inflammation[50].

Another pathological disease of pancreas is chronic pancreatitis (CP) identified as a fibrotic and inflammatory syndrome [51]. Almost 10% of AP patients turn into clinical evaluation of CP [52]. In addition to the risk factors of acute pancreatitis, metabolic abnormalities, genetics, and autoimmune responses can also induce the pathophysiology of chronic pancreatitis. In the long term, this chronic inflammation of pancreas would end up with pancreatic cancer. It is defined by importunate injury of exocrine and endocrine compartments, therefore CP patients present clinical symptoms of exocrine and endocrine deficiencies associated with pancreatic atrophy, loss of acinar cells, and function of islet cells [53].

Pancreatic cancer is one of the deadliest cancer type and holds fourth place in cancer-related deaths [54,55]. So far, pancreatic cancer still can not be detected efficiently by any screening methods or specific symptoms therefore most of the patients are diagnosed during terminal stage in which the disease is already locally advanced or metastasized to other organs [54]. Exocrine compartment originated pancreatic ductal adenocarcinoma (PDAC) is the most common subtype of pancreatic cancers. Around 90% of pancreatic ductal adenocarcinomas harbor *Kras* oncogenic mutation. *Tp53* (oncogenic or loss of function), *p16/CDKN2A* (loss of

function or complete loss), and *TGF-beta/SMAD4* (DPC4) (complete loss or loss of function, point mutation) are most frequently concurred genetic variances, following Kras [56–59]. In a recent publication, researchers distinguished several subtypes of PDAC by genomic analyses [59]. Regarding expression analysis and histopathological characterics of PDAC tissues, squamous, pancreatic progenitor, immunogenic, and aberrantly differentiated endocrine exocrine (ADEX) were defined [59]. By the help of these findings, it is believed that therapeutic modalities for PDAC might be identiified. Worse prognosis of PDAC patients associates with metastasis. An understanding of metastatic cascade in pancreatic cancer may hold a merit utility in determination prognosis and treatment options for PDAC patients.

3.2.3 Pancreatic Cancer, Autophagy and Metabolism

Autophagy and metabolic features become important emerging hallmarks of several cancers. Because of dense stromal reaction in PDAC, stromal components restrict availability of oxygen and nutrients for pancreatic cancer cells. Eventually, pancreatic cancer cells are contingent to various nutritional and metabolic amendments. Therefore, pancreatic cancer cells benefit use of autophagy, macropinocytosis and metabolic modifications to circumvent conditions with low nutrients and oxygen [60,61]. Their modified metabolism adventitously creates opposite effects on the microenvironment, e.g., by immunosuppression [62].

Pancreatic ductal adenocarcinoma cells effectively benefit from increased autophagy to proliferate and survive under several conditions [60]. Due to autophagy dependence of pancreatic cancer cells, researchers determined autophagy inhibition as a therapeutic approach. Antimalarial drug chloroquine remains one of the most important findings owing to its autophagy inhibitory effect via increasing lysosomal pH, tumor growth suppressing effect in vitro an in vivo and extending survival in xenograft murine autochthonous tumors [60]. Supportive findings could be beholded by pancreatic specific deletion of autophagy genes like Atg5 and Atg7, and it has been a subject of whether alterations of p53 determine the effect of autophagy in PDAC [63,64]. A first phase study of chloroquine as an adjuvant therapy with gemcitabine in patients with metastatic or unresectable pancreatic cancer is completed, however this combination still needs further assessment [65].

Another cellular process enabling cancer cells to degrade and use extracellular matrix (ECM) components to use as a supply for metabolic utilities is

macropinocytosis for pancreatic cancer cells [61]. Especially, Ras-transformed cancer cells exploit macropinocytosis to take up large soluble molecules like albumin from ECM [61]. This scavenging process can be inhibited by amiloride and inhibiton of macropinocytosis leads inhibiton of cancer cell proliferation and compromising in vivov tumor growth [61].

Pancreatic cancer cells have a comprehensive metabolic reprogramming, which is induced by mutational status mediated signaling pathways, the genuine interaction of the players of the tumor microenvironment, and their crosstalk with cancer cells [66]. Oncogenic *Kras* rewires metabolic activities of pancreatic cancer cells and several nutrients such as carbonhydrates, lipids, and amino acids are used by cancer cells to maintain cellular homeostasis and support proliferation of cell. In the list of nutrients, glucose is the main supply for proliferating cancer cells to produce more ATP and using its carbons for ribose biosynthesis and other building blocks like amino acids and lipids [67]. For proliferating cancer cells, another important nutrient is glutamine which is a non-essential amino acid (NEAA) and the most redundant amino acid in the blood circulation [68]. Glutamine has a pivotal role to sustain redox balance for PDAC cells [69]. Additionally, it holds an importance place to provide a supply of carbon and nitrogen to proliferating pancreatic cancer cells [70]. Oxidative phosphorylation and glycolysis are the main routes to counterbalance the metabolic demand of cancer cells. But the contribution of glycolytic ATP production, know as Warburg effect, covers over 50% of ATP content and oxidative phosphorylation still remains to promote cancer cell growth via providing building precursors generated in the tricarboxylic acid (TCA) cycle [71–73]. During deregulation of metabolic activities in cancer cells, mitochondrial dynamics can often adapt these alterations [74]. Mitochondria repeatedly tailor their structure, location and activities due to intracellular and extracellular changes [75]. Tailoring of mitochondrial dynamics mainly occurs via mitochondrial fission and fusion [76]. Mitochondrial quality can be maintained by mitophagy and this is also another component of mitochondrial dynamics [42]. The movement of mitochondria to other subcellular locations consummates four facets of mitochondrial dynamics [77]. All of these forms of mitochondrial dynamics are frequently dysregulated in several cancers and especially in pancreatic cancer [78]. Increased expression and activity of Drp1, molecular regulator of mitochondrial fission, have been connected with Ras-driven carcinogenesis, MAPK-dependent cancer expansion, stemness of tumor cells [79–82].

Thus, cumulative averments showing dysregulation of mitochondrial functions and dynamics in tumor progression shows that mitochondrial alterations are inevitable drivers of tumor growth and metastasis in pancreatic cancer.

3.3 Calcium Signaling and Its Role in Tumor Aggressiveness

Calcium (Ca^{2+}) is one of the most important cations in the cells with many functions in physiological and pathophysiological conditions. As a second messenger, calcium, is regulated by organelles like endoplasmic reticulum, golgi apparatus, mitochondria, and lysosomes which are controlling its sequestration and release [83]. In addition to regulatory organelles, there are also molecular regulators of calcium including transient receptor potential (TRP) channels, calcium release-activated calcium channel protein 1 (ORAI1) and stromal interaction molecule 1 (STIM1) [84].

Autophagy and lysosomal network bears several roles in Ca^{2+} signaling as an important hub [85]. Under starvation stress, lysosomes release Ca^{2+} via MCOLN1, thereby Ca^{2+} can enhance dephosphorylation of transcription factor EB (TFEB). After dephosphorylation, TFEB relocates to the nucleus and stimulates gene expressions of autophagic and lysosomal pathways [86]. During adaptation to different stressors, rewiring metabolic pathways can also alter intracellular metabolites. Especially, ADP-ribose (ADPR) is taken into consideration as a major metabolite for the transient potential receptor melastatin-2 (TRPM2) [87]. Lysosomes regulates intracellular Ca^{2+} flux via the interaction of ADPR and lysosomal membrane resided TRPM2 [88]. Most of the time, alterations in mitochondrial dynamics can interfere with calcium regulatory mechanisms. Therefore, metabolic changes in the cancer cells might be also linked to mitochondrial Ca^{2+} regulation [83]. Next to intracellular and extracellular stress signals bearing oncogenic mutations can also change the status of accumulation of Ca^{2+} in the mitochondria along with a metabolic switch. Herewith, modulation of Ca^{2+} signaling has been involved in cancer cell migration and metastatic cascade in many scenarios of tumor progression[84]. During migration, cancer cells display elevation in Ca^{2+} levels from the leading edge of the cells to the back, that is believed to be liable for cell retraction [89,90].

Another involvement of Ca^{2+} into metastatic cascade is enabled by calcium-binding proteins [91]. These protein family controls a broad spectrum of cellular functions via

acting as intracellular Ca^{2+} decoders and as extracellular parameters [92]. S100A4, as being an important member of this protein family, can intervene in survival, migration, and invasion of cancer cells [91]. S100A4 increases motility and invasion by way of increasing the cycle of myosin II filaments at the front edge and positively correlates with the expression pattern of metalloproteinase (MMP)-2 and MMP-9 respectively [93–95].

3.4 Tumor Aggressiveness : Metastasis

Metastatic diseases are esteemed as a reason of the greater part of cancer-related deaths [96]. In most of the patients, metastasis has ensued in due course of time for diagnosis, even though metastasis might not be observable symptomatically [97]. The spread of cancer cells from primary focus and colonization in distant target organs comprise multi stage processes, so called “the metastatic cascade” [98]. The pathophysiology of metastasis comprises multiple steps allying to cell-autonomous and non-autonomous properties [99]. Metastatic cascade starts with invasion of primary tumor into stroma and then it continues with intravasation into blood vessels or lymphatic system, entering to blood circulation and survival until future seeding into target organs. Then cancer cells get captured in target organ and after extravasation they adapt to new environment and colonize as metastatic disease [96]. Therefore, motility and invasion of cancer cells are really important features for metastatic cascade.

Local invasion of the primary tumor into its stroma can be facilitated by many mechanisms. Collective invasion of cancer cells could enable cancer clusters to seed metastatic cascade [100]. During constitution of invasion routes by collectively invading cancer cells, most of the studies have focused on the role of proteases in extracellular matrix (ECM) degradation [101]. Most of the proteases and ECM degrading cathepsins can be released from lysosomes via lysosomal membrane permeabilization (LMP), mitochondrial outer membrane permeabilization, and apoptosis [102,103]. Cathepsin (CTS) L,B ,S ,and D commit dual role for degradation of autohagic cargos and degradation of ECM as intra-lysosomal and extra-lysosomal activities respectively [101,104]. Especially, high levels of CTSB and CTSL are positively correlated with pancreatic cancer aggressiveness [105]. Recently, increased activities of lysosomal cathepsins were associated with tumor progression of several types of

cancer including pancreatic cancer. The combination of cathepsin-targeting approaches with already established chemotherapeutic regimens would be promising for cancer patients in the future.

Metastatic dissemination and colonization are presumably to be influenced by cells of the adaptive and innate immune systems [106]. Among the immune cells, most dominant cell group is macrophages in the tumor microenvironment. Macrophages are implausibly various type of cells, perpetual changing their functional status whereupon to circumferential stimuli[107]. Classically induced macrophages (M1) secrete pro-inflammatory cytokines and generally they act against to tumor. Instead of these macrophages, anti-inflammatory cytokines releasing macrophages (M2) resource for tumor associated macrophages (TAM) with their characterization[106]. This unrivaled subtype of macrophages called by TAM in the tumors has been classified as an important lieutenant to the establishment of a appropriate metastasis associated microenvironment via facilitating migration and invasion [108], altering composition of ECM [109], preparation of pre-metastatic niche [110], vitalizing metastatic outgrowth [111], and provoking angiogenesis [112]. Thus, TAMs have pivotal roles for tumor development, progression, and metastasis turning the light on for therapeutic approaches.

3.5 Aim

The main purpose of the present study was to reveal the role of *Atg5* in pancreatic cancer development and progression by using an *in vivo* model of pancreatic cancer. Pancreas-specific monoallelic (*A5+/-;Kras*), and biallelic (*A5;Kras*) loss of *Atg5* in oncogenic *Kras* expressing mice were generated, and compared them with mice with only oncogenic *Kras* harboring mice (controls). Pancreata were analyzed by histology and immunohistochemistry. Primary tumor cells were isolated and used to perform transcriptomics, metabolomics, intracellular calcium flux, extracellular cathepsin activity, and cell migration and invasion assays and their analyses. The isolated murine cancer cells were injected into wild type littermates via tail vein, and implanted as an orthotopic model to monitor tumor growth and metastasis. By using small hairpin RNAs, *Atg5* was knocked down as representing different dosages of *Atg5* in murine cancer cells, and migratory and invasive capacities of these cells were measured. Additionally, these cancer cells were injected to wild type littermates by tail vein to analyze metastatic loads. To confirm the relevance of this study, PDAC

samples were procured from independent patient cohorts and protein levels were measured with immunoblotting and immunohistochemistry to depict correlation of protein levels with metastasis and survival times of pancreatic cancer patients.

4 MATERIALS AND METHODS

4.1 Mice

4.1.1 Mouse models

- *Atg5*$^{flox/flox}$ [113]**:** Exon 3 of *Atg5* was flanked by two loxP sites.
- *Ptf1a-cre*^{ex1} [114]: Part of exon 1 (ex1) in the *Ptf1a* locus was replaced with the *Cre* recombinase.
- *GFP-LC3* transgenic mice [115]: Rat *LC3* was fused to *EGFP* at the N-terminus. Thus, *GFP-LC3* transgenic mice expressed LC3 coupled to EGFP. Formation of autophagosomes led to increased detection of GFP-LC3 puncta, enabling analysis of autophagy induction[34]. Background fluorescence was seen under conditions without autophagy stimulation. (TG(CAG-EGFP/Map1lc3b)53Nmz)
- *LSL-Kras*^{G12D} knock in mouse [116]: *Kras*$^{LSL-G12D}$ strain bears a *Kras* point mutation (G12D) whose expression is stopped by the presence of a *loxP*-sided stop codon. Cre-mediated recombination can remove the stop codon and then allow the oncogenic *Kras* protein expression.

Mouse strain combinations included:
Atg5$^{flox/flox}$*, Ptf1a-cre*^{ex1}*, LSL-Kras*^{G12D} mouse strains were interbred to generate compound mutant *Atg5*$^{flox/flox}$; *Ptf1a-cre*^{ex1}*; LSL-Kras*^{G12D} (termed as *A5;Kras*), *Atg5*$^{flox/+}$; *Ptf1a-cre*^{ex1}*; LSL-Kras*^{G12D} (termed as *A5+/-;Kras*) *and* ; *Ptf1a-cre*^{ex1}*; LSL-Kras*^{G12D} (termed as *Kras*). *GFP-LC3* transgenic mice were interbred with *A5+/-;Kras* mice to generate *A5;Kras* (termed as *GFP-LC3;A5;Kras*), *A5+/-;Kras* (termed as *GFP-LC3;A5+/-;Kras*) or *Kras* (termed as *GFP-LC3;Kras*) mice with concomitant GFP-LC3 expression were used to detect autophagosomes. Littermate mice without *Ptf1a-cre*^{ex1} expression were used for orthotopic transplantation and tail vein injections.

For all of the experiments in this research study, mice were housed under specific pathogen-free conditions with free access to food and water. All of the mice related procedures were evaluated and reviewed by the Zentrum für Präklinische Forschung

of the Technische Universität München, which follows the federal German guidelines for ethical animal treatment (Regierung von Oberbayern).

4.1.2 Orthotopic Transplantation

Sex-matched, 8 week old littermate mice of *A5+/-;Kras* (8 weeks old) were housed under specific pathogen-free conditions with free access to food and water. These mice were injected orthotopically into the pancreas with $1x10^6$ of either Kras or A5+/-;Kras tumor cells resuspended in a solution of Matrigel (Corning 354234). Suspension solution with Matrigel is diluted with DMEM without supplements in a ratio of 4/1. Orthotopic transplantations were made by using a 26G needle. Transplanted mice were sacrificed 30 d after implantation or earlier if they show sickness symptoms. Pancreatic tissues were collected, embedded in paraffin and stained with haematoxylin and eosin (H&E). Other organs like lung, liver, lymph nodes, kidney, spleen, and duodenum were also collected and processed in the same way.

4.1.3 Intra-Tail Vein Injections

Littermate mice of A5+/-;Kras mice at 8 weeks of age were injected intravenously (IV) by the way of tail vein with $1x10^6$ of either Kras or A5+/-; Kras tumor cell suspensions resuspended in 0.9% saline solution using a 26G needle. Intravenously injected mice were sacrificed 20 d after injection, or earlier if they present sickness symptoms. The lungs were collected, embedded in paraffin and stained with haematoxylin and eosin (H&E). Other organs as it is mentioned before were collected in a different tissue cassette. Mice were classified as metastasis positive or negative at the beginning with the presence of macroscopic pictures. Body weight of IV injected mice was measured to determine levels of cachexia and tumor progression.

4.1.4 Macrophages Depletion by Liposomal Clodronate

For macrophage depletion in wildtype mice, clodronate-loaded liposomes (CP-010-010, Liposoma) were used. As control, mice were injected with control liposomal suspensions in PBS. For the depletion of macrophages, administration of liposomal clodronate or control liposomes were done via intraperitoneally (ml/ mouse). Prior to tumor cells tail vein injection 8, 4 days before 0.2 ml liposomes were injected. On the

same day of tumor cells IV injection, mice have received 0.1 ml liposomes as last injection before IV injection of cancer cells. After tail vein injection, at 4^{th} , 8^{th} , 12^{th} , 16^{th} and 20^{th} days, IV injected mice have received 0.1 ml liposomes (Table 1).
Liposomal clodronate and PBS liposomes treated mice were undergone to injection of A5+/-; Kras cells (biological duplicates) into the tail vein. Experiments were performed with at least 5 mice per each group. Liposomes treated mice and IV injected mice were sacrificed 21 days after tail vein injection considering their sickness. Lungs and other metastatic target organs as liver were collected. Spleens of these mice were analyzed after the experiments for several stainings.

Table 1 : Schedule for Liposomal Treatment

Prior to tail vein injection			After tail vein injection		
Day -8	Day -4	Day 0	Day 4/ 8	Day 12/16	Day 20
0,2 ml	0,2 ml	0,1 ml	0,1 ml	0,1 ml	0,1 ml

4.1.5 Chronic Pancreatitis Model

Chronic cerulein injections into *A5;Kras*, *A5+/-;Kras*, and *Kras* mice to mimic chronic pancreatitis-mediated promotion of PDAC. Established protocol of chronic pancreatitis induction is used involving intraperitoneal injections of the cholecystokinin analog cerulein, which activates pancreatic enzymes and induces pancreatic damage/ inflammation. Mice (8 weeks of age) were injected for 5 days, once per day with 0,1 mg/ g body weight (American peptide Cerulein 46-1-50) and sacrificed one month after the last injection.

Schema 1: Chronic Pancreatitis Induction Schedule

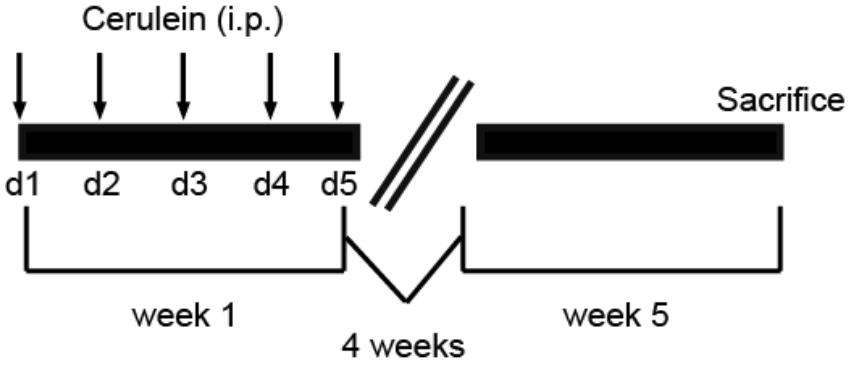

4.2 DNA/RNA studies

4.2.1 Mouse genotyping

Genotyping of mice was performed by DNA extraction from the tail tip of mice. Tail tips were obtained from mice at 4 weeks of age (standard genotyping) or after sacrifice (post-genotyping) to verify genotype. Tails were lysed in Tail Lysis Buffer (100mM TRIS/HCl (Sigma) pH 8.5; 200mM NaCl (Sigma); 5mM EDTA (Sigma) pH 8.0; 0.2% SDS (Sigma); 5% Proteinase K (Roche)) for 2-12 hours at 60°C. During and after the incubation, samples were thoroughly mixed and incubated for 10 minutes at 95°C to inactivate the proteinase K. To dilute the DNA, dH2O (900µl) was added. Genotyping PCR was performed with 3-5 µl of DNA using the RedTaq Ready Mix (Sigma). A standard PCR protocol was applied (Table 2). All primers (Table 3) were used at a final concentration of 10 pM. Mice were genotyped with the assistance of Alexandra Berninger and Marlena Kowalska.

Table 2: Genotyping PCR standard protocol.

Step	Temperature	Time	Cycle number
Pre-incubation	95°C	5 min	1x
Amplification	95°C 60°C 72°C	30 sec 30sec 60 sec	35x
Cooling	4°C	∞	1x

Table 2: Genotyping primer sequences and product sizes.

Name	Primer forward (5´-3´)	Primer reverse (5´-3´)	Product (bp)
Atg5 wildtype	GAATATGAAGGCAC ACCCCTGAAATG	GTACTGCATAATGGTTT AACTCTTGC	350
Atg5$^{F/F}$	ACAACGTCGAGCAC AGCTGCGCAAGG	GTACTGCATAATGGTTT AACTCTTGC	700
GFP-LC3	TCCTGCTGGAGTTC GTGACCG	TTGCGAATTCTCAGCC GTCTTCATCTCTCTCG C	400

Cre	ACCAGCCAGCTATC AACTCG	TTACATTGGTCCAGCC ACC	Wildtype: 350 Mutated: 200
	CTAGGCCACAGAAT TGAAAGATCT	GTAGGTGGAAATTCTA GCATCATCC	

4.2.2 RNA extraction

For RNA extraction, mice were sacrificed and samples of the pancreas and cancer cells were immediately removed, homogenized in RLT lysis buffer (1015762 Qiagen, Hilden, Germany) supplemented with 1% β-mercaptoethanol (M6250 Sigma) and snap frozen. Subsequently, RNA was extracted from pancreatic tissues and *Kras* and *A5+/-;Kras* cells using the RNeasy Mini Kit (74104 Qiagen). NanoDrop 2000 spectrophotometer (Peqlab, Erlangen, Germany) was used to determine RNA concentration and RNA purity through the absorbance ratios at 260 nm/280 nm and 260 nm/230 nm.

4.2.3 cDNA synthesis

SuperScript II Reverse Transcriptase (18064-014 Invitrogen, Darmstadt Germany) along with 1-5 µg RNA was used for complementary DNA (cDNA) synthesis. The reaction mix included oligo(dt) primer. cDNA obtained from the reaction was quantified and concentration set to 20 ng/µl.

4.2.4 Quantitative real time PCR analysis

Quantitative RT-PCR was performed on a LightCycler 480 (Roche) using the LightCycler 480 Sybr Green Master Mix 1 (Roche). Reaction conditions can be seen in table 4. 100 ng cDNA were used as a template. Target mRNA expression was normalized to endogenous *Cyclophilin* and quantified by the delta-delta CT method ($2^{\text{DeltaCT(Cyclophilin)} - \text{DeltaCT(target gene)}}$). Melting curves were evaluated to verify primer specificity. Primers are listed in table 5.

Table 3: qRT-PCR program.

Step	Temperature	Time	Cycle number
Pre-incubation	95°C	10 min	1x
Amplification	95°C 60°C 72°C	10 sec 20 sec 10 sec	45x
Melting	95°C 55°C 98°C	1 min 1 sec Continuous 0.11°C/sec	5 acquisitions/sec
Cooling	37°C	5 min	1x

Table 4: qRT-PCR primer sequences and product sizes.

Name	Primer forward (5´-3´)	Primer reverse (5´-3´)
Sod1	GTCCGTCGGCTTCTCG TCT	CACAACTGGTTCACCG CTTG
Sod2	ACACATTAACGCGCAG ATCA	ATATGTCCCCCACCAT TGAA
Nrf1	TCTCACCCTCCAAACC CAAC	CCCGACCTGTGGAATA CTTG
Nrf2	TTCTTTCAGCAGCATC CTCTCCAC	ACAGCCTTCAATAGTC CCGTCCAG
Xbp1	ACACGCTTGGGAATGG ACAC	CCATGGGAAGATGTTC TGGG
Cyclophilin A	ATGGTCAACCCCACCG TGT	TTCTGCTGTCTTTGGAA CTTTGTC

4.2.5 Detection of unspliced and spliced *Xbp1*

For detection of spliced *Xbp1*, cDNA was subjected to PCR with a primer set detecting both unspliced and spliced *Xbp1* (unspliced *Xbp1u* 171 bp, spliced *Xbp1s* 145 bp) (Table 5). PCR products were separated by agarose gel electrophoresis. PCR conditions can be seen in Table 6. *Cyclophilin* was used as control.

Table 5: PCR conditions for detection of spliced and unspliced *Xbp1*.

Step	Temperature	Time	Cycle number
Pre-incubation	94°C	4 min	1x
Amplification	94°C	10 sec	35x
	65°C	30 sec	
	72°C	30 sec	
Extension	72°C	10 min	1x
Cooling	4°C	∞	1x

4.2.6 Agarose gel electrophoresis

For agarose gel electrophoresis, agarose (Biozym, Hess. Oldendorf) was dissolved by heating in 1xTAE-Buffer (0.4 M Tris, 0.2 M acetic glacial acid, 0.01 M EDTA x NA_2 x $2H_2O$) at a concentration from 1 to 3% (w/v), dependent on PCR-product size. After cooling down to approximately 50°C, ethidium bromide (Sigma) was added to the agarose solution at a final concentration of 0.5 μg/ml. The agarose solution was poured into an electrophoresis chamber and allowed to polymerize. PCR-products diluted in loading buffer (Peqlab) along with a DNA-ladder (Peqlab, 1 kb) were run horizontally at 100 V. Documentation was performed by UV-light (EX/EM 312/516-518 nm, GelDoc^{TM}XR system)

4.2.7 Microarray analysis

For transcriptomic analysis, *Kras* and *A5+/-; Kras* tumor cells were harvested after PBS-washing in RLT lysis buffer supplemented with 1% β-mercaptoethanol, as described above. Cell suspensions were snap frozen and stored at -80°C. RNA isolation from tumor cell suspensions and Affymetrix GeneChip (*Mus musculus*) Mouse Gene 1.0 ST Array was conducted by the service facility KFB Center of Excellence for Fluorescent Bioanalytics (Regensburg, Germany, www.kfb-regensburg.de). Microarray data were analyzed by using the Gene Set Enrichment Analysis Software (GSEA) provided by the Broad Institute. A Nominal Enrichment Score (NES) of ≥1.0 and a nominal p-value of <0.05 were used to evaluate significantly upregulated pathways according to KEGG and Transcription Factor Binding Motif databases. Pathways were subsequently separated into groups depending on their description in the respective database. A heat map of the most

highly regulated genes computed by GSEA was used and the genes were further classified according to their function. Genes belonging to one functional group were depicted as percentage related to the entire number of highly regulated genes. A NES versus nominal p value diagram was provided to indicate the total number of regulated (NES≥0.5) and significantly regulated (NES≥1.4, nominal p value< 0.05) pathways detected in the KEGG database. Microarray data are available in the ArrayExpress database at EMBL-EBI (https://www.ebi.ac.uk/arrayexpress/) under accession number E-MTAB-6275.

4.3 Histology

4.3.1 Tissue sections

Paraffin sections

Mouse tissue samples were fixed in 4% PFA (Merck, Darmstadt, Germany)/PBS for 12-18 h, dehydrated and embedded in paraffin. A microtome (HM 355 S, MICROM, Walldorf, Germany) was used to cut 3.0-5.0 µm thick sections. Sections were mounted on adhesive-coated slides (SuperFrost® Plus, Menzel, Braunschweig, Germany) and air-dried at approximately 25°C for 12-18 h. Sections were kept at 25°C until further analysis.

Cryo-sections

Pancreatic tissue was snap frozen in freezing medium (Tissue-Tek O.C.T. Compound, Weckert Labortechnik, Kitzingen, Germany) and stored at -80°C. A cryotome (Cryo-Star HM 560 MV, MICROM) was used to cut 6-10 µm thick sections. Sections were mounted on adhesive-coated slides (SuperFrost® Plus, Menzel) and kept at -20°C until further analysis.

4.3.2 Haematoxylin and eosin (H&E) staining

For H&E staining, paraffin-embedded tissue sections were deparaffinized in Xylol (Merck) for 2 x 5 minutes followed by rehydration in ethanol (100%, 96%, 70%; 3 minutes each) and water (2 x 3 minutes). The slides were incubated in haematoxylin solution (Merck Millipore, Billerica, MA) for 5 minutes, washed with running tap water for 10 minutes and incubated in eosin solution (Merck) for 3.5 minutes. Dehydration

was performed with 96% Ethanol and Isopropanol for 25 sec each and xylol for 2 x 3 minutes. Slides were subsequently covered with mounting medium (Pertex, Medite GmbH) and coverslips (Merck). Axiostar Plus (Carl Zeiss, Göttingen, Germany) was used for histological analysis.

4.3.3 Immunohistochemistry

For immunohistochemistry, slides were de-waxed and rehydrated as described under 4.3.2. After deparaffinization and rehydration, heat induced antigen retrieval was done by shortly boiling the slides in 0.01 M citrate buffer (pH 6.0) followed by sub-boiling for 10 minutes. Slides were allowed to cool down at approximately room temperatures for 20 minutes in citrate buffer and washed 2 x 5 minutes with water. Endogenous peroxidase was blocked with 3% hydrogen peroxide for 15 min at approximately 25^{o}C in the dark and slides were washed 2 x 5 minutes with wash buffer (TBS, TBS-T, PBS or PBS-T (Table 7) depending on the primary antibody). Unspecific binding was blocked with 5% serum blocking solution (5% rabbit or 5% goat serum, according to the secondary antibody, in wash buffer) for 1 h at approximately 25°C. Slides were then incubated with the primary antibody diluted in blocking solution (or wherever indicated in SignalStain antibody diluent, 8112 Cell Signaling Technology, Danvers, MA) for 12-18 h at 4°C. Primary antibodies used include: anti-BrdU (1/250) (MCA2060 AbD Serotec), anti-F4/80 (1/100) (MF-48000 Invitrogen), anti-CK19 (1/200) (TROMA III Developmental Studies Hybridoma Bank), anti-Arginase 1 (1/500) (610708 BD Transduction Laboratories), anti-S100a4 (1/800) (13018 Cell Signaling Technology), anti-MMR/ CD206 (1/100) (AF2535 R&D systems Biotechne), anti-Atg5 (1/100) (NB110-53818 Novus Biologicals), anti-p62 (1/100) (GP62-C Progen), and anti-LC3 (1/100) (PD014 MBL International). Secondary antibodies including biotinylated anti-rabbit in goat (BA 1000 Vector), anti-mouse in goat (BA 9200 Vector), and anti-rat in rabbit (BA 4000 Vector) were applied for 1h at RT and avidin-biotin peroxidase complex for biotinylated secondary antibodies was then added according to manufacturer directions (Vector Laboratories, CA). Staining was developed with DAB reagent (Vector Laboratories, CA). For Arginase 1 and S100a4 detection Streptavidin/Biotin blocking kit (SP2002 Vector) was used during the staining procedure to reduce background, according to manufacturer instructions. Hematoxylin was used for counterstaining and slides were consequently dehydrated and mounted as mentioned (4.3.2).

Table 7: Buffers used for washing.

Name	Components	pH
TBS	20 mM Tris, 137 mM NaCl	7.6
TBS-T	TBS-buffer, 0.1% (v/v) Tween-20	7.6
PBS	137 mM NaCl, 2.7 mM KCl, 10 mM Na_2HPO_4, 10 mM KH_2PO_4	7.4
PBS-T	PBS-buffer, 0.1% (v/v) Tween-20	7.4

4.3.4 Co-immunofluorescence

Cryo-sections of GFP-LC3 transgenic pancreas were processed as described (4.3.1-3). Unspecific binding was blocked with 5% serum blocking solution (5% goat or 5% rabbit serum, according to the secondary antibody, in wash buffer (table 7)) for 1 h at approximately RT and incubated over night at 4°C with the primary antibody. Primary antibody anti-CK19 (1/200; TROMA III Developmental Studies Hybridoma was diluted in blocking solution and at the following day, slides were washed 3 x 5 minutes with wash buffer and secondary anti-rat in goat Alexa Fluor 568 nM (1/300; A11077 Invitrogen) was applied for 1 h at approximately RT. In the end, the slides were washed and covered with DAPI containing mounting medium (H-1200 Vector Laboratories) and analyzed by fluorescence microscopy (Axiostar Plus FL, Carl Zeiss).

4.3.5 Detection of GFP-LC3 puncta

GFP-LC3 transgenic mice with or without concomitant *Kras* expression were sacrificed after standard fed conditions. Pancreas was snap frozen in freezing medium (Tissue-Tek O.C.T. Compound, Weckert Labortechnik, Germany) and 7-10mm thick cryo-sections were mounted on adhesive-coated slides. Sections were air dried, fixed in 100% ethanol for 8 minutes at RT, washed with PBS and covered with DAPI containing mounting medium (H-1200 Vector Laboratories, CA). Sections were processed and kept in the dark until analysis. Puncta formation was detected by analysis of green fluorescence (EX/EM 470/525nm) with fluorescence microscopy (Zeiss Axiovert 200M).

4.3.6 ADM and PanIN Quantifications

Paraffin-embedded tissue sections from 4-week old *Kras*, *A5+/-; Kras*, *A5; Kras* were stained for H&E and photographed at 100x magnification. The number of Acinar to Ductal Metaplasias was determined in each picture using Zeiss axiovision software. Measurements from multiple photographs per tissue slide were summed up and expressed as ADM per High Power Field (HPF). Results were then averaged according to genotype. In a similar fashion, paraffin-embedded tissue sections from 9- and 18-week old *Kras*, *A5+/-; Kras*, *A5; Kras* were stained for H&E and photographed at 100x magnification. Pancreatic Intraepithelial Neoplasias (PanINs) were classified according to PanIN-1/-2/-3 and total numbers were expressed as PanIN/HPF. Results were then averaged according to genotype and age group.

4.3.7 Quantification of Macrophage Infiltration (F4/80-Positive) and M2 Polarized Macrophages (CD206-positive)

For quantification of F4/80-positive macrophages in the lungs of tail vein-injected mice, tissue sections were stained for F4/80 via immunohistochemistry, as described above. Sections were subsequently photographed at 200x magnification. Number of positive cells was determined with Zeiss axiovision software. Sum from multiple photographs per tissue slide were generated and expressed in relation to the number of high power fields counted. Results were then averaged by genotype.
F4/80-positive and CD206-positive macrophages were also quantified in the original tumors of *Kras* and *A5+/-;Kras* mice. For this, tissue slides were stained with the respective antibodies and the % of positive nuclei/ all nuclei were determined.

4.3.8 Quantification of Relative Pancreatic Weight, Tumor Incidence, Metastasis Incidence, Tumor and Metastasis Burden

Kras, *A5+/-; Kras*, and *A5; Kras* mice were sacrificed at 4, 9, and 18 weeks of age or at the time point of sickness. Relative pancreatic weight was calculated from the pancreas and body weight obtained during sacrifice (pancreas weight/ body weight). Tumor incidence and metastasis incidence (% of tumor or metastasis-positive mice relative to all mice sacrificed) was calculated after histological examination. Metastasis-positive mice were mice with metastasis in liver, lung, or diaphragm from

the pool of pancreatic tumor-positive mice. Ascites, lymph node, spleen, or kidney infiltration was also evaluated.

For quantification of primary tumor and metastasis burden (in all orthotopic transplantation and tail vein injection experiments) 2 mm-tissue slices were stained with H&E. Per H&E slide multiple pictures at 100x magnification were taken. Area (mm^2) of tumor foci in pancreas and/ or lung tissues was calculated and expressed as % to all tissue area using a proprietary software package (Zeiss Axiovision, Oberkochen, Germany). Statistical analysis was done in between the genotypes (mean ± standard deviation (SD), Student t test).

4.3.9 Human PDAC Samples

For ATG5 immunoblotting, a total of 67 human PDAC samples (Supplementary Table 2, Cohort 1) collected from the Institute of Pathology at the Technical University Munich, were analyzed as described above. Band density was quantified by using ImageJ and normalized to β-Actin. From these 67 patients, n=56 with known survival were grouped into ATG5 low-moderate expression (ATG5/ β-Actin ratio below 0,5) and high expression (ATG5/ β-Actin ratio equal/ above 0,5) and used for Kaplan-Meier survival analysis with GraphPad Prism.

For ATG5 immunohistochemistry, two different cohorts (Cohort 2 and Cohort 3) were used. Cohort 2 consisted of 26 primary PDACs and their corresponding distant metastases that were resected between 2008 and 2013 at the University Hospital Heidelberg. Primary tumor samples were used for ATG5 immunohistochemistry as described below for Cohort 3 and 20 of these were evaluated as described below for Cohort 3. In this analysis 3 patients from the Cohort 3 also exhibiting metastasis were included as well. The percentages of patients with metastasis in the low-moderate and in the high ATG5-expressing groups were calculated as described below for Cohort 3.

Cohort 3 consisted of a patient cohort with primary resected PDACs. The cohort was investigated previously in several studies [117–119] and included 200 individuals (Supplementary Table 3) that received partial pancreatoduodenectomy for PDAC between 1991 and 2006 at the Charité University Hospital Berlin. The use of this tumor cohort for biomarker analysis has been approved by the Charité University ethics committee (EA1/06/2004). Tissue microarrays were generated as previously described [117,120]. In detail three tumor cores (diameter 1.5 mm) of representative

tumor areas selected by a board certified pathologist on H&E stained slides were punched out of formalin-fixed paraffin embedded (FFPE) tissue blocks and arranged in a newly generated paraffin block. TMAs were made using a tissue microarrayer (Beecher Instruments, Sun Praierie, USA). Staging of both cohorts followed the WHO recommendations at the time of cohort generation (TNM-classification of the 7th edition). Clinical and demographic information was obtained from the respective institutional patient databases, by reviewing medical charts and pathological reports. Patient follow-up data were obtained from clinical records and via direct contact with patients and/ or their relatives. For Immunohistochemistry, 2µm-thin sections prepared with a rotary microtome (HM355S, ThermoFisher Scientific, Waltham, USA) were collected from 134 patients in this cohort. Immunohistochemistry was performed using a Bond RXm system (Leica, Wetzlar, Germany, all reagents from Leica) with a primary antibody against ATG5 (NB110-53818 Novus Biologicals). Briefly, slides were deparaffinized using deparaffinization solution, pretreated with Epitope retrieval solution 1 (corresponding to citrate buffer pH 6) for 20 minutes. Antibody binding was detected with a polymer refine detection kit without post primary reagent and visualized with DAB as a dark brown precipitate. Counterstaining was done with hematoxyline. The membranous ATG5 was scored according to the percentage and intensity of positive cells on a 0 to 3+ scale (negative as score 0, faint expression as score 1+, moderate expression as score 2+ and strong expression as score 3+; see FIgure 7B for a panel of staining). Kaplan-Meier survival analysis was performed by GraphPad Prism with a total of 79 patients from the 134. Patients with no available survival and patients with no death follow up were removed from the analysis. The two groups in the Kaplan-Meier analysis included low-moderate ATG5-expressing patients (with scores 1 and 2) and high ATG5-expressing patients (score 3). Lymph node status and resection status in these patients was expressed as % patients referring to the total patients belonging to the two groups. An overview of the three different cohorts used can be found in the Table 8.

Table 8: PDAC Patients Cohorts

Cohort number	Status	Site	Analysis	Number of patients
1	Postoperative	Primary	Western blot	56
2	Palliative/ metastatic	Primary	IHC	23
3	Palliative	Primary	IHC	79

4.3.10 Transmission Electron microscopy (TEM)

Cells were fixed in 2.5% electron microscopy grade glutaraldehyde in 0.1 M sodium cacodylate buffer, pH 7.4 (Science Services, Munich, Germany), post-fixed in 2% aqueous osmium tetraoxide *(Dalton, 1955*), dehydrated in gradual ethanol (30–100%) and propylene oxide, embedded in Epon (Merck), and cured for 24 hours at 60°C. Semithin sections were cut and stained with toluidine blue. Ultrathin sections of 50 nm were collected onto 200 mesh copper grids, stained with uranyl acetate and lead citrate, before examination by TEM (Zeiss Libra 120 Plus, Carl Zeiss NTS GmbH, Oberkochen, Germany). Pictures were acquired using a Slow Scan CCD-camera and iTEM software (Olympus Soft Imaging Solutions, Münster, Germany). TEM sample preparation was done with the help of Gabriele Mettenleiter. TEM image analysis was done with the help of Dr. Michaela Aichler.

4.4 *In Vitro* Experiments and Proteinbiochemistry

4.4.1 Measurement of Serum Amylase and Lipase

Serum was collected from mice immediately after sacrifice at 13 weeks of age after 4 weeks CP induction and diluted 1/10 with 0.9% NaCl. Amylase activity (AMYL2 Cobas, Roche) was evaluated by a colorimetric assay in line with the IFCC method. Lipase activity (LIPC Cobas, Roche) was evaluated via DGGR substrate-based assay.

4.4.2 Tumor Cell Isolation and Cultivation

Primary pancreatic tumor cell lines were established from isolated murine pancreatic tumors. To establish the cancer cell lines, pieces of pancreatic tumor tissues from Kras, A5+/-; Kras, and A5; Kras mice were placed in full culture medium (see below) and cancer cells were allowed to grow out of the tissue. Cell lines were usually cultured under standard conditions (5% CO_2, 37 C) in culture media (Dulbecco's modified Eagle medium (DMEM) supplemented with 10%FBS (#10082147; Gibco), 1% PenStrep (#1500-063; Gibco), 1% Non-Essential-Amino-Acids (NEAA #11140050; Gibco)). On average, cells were passaged 5 times prior to any experiments.

4.4.3 In Vitro Cathepsin Activity Measurements

Activities of cathepsins B, L, and D were intra- and extracellularly assessed in cell lysates and culture media of primary pancreatic tumor cell lines. Tumor cells were separated from culture media by centrifugation at 1000 g for 10 min. Then, cell pellet and culture medium were snap frozen. After thawing tumor cells were subsequently resuspended in ice-cold homogenization buffer (5 mM MOPS pH 6.5, 250 mM sucrose, 1 mM Mg_2SO_4, 0.13% Triton X100l) and lysed by sonication. Cathepsin B and -L were determined as Ca074- and N1760- sensitive activity in assay buffer (50 mM sodium phosphate buffer [pH 5.5], 1 mM EDTA, and 1 mM dithiothreitol) using the fluorogenic substrates Z-Arg-Arg-7-amino-4-methylcoumarin A (10µM, #31213-v, Pepta Nova) and Z-Phe-Arg-7-amino-4-methylcoumarin (10µM, #3095-v, Pepta Nova), respectively. Cathepsin D activity was measured in 50 mM sodium acetate buffer pH 4.0 using the fluorogenic substrate Mca-Gly-Lys-Pro-Ile-Leu-Phe-Phe-Arg-Leu-Lys(Dnp)-D-Arg-NH2 (10µM, #3200-v, Pepta Nova). The release of 7-amido-4-methylcoumarin was kinetically monitored over 10 minutes at the excitation/emission wavelength of 360/438 nm in a Safire microplate reader (Tecan, Grödig, Austria) by spectrofluorometry. Intra- and extracellular portions of cathepsin activities were normalized to the protein concentration in cell lysates determined by BioRad Protein Assay Kit.

4.4.4 Subcellular Fractination by Isopycnic Percoll Density Centrifugation and Measurement of GLDH Activity

To analyze distribution and integrity of mitochondria in subcellular fractions pelleted tumor cells harvested from primary pancreatic tumor cells lines (produced as described above) were resuspended in HS buffer (250mM sucrose, 10 mM citric acid, 0.5 mM EGTA, 0.1 mM MgSO4 [pH 6.0]) and homogenized by 5 strokes using a Dounce homogenizer. After centrifugation at 100g post-nuclear supernatant was applied onto an isotonic 50% (v/v) Percoll/HS buffer solution (described above) at pH 7.27 and subsequently separated by isopycnic centrifugation at 50,000 g for 45 min at 4°C. After separation the percoll gradient was portioned in 46 fractions using a peristaltic pump beginning from the bottom and fractions were stored at -80°C until further use.

Activity of GLDH as a marker of mitochondrial distribution in subcellular fractions was determined spectrophotometrically at 340 nm according to $NADH_2$ oxidation with 2-oxoglutarate and NH_4^+ as a substrate by the method of E. Schmidt [121].

4.4.5 Protein Extraction and Quantification

Protein extraction was performed on ice. Snap frozen cell pellets were lysed in ice-cold protein lysis buffer (IP-buffer: 50 mM HEPES, pH 7.9, 150 mM NaCl, 1 mM EDTA, pH 8.0, 0.5% (v/v) NP-40, 10% (v/v) Glycerol) freshly supplemented with a cocktail of protease (2% (v/v))/phosphatase (1% (v/v)) inhibitors (SERVA, Heidelberg, Germany). Lysates were incubated for 10 min at 4°C and subsequently centrifuged (13,000 rpm, 30 min, 4°C). Supernatants

were collected and centrifuged again (13,000 rpm, 5 min, 4°C) to assure entire removal of cell debris. Protein concentration was approximated from a 1/10 dilution of the supernatant in IP-buffer with the Bio Rad Protein Assay Kit (Bio Rad, München, Germany) by mixing 250 µl Bio Rad Protein Assay Kit (diluted 1/5 in H_2O) with 2,5 µl protein dilution in a 96-well plate. BSA (1 mg/ml; Sigma) was used as a standard and IP-buffer was used as blank. In pursuit a 10 min incubation at approximately 25°C, extinction at 595 nm was measured and protein concentration was determined by the standard curve. Samples were subsequently adjusted to 4 µg/µl with 5 x Laemmli buffer (300 mM Tris-HCl, pH 6.8, 10% (w/v) SDS, 50% (v/v) Glycerol, 0.05% (w/v)

Bromphenole blue, 5% (v/v) β-mercaptoethanol), heated for 5 min at 95°C, cooled down, centrifuged shortly and stored at -80°C until further use.

4.4.6 SDS-PAGE

SDS-polyacrylamide gel electrophoresis for protein separation and consecutive western blot analysis was performed in a Mini-Protean® 3 Cell System (Bio Rad). 50-80 µg protein per sample (contingent upon the protein of interest) in Laemmli-buffer (mentioned above (4.4.5)) were denatured by heating at 95°C for 5 min. After cooling down at RT and a short centrifugation, protein samples were loaded onto the gel. A protein standard (Bio Rad) was used to conclude kDa-size of the proteins. The gel made up of an upper Stacking gel (10% polyacrylamide concentration) and a lower Separating gel (7.5-15% polyacrylamide concentration depending on protein size). Gel run was implemented in Running buffer at 70 V for 20 min followed by 90-120 V (depending on polyacrylamide concentration) until protein separation (depending on the size of the protein). Table 9 describes the itemized contents of the buffers used for SDS-PAGE and Table 10 and 11 depict how the gels were drained.

Table 9: Detailed components of buffers used for SDS-PAGE.

Name	Components	pH
Stacking Gel Buffer	0.5 mM Tris	6.8
Separating Gel Buffer	1.5 mM Tris	8.8
Running Buffer	25 mM Tris-HCL, 192 mM Glycine, 0.1% (w/v) SDS	-

Table 10: Ingredients of SDS-Collection Gels.

dH_2O	3.0 ml
Stacking Gel Buffer	1.3 ml
30%/0.8% Acrylamide/Bis solution (Roth, Karlsruhe, Germany)	750 µl
10% SDS	50 µl
10% APS (Sigma)	25 µl
TEMED (Fluka, Buchs, Schweiz)	10 µl

Table 11: Ingredients of Separating gels in accordance with varying polyacrylamide concentration (for 1.5mm plates).

Concentrations	7.5%	10%	12%	15%
dH_2O	4.9 ml	4.1 ml	3.4 ml	2.5 ml
Separating Gel Buffer	2.6 ml	2.6 ml	2.6 ml	2.6 ml
30%/0.8% Acrylamide/Bis solution	2.5 ml	3.3 ml	4.0 ml	5.0 ml
10% SDS	100 µl	100 µl	100 µl	100 µl
10% APS	50 µl	50 µl	50 µl	50 µl
TEMED	15 µl	15 µl	15 µl	15 µl

4.4.7 Western blot

Following SDS-PAGE (mentioned in 4.4.6), proteins were transferred onto a PVDF membrane of Nitrocellulose membrane depending on a protein of interest (0.45 or 0.2 µm pore size, Merck Millipore) by western blot in the Mini Trans-Blot Cell™ System (Bio Rad). PVDF membranes were hydrophilized prior to usage in 100% methanol for 1 min, followed by washing in water and Transfer buffer (Table 11). Nitrocellulose membranes did not need activation with 100% methanol. Western blot was performed in Transfer buffer (pre-cooled to 4°C) on ice at 390 mA for 1-2 h (depending on protein size). After transferring proteins, membranes were washed shortly in TBS-T or PBS-T (Table 7) and incubated for 1 h at RT on a shaker in blocking solution (Table 12) to block unspecific binding of the antibodies. Primary antibody incubation was completed in antibody solution (Table 12) approximately 18 h at 4°C on a shaker. The primary antibodies used included: The primary antibodies used include: Anti-Atg5 (1/1000) (NB110-53818 Novus Biologicals), anti-p62 (1/1000) (GP62-C Progen), anti-LC3 (1/1000) (PD014 MBL International), anti-Cathepsin B (1/5000) (AF965, R&D Systems), anti-p53 (1/500) (NCL-p53-CM5p Novocastra), anti-Cathepsin L (1/5000) (AF1515, R&D Systems) anti-Cathepsin D (1/5000) (cs-10725, Santa Cruz Biotechnology), anti-phospho-AMPKa (1/1000) (2535 Cell Signaling Technology), anti-AMPKa (1/1000) (2532 Cell Signaling Technology), anti-phospho-S6 (1/1000) (2211 Cell Signaling Technology, anti-SOD2 (1/1000) (ADI-SOD-111 Enzo), anti-BiP (1/1000) (AB21685 Abcam), anti-MitoProfile Total OXPHOS Rodent Western Blot antibody cocktail (1/1000) (MS604 Mitosciences), anti-β-Actin (1: 2000) (A5441, Sigma). After incubation, membranes were washed 3 x

5 min with TBS-T or PBS-T and the secondary antibody was added in antibody solution (Table 12) (horseradish peroxidase-conjugated anti-mouse (1/2000; NA931V GE Healthcare), anti-rabbit (1/2000; NA934V GE Healthcare), or anti-guinea pig (1/2000; A7289, Sigma)) for 1 h at RT on a shaker. Before development, membranes were washed again 3 x 5 min with TBS-T or PBS-T. Development of membranes was performed with the Amersham ECL™ western blot detection reagent (GE Healthcare, Buckinghamshire, UK) and the Amersham Hyperfilm™ ECL (GE Healthcare). Exposure of films to membranes diversed (3 sec-1 h) contingent upon the signal acquired from the protein of interest.

Table 12: Components of solutions used for western blot.

Name	Components
Transfer buffer	25 mM Tris-HCl, 192 mM Glycine, 20% (v/v) Methanol
Blocking solution	5% BSA or 5-10% milk in TBS-T or PBS-T (depending on antibody)
Antibody solution	2% BSA or 2% milk in TBS-T or PBS-T (depending on antibody)

4.4.8 Transmission Electron Microscopy (TEM)

For TEM *Kras* and *A5+/-; Kras* cells were collected when they have 20-30% confluency and fixed in 2.5% electron microscopy grade glutaraldehyde in 0.1M sodium cacodylate buffer pH 7.4 (Science Services, Munich, Germany), postfixed in 2% aqueous osmium tetraoxide [122], dehydrated in gradual ethanol (30–100%) and propylene oxide, embedded in Epon (Merck, Darmstadt, Germany) and cured for 24 hours at 60°C. Pellets were cut in semithin sections and stained with toluidine blue. Ultrathin sections of 50nm were collected onto 200 mesh copper grids, stained with uranyl acetate and lead citrate before examination by transmission electron microscopy (Zeiss Libra 120 Plus, Carl Zeiss NTS GmbH, Oberkochen, Germany). Pictures were acquired using a Slow Scan CCD-camera and iTEM software (Olympus Soft Imaging Solutions, Münster, Germany)

4.4.9 Measurement of Mitochondrial Metabolism by Seahorse Extracellular Flux

Measurements of oxygen consumption rate (OCR) were performed with a XF extracellular flux analyzer as described previously (Oelkrug R, Goetze N, Exner C, Lee Y, Ganjam GK, Kutschke M, Muller S, Stohr S, Tschop MH, Crichton PG, Heldmaier G, Jastroch M, Meyer CW. Brown fat in a protoendothermic mammal fuels eutherian evolution. Nature communications 2013;4:2140). Briefly, *Kras* and *A5+/-;Kras* tumor cells were seeded at a density of $1X10^5$ cells per well in a XF24 cell culture microplate. DMEM (4.5 g/L glucose, +L-Glutamine, -Pyruvate, pH 7.6 at RT) supplemented with 10% heat inactivated FBS (Gibco) and 1% Pen/Strep was used for cell culturing. On the day of assay (24h after seeding), medium was exchanged to non-carbonated Seahorse measurement medium and the XF24 plate was transferred to a temperature-controlled (37 °C) XF24 Extracellular Flux analyzer (Seahorse Bioscience) and equilibrated for 10 min. To determine the basal respiration four assay cycles (1-min mix, 2-min wait and 3-min measuring period) were used. Then oligomycin (4 µM) was added by automatic pneumatic injection (three assay cycles) to inhibit ATP synthase and thus approximate the proportion of respiration used to drive ATP synthesis versus proton leak-linked respiration. Oligomycin was followed by an injection of FCCP (carbonyl cyanide p-trifluoromethoxyphenylhydrazone) (0.5 µM) to completely dissipate proton motive force and maximally stimulate mitochondrial respiration (three assay cycles), thus determining spare respiratory capacity and substrate oxidation capacity. An injection of rotenone (4 µM) and antimycin A (2 µM) was used to correct for the non-mitochondrial respiration rate (three assay cycles), which was subtracted from all the other rates. Coupling efficiency was calculated as the oligomycin-sensitive fraction of mitochondrial respiratory activity, estimating the proportion of basal respiration used to drive ATP synthesis. To determine extracellular acidification rates (ECARs) for glycolysis, experiments were ended by injection of 2-DG (2-deoxy-D-glucose, 100 mM), correcting for non-glycolytic acidification. Injection of 2-DG enabled calculation of glycolytic acidification. Data obtained after oligomycin treatment induce glycolytic capacity. OCR was plotted against ECAR to illustrate oxidative versus glycolytic metabolism in cancer cells. Raw data were normalized to either protein or DNA content (ng).

4.4.10 Cellular Morphology Analysis and Quantification of Cell Proliferation

To analyze cell morphology, *Kras* and *A5+/-; Kras* were seeded in 6-well plates. 24h after seeding, pictures were acquired with the Zeiss Axiovision Imager A1 using a magnification of 100x. For quantification of proliferation, $5x10^4$ *Kras* and *A5+/-; Kras* cells were seeded per well in a 6-well plate. The culture media was changed every other day. Cells were counted after trypsinization every 24 hours up to 120 hours using the neubauer counting chamber. Full medium Dulbecco's modified Eagle medium (DMEM) supplemented with 10%FBS (#10082147; Gibco), 1% PenStrep (#1500-063; Gibco), 1%NEAA (#11140050; Gibco) was used for cell culture.

4.4.11 Autophagic Flux Measurement using Cyto-ID

To analyze autophagosome accumulation, *Kras* and *A5+/-; Kras* were seeded in triplicates in 96-well plates and allowed to adhere overnight. Half of the cells were kept in full medium and compared to cells cultivated overnight in serum-free medium. Autophagosome accumulation was analyzed by using the CYTO-ID Autophagy Detection Kit (Enzo, ENZ-51031) according to the manufacturer's instructions. Fluorescence was detected using a Varioscan Lux (Thermo scientific) microplate reader.

4.4.12 Colony Formation Assay and Cell Treatments

For the colony formation assay, $3x10^2$ *Kras* and *A5+/-; Kras* cells were plated in triplicates six-well plates and grown for 10d in culture media. Colonies were stained with 2% crystal violet (C3886; Sigma), washed with water, and their area was quantified using ImageJ. Treatments during the clonogenic assays include: 10% FCS-containing medium, serum-free HBSS-containing medium (Hanks´Balanced Salt Solution GIBCO-14025092, 1:20 dilution of normal medium), chloroquine in full medium (2μM and 6 μM, C6628 SIGMA), 6-Aminonicotinamide in full medium (10μM and SIGMA-A68203), Rotenone in full medium (15nM and SIGMA-R8875), Galactose and Glutamine in glucose free medium (Galactose 10mM and Glutamine 4mM, D-(+)-Galactose, SIGMA-G5388 and GlutaMAX-I, GIBCO-35050061, DMEM,

no glucose, GIBCO-11966-025), High Glucose in glucose free medium (25mM and GIBCO-A2494001).

4.4.13 Anoikis Assay

For the anoikis assay, 6-well plates were coated with poly-HEMA (20mg/ml) (P3932; Sigma) dissolved in 96% ethanol. $5x10^5$ *Kras* and *A5+/-; Kras* cells were seeded in triplicates and cultured for 48h in culture media. Surviving cells in the media were calculated using the neubauer counting chamber.

4.4.14 Boyden Chamber Migration and Invasion Assay

$1.5x10^5$ *Kras* and *A5+/-; Kras* cells were seeded in triplicates in 6-well plates till confluence. 100 µL serum free medium was added to upper chamber and 200 µL cells were added to chamber ($2,5x10^5$/mL in serum free medium). 750 µL full medium was added to lower chamber. Boyden-Chamber Assay plate was incubated at 37°C for 12-16 hours. After incubation, medium was removed from upper chamber and chambers were washed twice with PBS. Cells were fixed with formaldehyde (3,7% in PBS) for 2 minutes and washed with PBS twice. To permeabilize cells, 100% methanol was added to chambers for 20 minutes. After removing methanol chambers were washed twice with PBS. Chambers were place into wells and stained with Giemsa at room temperature for 15 minutes. After removing Giemsa solution, chambers were washed twice with PBS. Non-migrated cells were scraped off with cotton swabs from the membranes. Migrated cells were counted under a light microscope.

For invasion assay, 6.5mm Transwell (#CLS3464; Sigma, Corning Costar, USA) with 8.0 µm Pore polyester membrane insert was used in 24-well culture plates. The upper surface of the membrane was coated with 100ml mixed matrigel (corning Life Sciences) per well. The matrigel was incubated at 37°C for gelling. $5x10^4$ *Kras* and *A5+/-; Kras* cells were seeded in triplicates with 200µl serum-free DMEM in the upper chamber. The lower chamber was filled with 750 µl of culture media. After 48h, the cells were fixed by formaldehyde 3.7% in PBS, permeabilized with 100% methanol and stained with crystal violet. Cells that invaded to the lower surface area of the membrane were calculated by counting stained cells. E64d (100 µM and E3132-SIGMA) was used to inhibit cathepsin activity. Filopodia were quantified after 36h of seeding.

4.4.15 Cytokine Array

In order to detect cellular cytokine profile supernatants of *Kras* and *A5+/-; Kras* cells were collected and processed as described above for immunoblotting. Lysates were then used according to the manufacturer's instructions (Mouse Cytokine Array Panel A, Catalog Number ARY006, R&D Systems). Pixel intensity of individual plots was quantified using ImageJ software. The average of two spots corresponding to one cytokine was used to compare cytokine profile according to genotype.

4.4.16 Macrophage Differentiation Assay

To detect the effect of *Kras* and *A5+/-; Kras* cells on macrophage phenotype, *Kras* and *A5+/-; Kras* cells were seeded in 6-well plates and cultivated for 48h. Supernatants were collected and applied on Raw macrophages (RAW 264.7 (ATCC® TIB-71™) cultivated in Dulbecco's modified Eagle medium (DMEM) supplemented with 10%FBS (#10082147; Gibco), 1% PenStrep (#1500-063; Gibco), 1%NEAA (#11140050; Gibco). Macrophage phenotype was monitored and assessed by microscopy as described [123].

For Arginase-1 Immunofluorescence macrophages were treated as described above and subsequently stained with anti-Arginase 1 (1/500) (610708 BD Transduction Laboratories). Briefly, unspecific binding was blocked with 5% serum at RT and cells were incubated over night at 4°C with the primary antibody. At the following day secondary antibody anti-mouse in goat Alexa Fluor 488 (1/300) (A-11001 Invitrogen) was applied for 1h at RT. In the end, slides were covered with DAPI containing mounting medium (H-1200 Vector Laboratories) and analyzed with fluorescence microscopy (Zeiss Axiovert 200M).

4.4.17 Measurement of Cytoplasmic Ca^{2+} Response

To measure Ca^{2+} responses, *Kras* and *A5+/-; Kras* cells were loaded with Fluo-4 by incubation with Fluo-4/AM (5µM) for 60min at room temperature (approximately 23°C) in Na-Hepes-based solution (140mM NaCl, 4.7mM KCl, 1.13mM $MgCl_2$, 10mM HEPES, 10mM Glucose, 1.8mM $CaCl_2$, pH7.4). After that cells were washed by perfusion (gravity-based perfusion system) with the Na-Hepes-based solution and imaged every 2sec over a time period of 800sec using a Zeiss 510 confocal made (excitation 488nm, emission LP505). Heat Inactivated FBS (0.01% or 0.05% diluted

in the Na-Hepes-based solution) was applied when 200sec of recording were reached.

Fluorescent responses (F) were normalized to fluorescence F_0 recorded before the addition of FBS (average fluorescence value for measurements recorded during 190 - 200sec time interval). Amplitude of cytosolic Ca^{2+} responses was determined by the equation $((F_{max}-F_0)/F_0 = DF_{max}/F_0$, with F_{max} corresponding to the maximum Fluo-4 fluorescence measured during the 200-500sec interval. Amplitude of cytosolic Ca^{2+} responses of each single cell over 5min of FBS application was measured and the amplitudes were then averaged for each genotype (n > 170 cells for each genotype). Cells responding to FBS were defined as cells exciding 20% elevation threshold of normalized fluorescence (F/F_0) in the first 5min of FBS application.

4.4.18 Knockdown of mAtg5

Transfection of 293T cells for production of lentiviral particles

5 x 10^6 293T cells were seeded in 10 cm dishes. After one day, media was replaced and co-transfection of transfer plasmids purchased from Sigma Aldrich (TRCN0000327456 (54% knockdown, validated), TRCN0000327358 (58% knockdown, validated), TRCN0000363558 (81% knockdown, validated), TRCN0000375754 (86% knockdown, validated), and TRCN0000099432 (94% knockdown, validated)) with lentiviral packaging plasmids (pMD.GP, pRSV-rev, pMD.G) was performed using lipofectamine 2000 (Thermo Fisher Scientific). shRNA that does not target any known human or mouse gene (shNT) was used as a control. Two days later, lentiviral particles were harvested from the supernatant and frozen at -80°C.

Transduction of target cells with mATG5 knockdown constructs

Target *Kras* cells were seeded in 6 cm dishes. One day later, media was aspirated and 1 ml of lentiviral suspension was added to cells in presence of 8 µg/ml Polybrene (Sigma Aldrich). After 2 h at 37°C, 4 ml media was added. Selection of transduced cells was performed using 10 µg/ml puromycin.

Experimental analysis

Cells were tested in western blotting for Atg5, LC3, and β-Actin expression (as described below) and the knockdown percentage was confirmed. Cells with 54%, 58%, 81%, 86%, and 94% mAtg5-knockdown were further used in colony formation

(full medium, 10% FCS), Boyden Chamber migration, invasion, and tail vein injection experiments as described below. Experiments were performed in triplicates.

4.5 Non-targeted Metabolomics Profiling

LC-MS/MS–based non-targeted metabolomics analysis was conducted at the Genome Analysis Centre, Helmholtz Zentrum München as previously described [124]. About $1x10^6$ pancreatic cancer cells were required for the analysis. In brief, $0.375x10^6$ *Kras* or *A5+/-; Kras* cells were seeded in duplicates in a 6-well plate with 2 ml culture medium and grown for 48h until 80-90% confluent and an approximate number of $0.5x10^6$ was reached. Cells were washed two times with PBS (37°C). Dry ice cold 80% v/v methanol (400 ml) containing 4 recovery standard compounds to monitor extraction efficiency was added to the cells to cover them immediately. Cells were scraped and the cell suspension was transferred into precooled (dry ice) 2 ml screw cap micro tubes (Sarstedt Micro tube 2 ml, PP (Reference #: 72.694.005)) filled with 160 mg glass beads. Another 100 ml of dry ice cold methanol extraction solvent to wash the well was added and transferred to the micro tube. Suspensions of two 6-wells were pooled into one tube to obtain a sample of $1x10^6$ cells in 1 ml cell suspension. The samples were stored immediately at -80°C until metabolomic analysis was performed. The metabolites were assigned to cellular pathways based on PubChem, KEGG, and the Human Metabolome Database. Metabolic pathways were described as significantly up- or down-regulated, when metabolites assigned to those specific pathways were increased or decreased, respectively.
Data was obtained at the Institute of Experimental Genetics and at the Institute of Bioinformatics and Systems Biology, Helmholtz Zentrum Munich, Germany, in the in the lab of Prof. Jerzy Adamski with the help of Dr. Anna Artati and in the lab of Dr. Werner Roemisch-Margl respectively.

4.6 Statistics

Data are displayed as averages ± standard deviations (SD). Parameters for the groups were compared by Mann-Whitney test or two-sided Student's t-tests as appropriate and statistical significance was set at $*P<0.05$, $**P<0.01$, $***P<0.001$. The statistical software Prism 5 (GraphPad Software, Inc.) was used for analysis.
The oncomine database (www.oncomine.org) was used to search for autophagy and

lysosomal function-associated genes. GO Biological Process-Autophagy or GO Cellular Component-Lysosome was used as concept; primary filters selected were Cancer versus Normal Analysis and Pancreatic Cancer; pathology subtypes M1+, N1+, T4 according to TNM-staging were subsequently applied. DNA Copy Number (log2 copy number units) retrieved from the Cancer Genome Atlas (TCGA Research Network, http://cancergenome.nih.gov/) was used to illustrate copy number gain or loss in human pancreatic cancer samples versus normal pancreas samples.

5 RESULTS

5.1 Autophagy in the pancreatic cancer

5.1.1 Autophagy is induced during pancreatic tumorigenesis.

Autophagic induction has an inevitable role for pancreatic cancer growth[60]. In order to demonstrate that autophagy occurs during pancreatic carcinogenesis, we have visualized autophagy as GFP-LC3 positive autophagosomes using GFP-LC3 transgenic mice (Figure 2A). Under normal fed conditions, GFP-LC3 signals were visible in acinar cells. During pancreatic carcinogenesis, autophagosomes were distinguishable in pre-malignant acinar-to-ductal metaplasias (ADM), pancreatic intraepithelial neoplasias (PanIN), in conjunction with in fully developed pancreatic tumors and metastasis (liver) of *GFP-LC3; Kras* mice. PanIN-adjacent normal acinar cells were deficient in GFP-LC3-positive puncta, in spite of harboring the oncogenic *Kras*^{G12D} mutation(white star, Figure 2A).

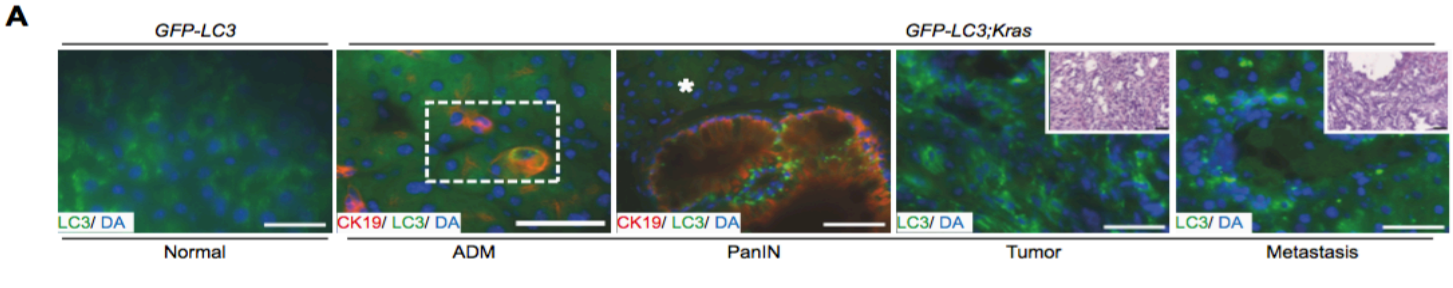

Figure 2: Autophagy is detectable and inducible in the pancreas. (**A**) Autophagy in the pancreas of GFP-LC3 transgenic mice under normal conditions and during PDAC progression in *GFP-LC3;Kras* mice. Tumor and liver metastasis are shown; white square/ white asterisk indicate ADM/ PanIN-adjacent acinar cells (DA=DAPI) **(B)** GFP-LC3 and CK19 immunofluorescence of *A5;Kras* mice expressing transgenic GFP- LC3; white arrowhead indicates diffuse GFP-LC3 staining; nuclei are detected with DAPI. Scale bars equal 50µm.

Thus, autophagy was not detectable in *A5;Kras* as it is in *GFP-LC3; Kras* mice (Figure 2B). LC3 signals were observed as diffuse staining. Therefore, autophagy is occurring in each stage of pancreatic tumor formation and metastasis.

5.1.2 Allelic dosage of Atg5 influences pancreatic tumorigenesis.

To interpret the role of autophagy during PDAC, we have generated mice with homozygous (*A5;Kras*) and heterozygous (*A5+/-;Kras*) deletion of Atg5 and compared them to autophagy competent *Kras* mice. As already shown [63,64], total loss Atg5 hastens tumor initiation by significantly augmenting ADM (Figure 3A, C) and increasing pancreas/body weight index at 4-weeks of age (Figure 3B); nevertheless, *A5;Kras* mice only progress to PanIN-1 at 9-weeks of age (Figure 3C, D) and do not advance more malignant steps of this disease (Figure 3D).

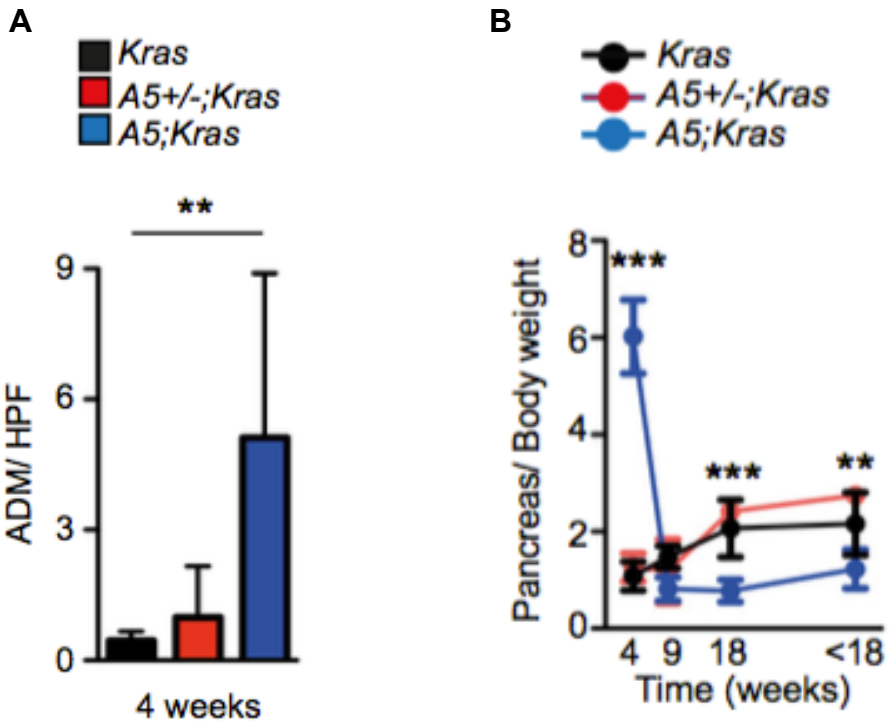

C

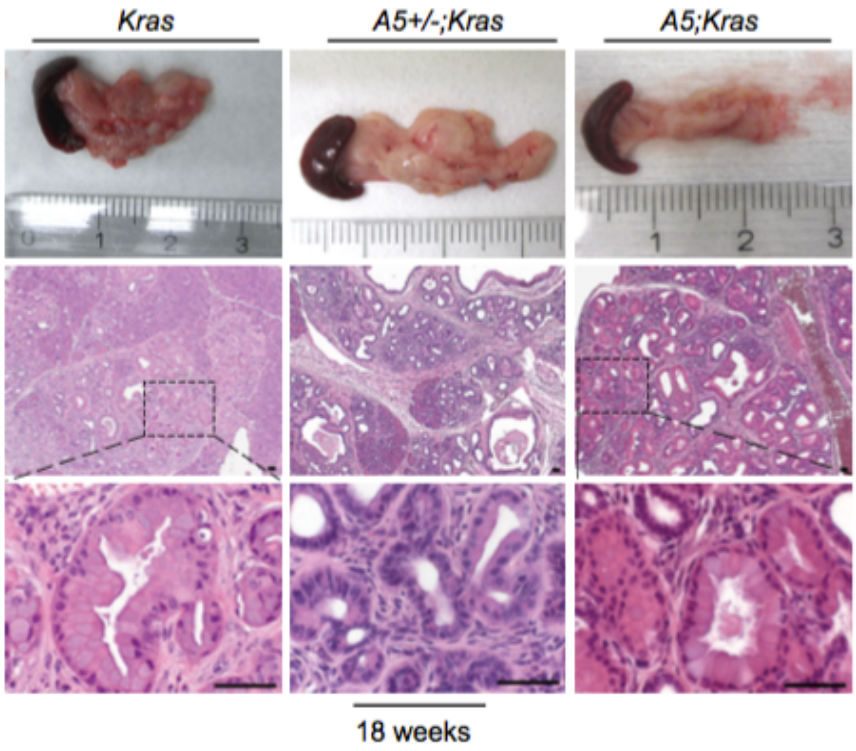
Kras
A5+/-;Kras
A5;Kras
18 weeks

D

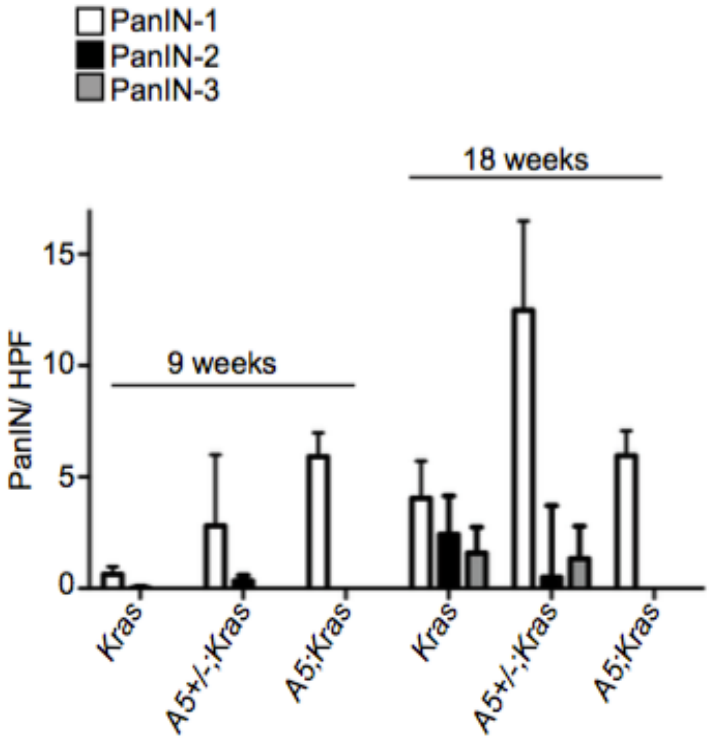
PanIN-1
PanIN-2
PanIN-3
18 weeks
9 weeks
PanIN/ HPF
15
10
5
0
Kras
A5+/-;Kras
A5;Kras
Kras
A5+/-;Kras
A5;Kras

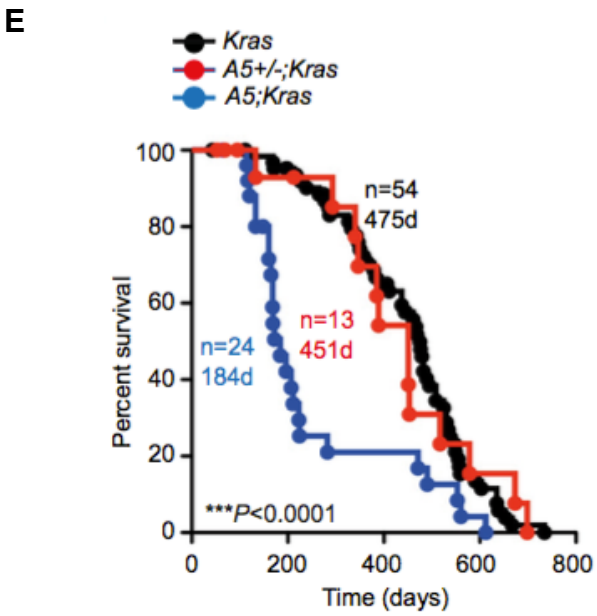

Figure 3: Atg5 allelic status influences tumor progression. (**A**) Quantification of Acinar-to-Ductal Metaplasia (ADM) per High Power Field (HPF) in 4-week old *Kras, A5+/-;Kras, A5;Kras* mice (n≥4). **(B)** Pancreas/Body weight ratio in 4-/9-/18/ and more than 18-week old *Kras, A5+/-;Kras, and A5;Kras* mice (n≥3). **(C)** Macroscopic and microscopic appearance of pancreata from 18-week old Atg5 deficient (*A5;Kras*) and Atg5 heterozygous mice (*A5+/-;Kras*) compared to 18-week old Atg5 proficient mice (*Kras*); oncogenic Kras is expressed in all groups of mice. **(D)** Quantification of PanIN-1/-2/-3 per High Power Field (HPF) in 9-/ 18-week old *Kras, A5+/-;Kras*, and *A5;Kras* mice (n≥3). **(E)** Kaplan-Meier survival curve of *Kras* (n=54), *A5+/-;Kras* (n=13), and *A5;Kras* (n=24) mice (Median survival 475, 451, 184 days respectively; ****P<0.0001* comparing *Kras* and *A5;Kras*). Mean±SD, **P<0.05, **P<0.01, ***P<0.001*. Scale bars equal 50µm.

In genuinely, A5;Kras mice have decreased survival (Figure 3E) affiliated with severe pancreatic degeneration as shown by a certainly lower relative pancreatic weight starting at 18 weeks of age (Figure 3B). *A5+/-;Kras* mice (Table 13) did not distinct in ADM/ PanIN formation, pancreas/ body weight ration or survival compared to *Kras* mice (Figure 3A, B, C, D, E).

5.1.3 Allelic dosage of Atg5 do not change chronic pancreatitis induced pancreatic cancer progression.

To analyze the possibility of tumor development in *Atg5*-deficient mice expressing mutant *Kras* and chronic pancreatitis induced pancreatic carcinogenesis, chronic cerulean injections were performed into *A5;Kras*, *A5+/-;Kras*, and *Kras* mice to mimic chronic pancreatitis-mediated promotion of PDAC. Measurement of serum amylase

and lipase levels were used to determine pancreatic tissue damage and pancreatitis responses. Amylase and Lipase (U/dL) levels were not different in between the groups (Figure 4A). Tumor progression in each group was quantified by counting ADM and PanIN structures in H&E tissue slides of *Kras*, *A5+/-;Kras*, and *A5;Kras* mice (Figure 4B). Notably, ADM and PanIN formation were not different in between the genotypes. Accordingly, chronic pancreatitis does not contribute to tumor progression in *A5;Kras* mice.

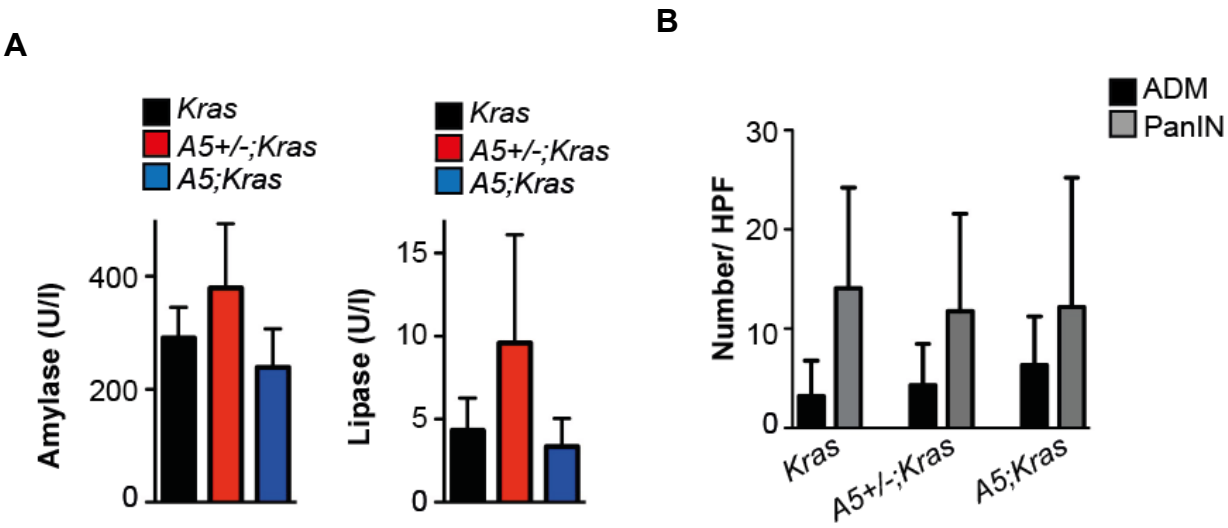

Figure 4: Chronic pancreatitis induced tumorigenesis is not changed by the levels of Atg5. (A) Serum Amylase (left) and Lipase (right) levels (U/dl), measured in *Kras*, *A5+/-;Kras*, and *A5;Kras* mice one month after last cerulein injection (n>3). **(B)** Quantification of Acinar-to-Ductal Metaplasia (ADM) and Pancreatic Intraepithelial Neoplasia (PanIN) per High Power Filed (HPF) based on H&E of *Kras*, *A5+/-;Kras*, and *A5;Kras* mice one month after last cerulein injection (n>3). Mean±SD

5.1.4 Monoallelic loss of Atg5 alters tumor incidence and metastatic load.

Monoallelic loss of *Atg5* significantly boosted tumor and metastasis incidence, determined at the time of sacrifice, in comparison with autophagy competent and autophagy impaired genotypes (Figure 5A, B, C). As depicted in Figure 5A, primary tumors developed in *A5+/-;Kras* mice were characterized by a high level of histologic malignancy; concurrent with multiple metastatic foci in target tissues (Table 13). This observed phenotype was not present in autophagy proficient *Kras* mice. Consequently, monoallelic and not biallelic loss of Atg5 gravely determines pancreatic tumor initiation, progression, and metastasis.

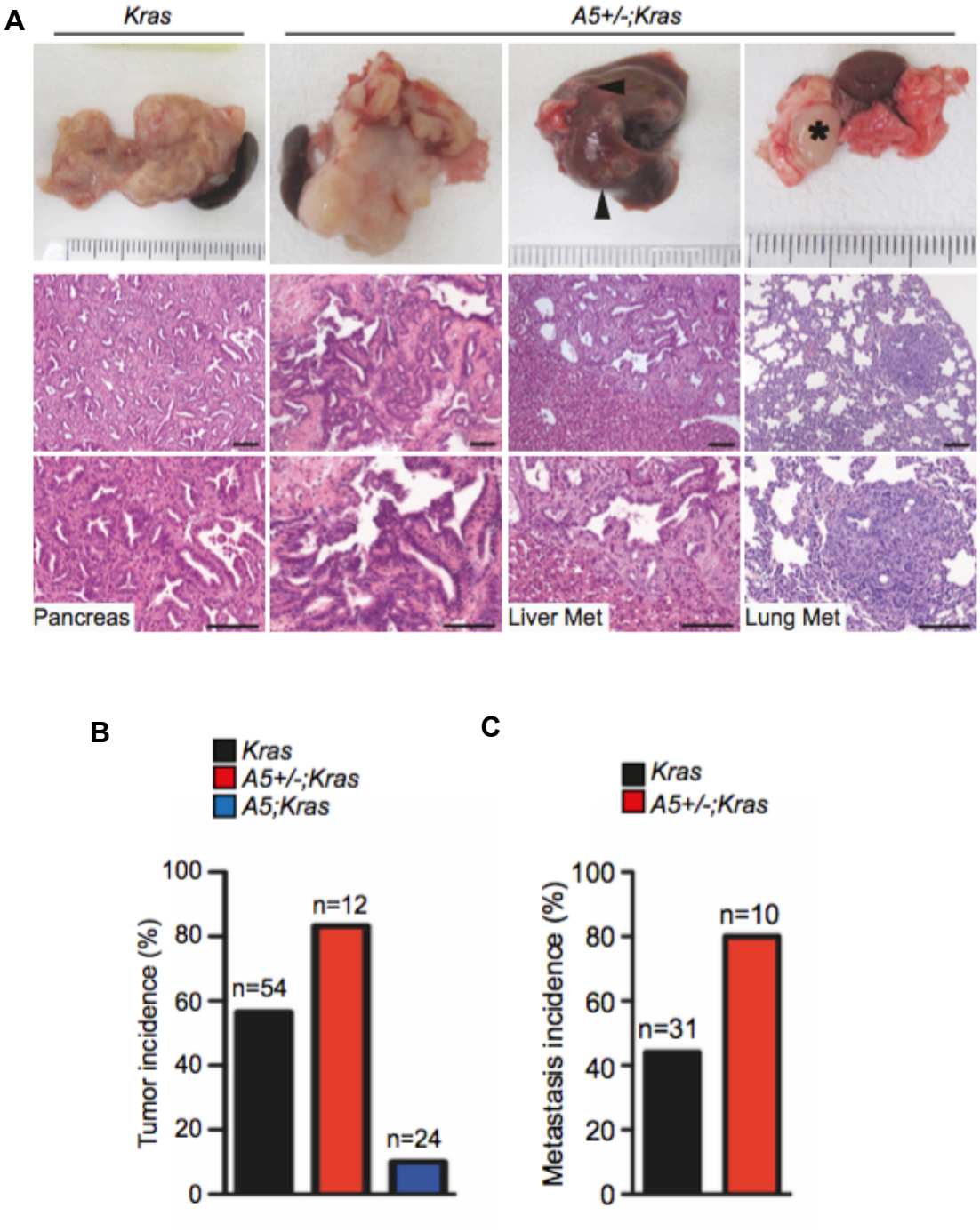

Figure 5: Monoallelic loss of Atg5 alters tumor incidence and metastatic load. **(A)** Representative pictures of pancreatic, liver, and lung tumors from *Kras* and *A5+/-;Kras* mice; black arrowheads/ asterisk point to metastatic focus in liver/ lung respectively. **(B)** Tumor incidence (%) in *Kras* (n=54), *A5+/-;Kras* (n=12), and *A5;Kras* (n=24) mice. **(C)** Metastasis incidence (%) in *Kras* (n=31) and *A5+/-;Kras* (n=10) mice. Scale bars equal 50µm.

5.1.5 Monoallelic loss of Atg5 does not change autophagic flux *in vivo* and *in vitro*.

The effect of monoallelic Atg5-loss on autophagy is analyzed *in vivo* and *in vitro*. Relative levels of autophagy in the original primary tumors were analyzed via Atg5, p62, LC3 immunohistochemistry. These autophagic targets were analyzed in pre-malignant and malignant *Kras* and *A5+/-;Kras* tissues. There was no difference between p62 and LC3 levels(Figure 6A, B). Essentially, reduction in Atg5 protein was obvious in *A5+/-;Kras* primary tumors and *A5+/-;Kras* cells (Figure 7A). Atg5 was also expressed in pre-malignant structures in *Kras* and *A5+/-;Kras* mice. p62 was only slightly expressed in cells of the tumor microenvironment (Figure 6A, B).
Morphology and proliferation of cancer cells were not affected by Atg5 levels (Figure 7B). Interestingly nevertheless, while autophagic flux was not different between *Kras* and *A5+/-;Kras* in vitro and in vivo (Figure 7A, B), autophagy regulation after treatment with autophagy inducers and inhibitors were altered (Figure 7C). Particularly, starvation with HBSS functionally altered Kras cells by significantly lowering colony numbers compared to 10% FCS-containing medium (Figure 7E). Colony formation in *A5+/-;Kras* cells was not compromised (Figure 7E). FCS-starvation caused an accumulation of LC3-II, which was indeed more apparent in *Kras* versus *A5+/-;Kras* cells after co-treatment with chloroquine (Figure 7C). Autophagic flux inhibition was justified by elevated p62 protein levels in both cell types, especially notwithstanding in *Kras* cells after co-treatment with chloroquine. AMPKalpha phosphorylation was lightly elevated in *A5+/-;Kras* cells, indicating that AMPKalpha endures sensitive to starvation in *A5+/-;Kras* cells (Figure 7C). Further, increasing chloroquine treatment significantly altered colony formation only in *Kras* cells (Figure 7D). Beyond any doubt, Cyto-ID-mediated quantification of autophagosomes after FCS- starvation depicted an increase in autophagosome numbers only in *Kras* cells, not in *A5+/-;Kras* cells (Figure 7F).

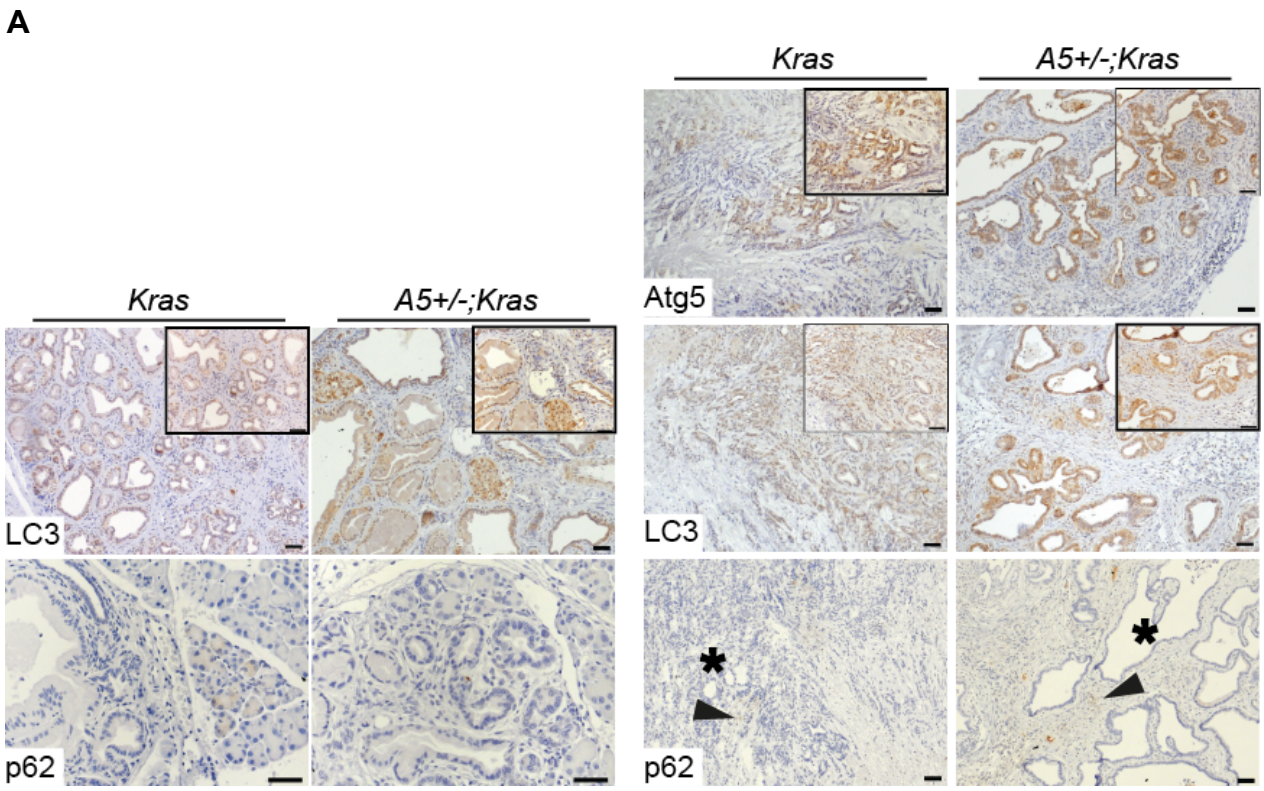

Figure 6: Monoallelic loss of Atg5 do not change autophagic flux in pre-malignant and malignant structures in the primary tumors. (A) Representative immunohistochemistry of Atg5, LC3, and p62 in *Kras* and *A5+/-;Kras* mice; on the left pre-malignant structures are highlighted whereas on the right more malignant structures and tumor lesions are shown. Asterisks highlight tumor structures and arrowheads tumor microenvironment (previous page). **(B)** Scoring (score 1 (faint) - score 3 (strong)) of Atg5, LC3, and p62 in *Kras* and *A5+/-;Kras* mouse tumors. Mean±SD, **P<0.05, ***P<0.001*. Scale bars equal 50µm

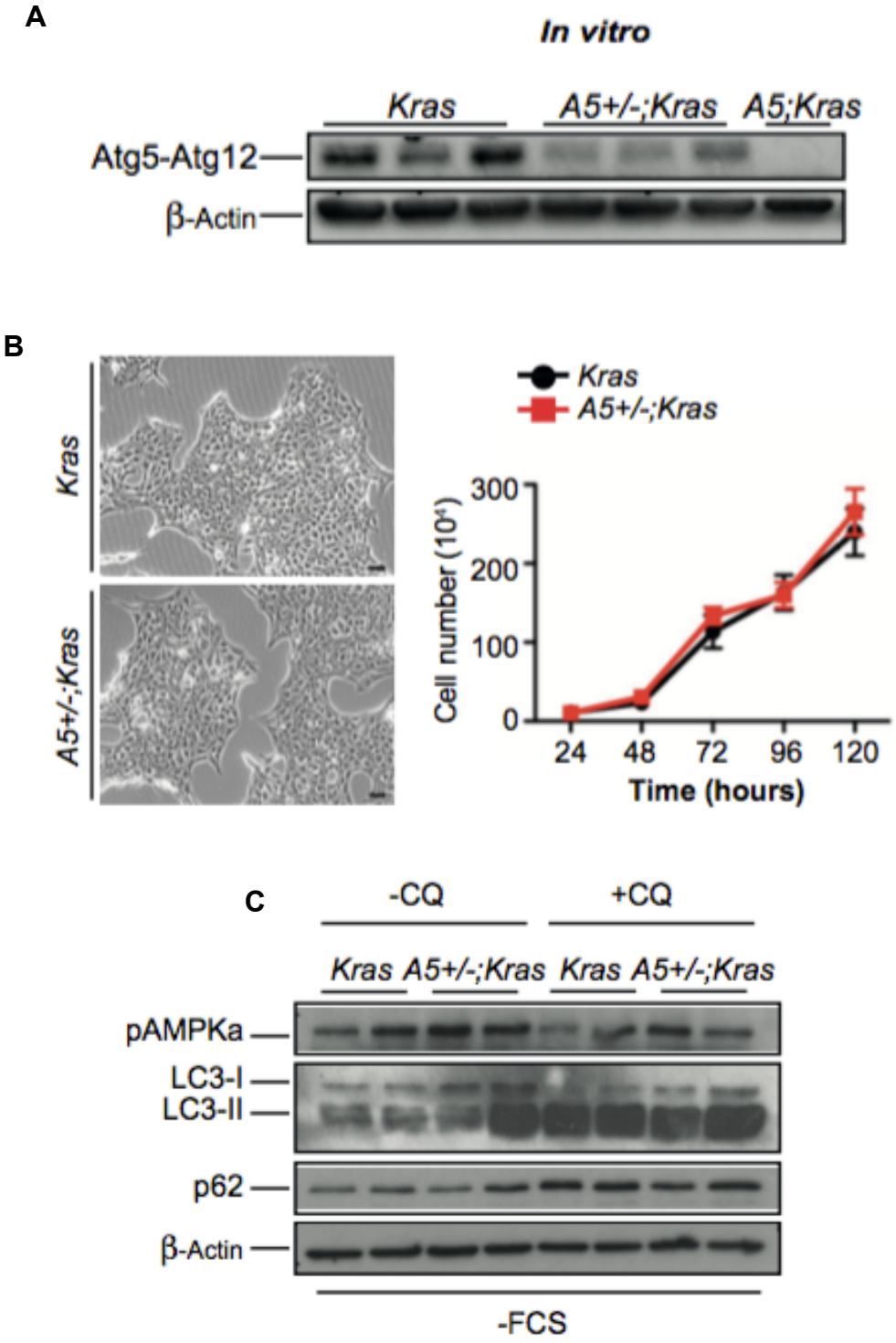
A
In vitro
Kras
A5+/-;Kras
A5;Kras
Atg5-Atg12
β-Actin
B
Kras
A5+/-;Kras
Kras
A5+/-;Kras
Cell number (10⁴)
300
200
100
0
24
48
72
96
120
Time (hours)
C
-CQ
+CQ
Kras
A5+/-;Kras
Kras
A5+/-;Kras
pAMPKa
LC3-I
LC3-II
p62
β-Actin
-FCS

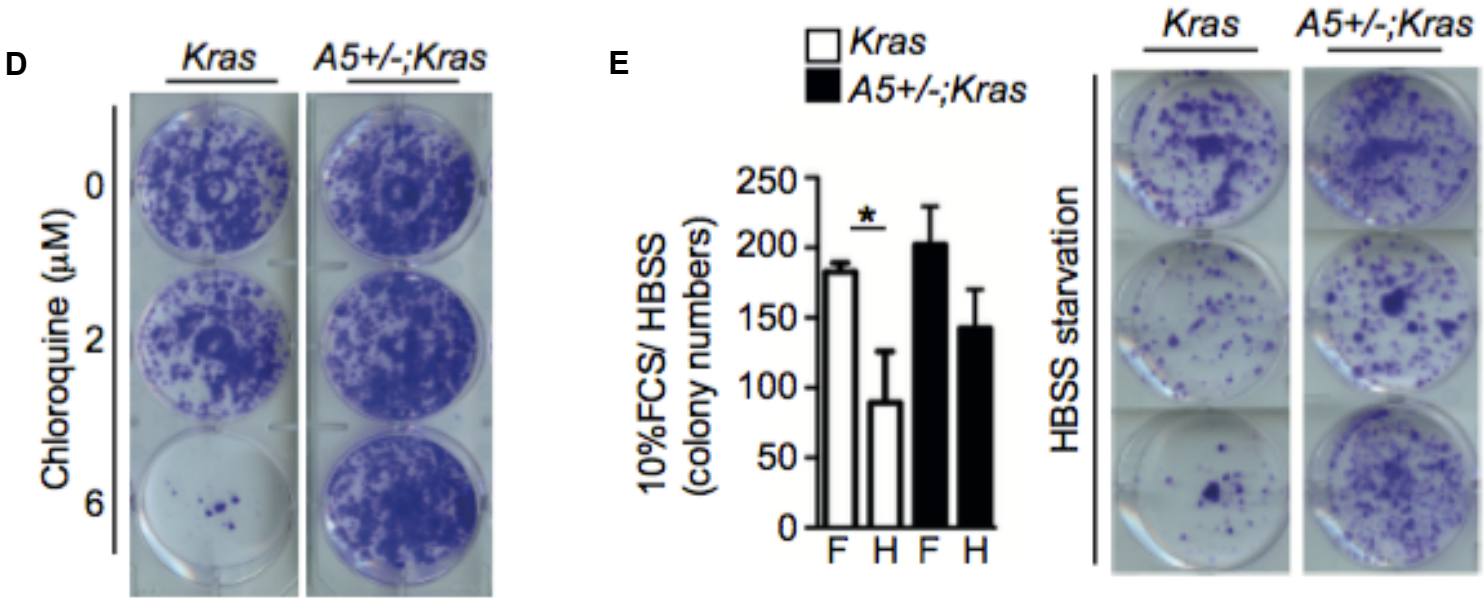

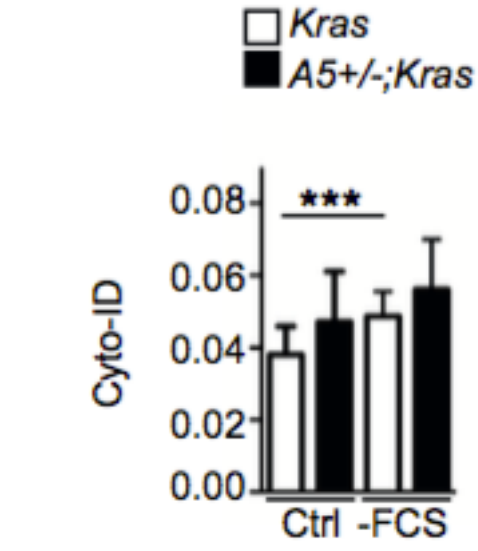

Figure 7: Monoallelic loss of Atg5 do not influence autophagic flux in cancer cells. (A) Atg5-detection in primary pancreatic tumor cells isolated from Kras, *A5+/-;Kras*, and *A5;Kras* mice. (**B)** Morphology of *A5+/-;Kras* and *Kras* cells (left); *Kras* and *A5+/-;Kras* proliferation curve showing cell number x 10^4 versus time (hours) after seeding (n=3) (right). **(C)** Phospho-AMPKa, LC3-I/ LC3-II, and p62 expression in Kras and A5+/- ;Kras cells, after FCS-starvation, with/ without chloroquine treatment (CQ) **(D)** Representative picture of colony formation capacity in *Kras* and *A5+/-;Kras* cells after CQ- treatment. **(E)** HBSS-starvation (n=3) (left); representative picture of colony formation capacity in *Kras* and *A5+/-;Kras* cells after HBSS-starvation (right). **(F)**Cyto-ID fluorescence in *Kras* and *A5+/-;Kras* cells after cultivation in medium with/ without FCS (n>3). Mean±SD, **P<0.05, ***P<0.001*.

Additionaly, treatment of *Kras* and *A5+/-;Kras* cells with various metabolic regulators (10% FCS, 6- AA, rotenone, galactose/ glutamine, high glucose) did not differentially affect the colony forming capacities of *Kras* and *A5+/-Kras* cells (Figure 8A, B, C, D, E).

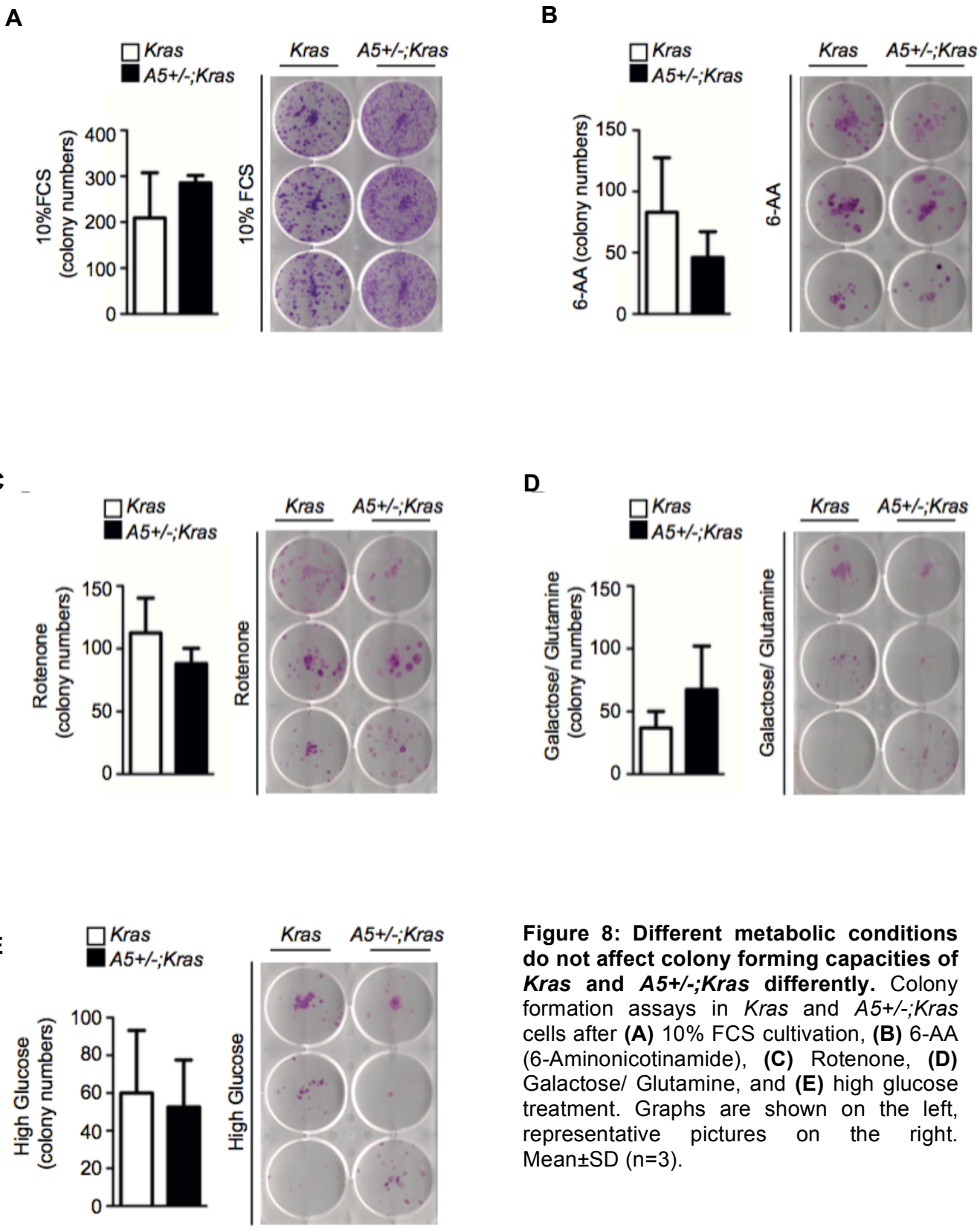

Figure 8: Different metabolic conditions do not affect colony forming capacities of *Kras* and *A5+/-;Kras* differently. Colony formation assays in *Kras* and *A5+/-;Kras* cells after **(A)** 10% FCS cultivation, **(B)** 6-AA (6-Aminonicotinamide), **(C)** Rotenone, **(D)** Galactose/ Glutamine, and **(E)** high glucose treatment. Graphs are shown on the left, representative pictures on the right. Mean±SD (n=3).

5.1.6 Monoallelic loss of Atg5 does not change basal canonical, non-canonical, selective autophagy regulator pathways in pancreatic cancer cells.

As it is mentioned before, monoallelic loss of Atg5 does not alter autophagic flux in pancreatic cancer cells. But cancer cells might also use multiple cellular processes like non-canonical, selective autophagy. Therefore, several markers were analyzed in both genotypes. To check autophagy dependence on mTOR regulation and metabolic regulation of autophagy, mTOR, AMPK and pS6 levels were analyzed and no significant difference was observed between the genotypes (Figure 9A).

Detection Ulk1-complex via pUlk1, Ulk1, Atg13, FIP200 western blot showed no difference between the genotypes (Figure 9B). Class III PI3K-complex regulator Beclin-1 was not different neither (Figure 9C). Main regulators of non-canonical autophagy, Atg16L1, Atg101, Lamp2a, Rab9, were not differently expressed (Figure 9D). As a ER-phagy selective autophagy regulator, no difference could be detected in CCPG1 levels (Figure 9E) [125]. Thus, monoallelic loss of Atg5 does not change autophagy related regulators in pancreatic cancer cells.

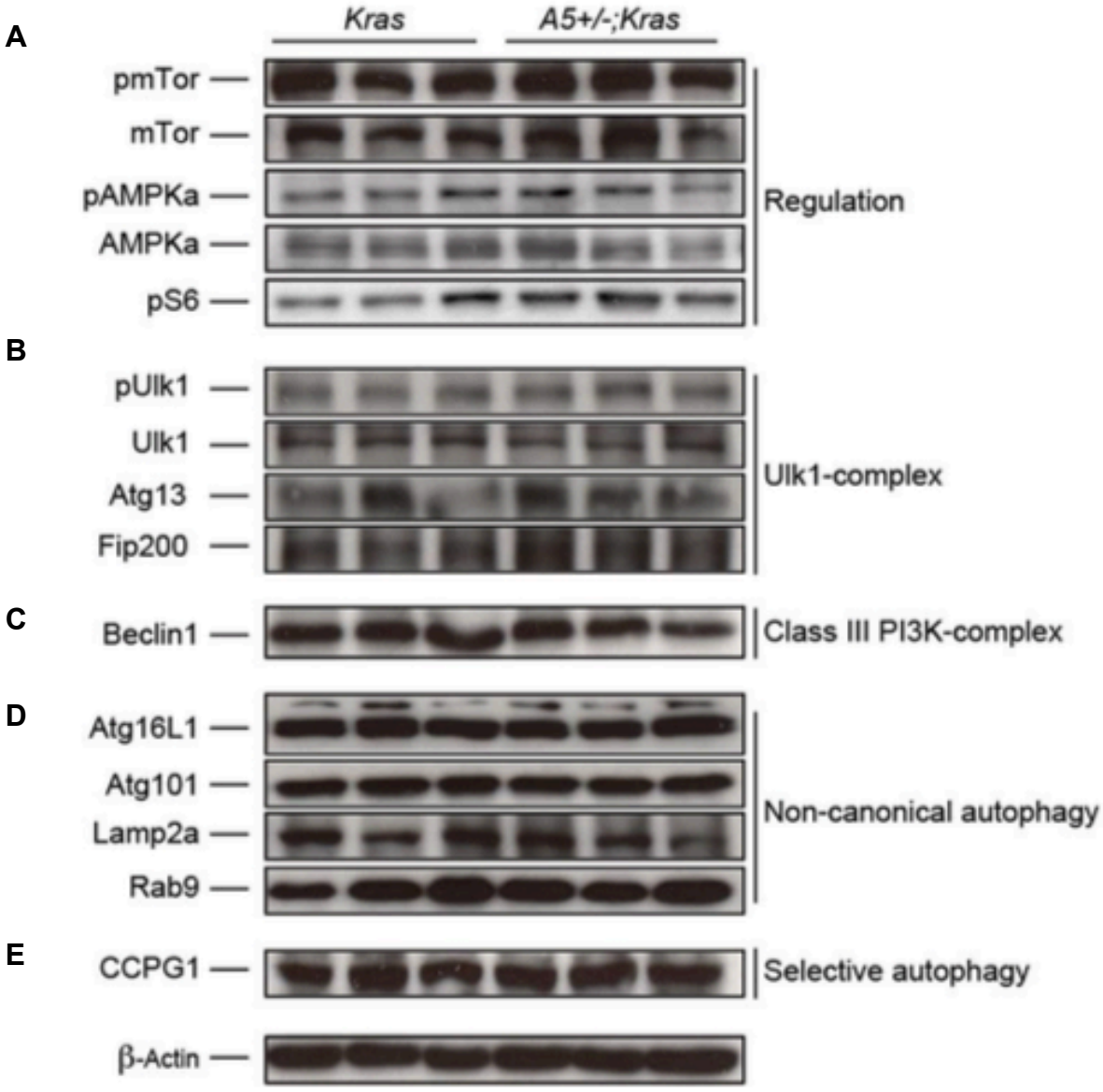

Figure 9: Monoallelic loss of Atg5 does not change basal canonical, non-canonical, selective autophagy regulator pathways in pancreatic cancer cells. Western blot detection of **(A)** autophagy regulation (pmTOR/ mTor, pAMPKa/ AMPKa, pS6), **(B)** Ulk1-complex (pUlk1/ Ulk1, Atg13, Fip200), **(C)** Class III PI3K-complex (Beclin1), **(D)** non-canonical autophagy (Atg16L1, Atg101, Lamp2a, Rab9), **(E)** selective autophagy of the endoplasmic reticulum (CCPG1). (previous page)

5.2 Role of Atg5 in Metastatic Properties of Cancer Cells

5.2.1 Monoallelic loss of Atg5 increases metastatic features *in vitro*.

During the time that *A5+/-;Kras* mice had more advanced tumor and metastasis incidence, Atg5-monoallelic loss on cancer cells was analyzed in terms of migratory and invasive potential of pancreatic cancer cells. Before checking their migratory and invasive capacity, anoikis resistance was analyzed to show their survival capacity after extracellular detachment. In vitro experiments with *Kras* and *A5+/-;Kras* cells revealed unquestionably boosted anoikis resistance (Figure 10A), migration, invasion (Figure 10B) and cell spreading in *A5+/-;Kras* cells (Figure 10C). All of these features shape metastatic capacities of cancer cells. Filopodia formation, a sign of cellular migration and spreading, was additionally clearly distinguishable in *A5+/-;Kras* cells while Kras cells present only small protrusions (Figure 10C).

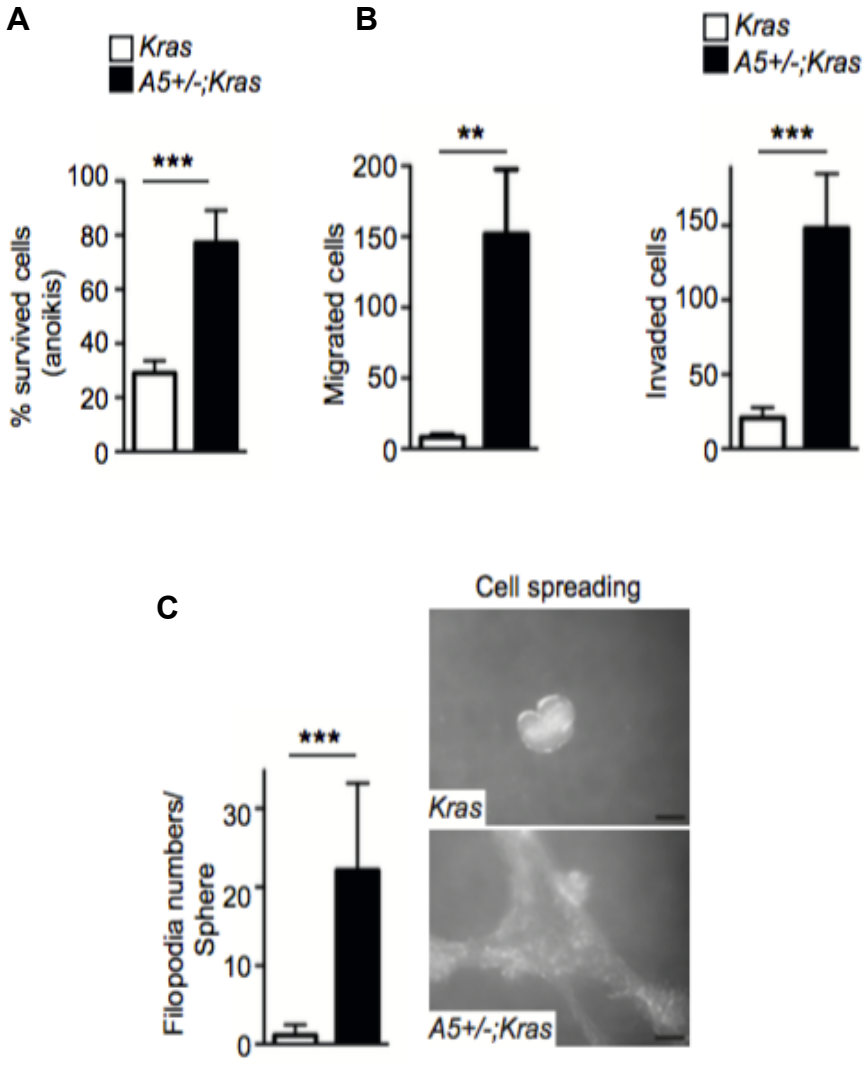

Figure 10: Monoallelic loss of Atg5 increases anoikis resistance, migration and invasion *in vitro*. (A) Anoikis assay with *Kras* and *A5+/-;Kras* cells (%). **(B)** Quantification of migration (left), invasion (right) **(C)** Filopodia numbers/ sphere with representative picture of cell spreading/ filopodia formation in *Kras* and *A5+/-;Kras* cells. Mean±SD (n>3), ****P<0.001, **P<0.01*. Scale bars equal 50µm. (previous page)

5.2.2 Monoallelic loss of Atg5 increases metastatic features *in vivo*.

Tumor formation after orthotopic transplantation was similar in *Kras* and *A5+/-;Kras* cell lines, with both cell lines forming CK19-positive ductal tumors, morphologically resembling primary tumors (Figure 12). Nevertheless, metastasis incidence (%) after orthotopic transplantation was significantly increased in *A5+/-;Kras* cells, with cells metastasizing to sites including lymph nodes, liver, lung, and spleen (Figure 11). In a second model for comparison of metastatic capacities, undoubtedly more lung tumors (%) were developed after tail vein injection of wild-type mice with *A5+/-;Kras* versus *Kras* cells (Figure 13A). Moreover to lung metastasis, some mice displayed liver and spleen metastasis, signifying higher aggressiveness of pancreatic tumor cells after losing one allele of Atg5 (Figure 13B). Re-isolation of *A5+/-;Kras* cancer cells from lung metastasis depicted more proliferative capacity compared to *Kras* cells (Figure 13B).

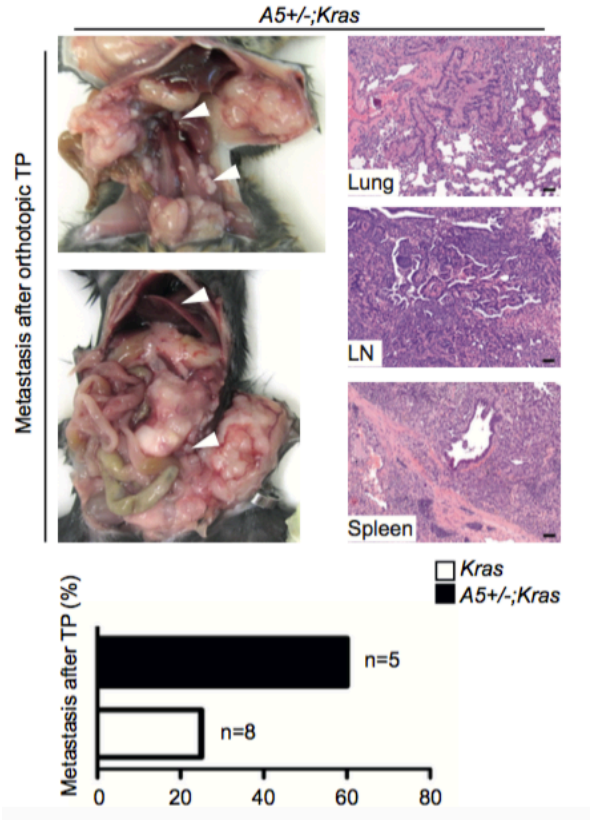

Figure 11: Monoallelic loss of Atg5 increases metastasis after orthotopic transplantation. Representative macroscopic and microscopic pictures of metastasis (lung, LN=lymph node, spleen) after TP of *A5+/-;Kras* cells into wildtype mice; white arrowheads indicate metastasis (top); metastasis incidence (%) after TP of *Kras* and *A5+/-;Kras* cells (n≥5) (bottom). Scale bars equal 50µm.

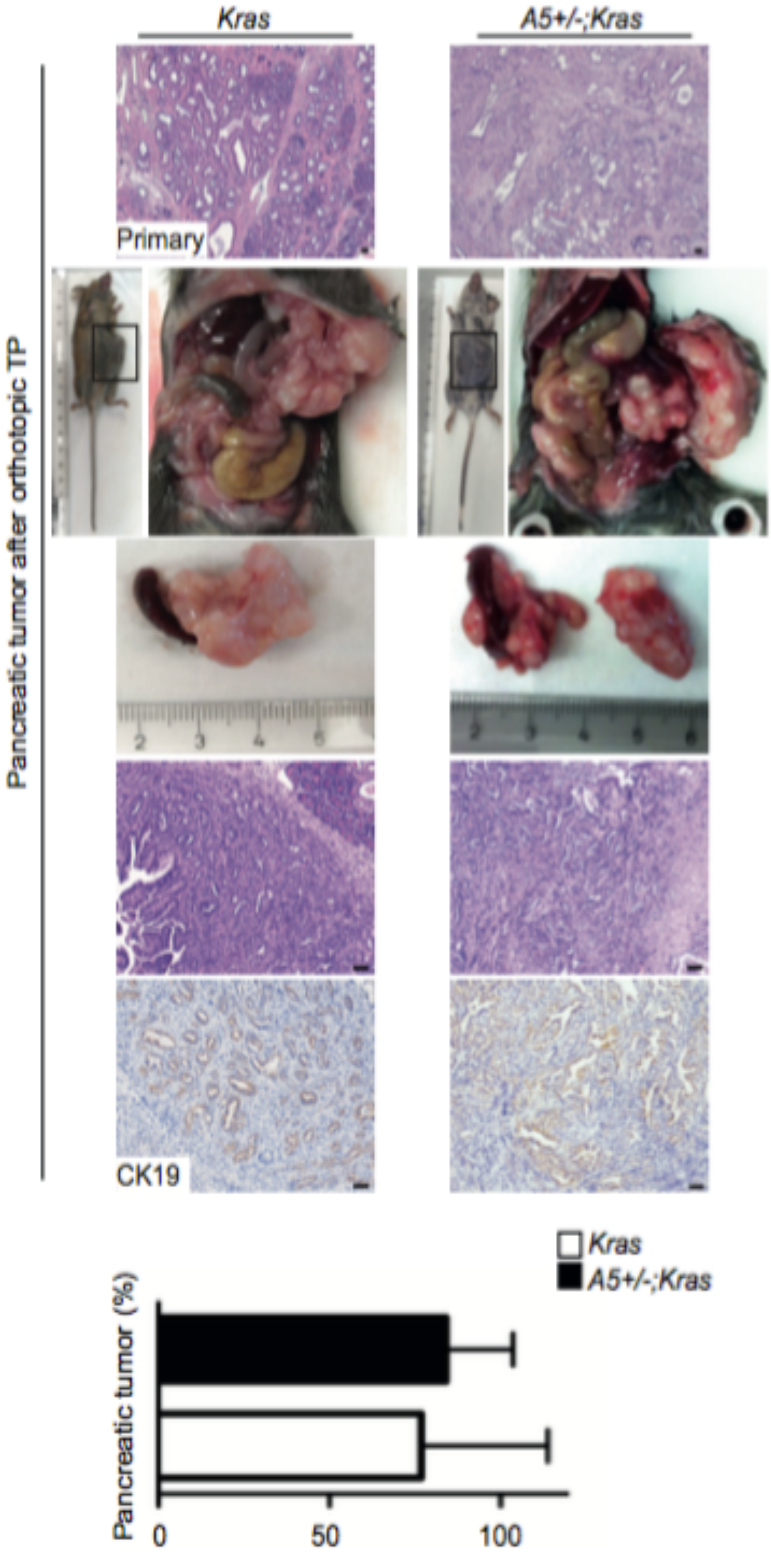

Figure 12: Monoallelic loss of Atg5 does not alter tumor growth after orthotopic transplantation. Representative macroscopic and microscopic pictures of pancreatic tumors from wildtype mice after orthotopic transplantation (TP) of *Kras* and *A5+/-;Kras* cells; primary tumors are shown on the top, tumors formed after transplantation in the fourth picture from the top, and CK19 immunohistochemistry on the bottom; Quantification of primary pancreatic tumor burden in mice after orthotopic transplantation of *Kras* and *A5;Kras* cell lines (% area of tumor tissue, n>3) (bottom). Scale bars equal 50µm.

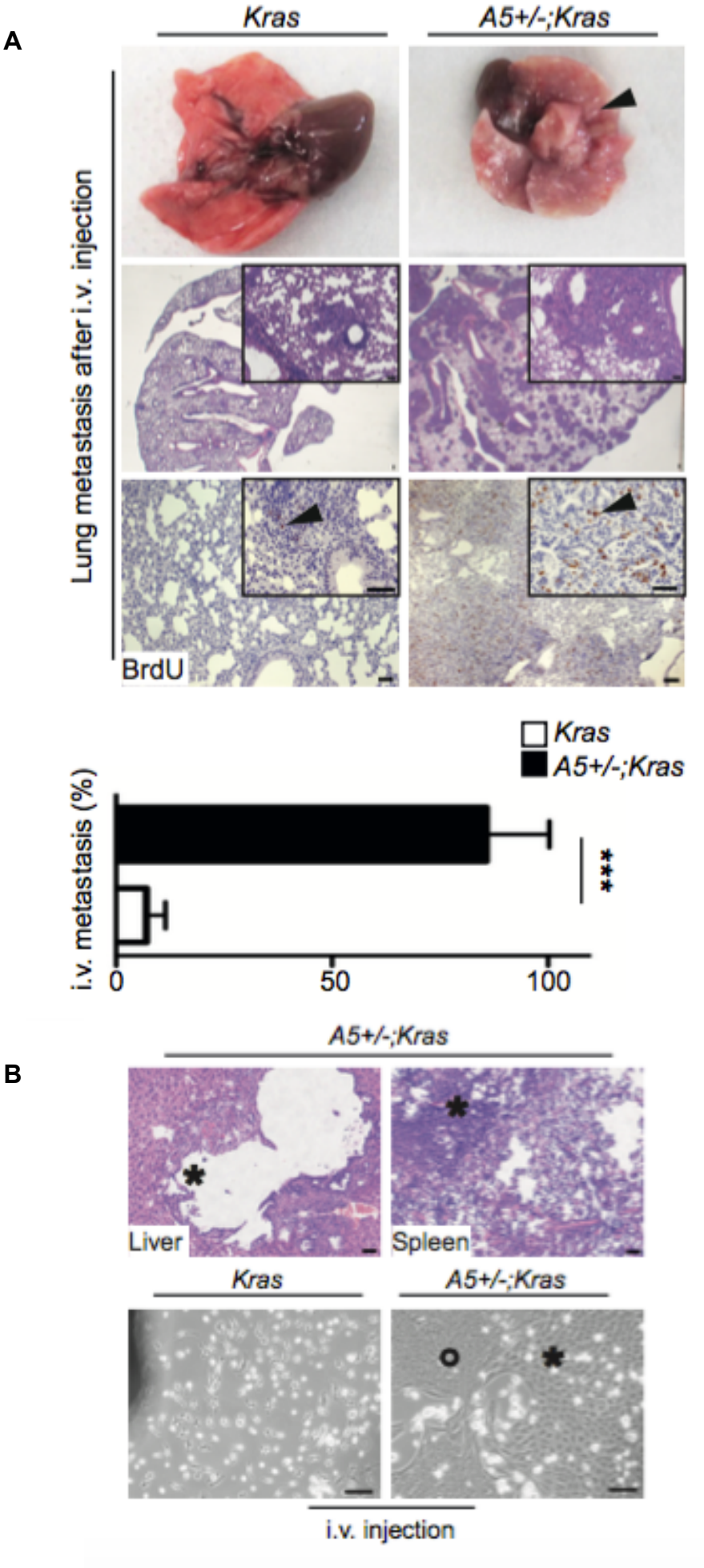
A
Kras
A5+/-;Kras
Lung metastasis after i.v. injection
BrdU
Kras
A5+/-;Kras
i.v. metastasis (%)
***
0
50
100
B
A5+/-;Kras
Liver
Spleen
Kras
A5+/-;Kras
i.v. injection

Figure 13: Monoallelic loss of Atg5 augments metastasis after intra-tail vein injection. (A) Lung tumors after tail vein injection (i.v.) of *Kras* and *A5+/-;Kras* cells; black arrowheads indicate tumors or BrdU- positive cells (top); quantification of lung metastasis (% area) after i.v. of *Kras* and *A5+/-;Kras* cells (n=6) (bottom). **(B)** H&E picture of liver and spleen metastasis after i.v. of *A5+/-;Kras* cells; asterisks indicate metastasis (top); representative bright field pictures of *Kras* and *A5+/-;Kras* cells isolated from the lung of wildtype mice after i.v.; asterisk and circle indicate two different cell populations (bottom). Mean±SD (n>3), ****P<0.001, **P<0.01*. Scale bars equal 50µm. (previous page)

5.2.3 Downregulation of Atg5 increases metastatic features *in vivo* and *in vitro*.

To exemplify the corporation between *Atg5* expression levels in PDAC-malignancy, *Atg5* was knocked down in *Kras* cell lines using shRNAs with various knockdown efficiencies (54%, 58%, 81%, 86%, and 94%). All shRNAs were able to affect *Atg5* expression levels with the above-mentioned efficiency at the mRNA (Figure 14) and protein level (Figure 15). As 58% *Atg5* knock down represents the situation after monoallelic loss of *Atg5*, these cells were used for further experiments. 94% *Atg5* downregulation having cells were also used to represent another dosage of *Atg5* in these experiments. Principally, knock down of *Atg5* by 58% or 94% significantly augmented migration and invasion *in vitro* (Figure 16A) along with lung metastasis (Figure 16B) *in vivo*. Downregulation of Atg5 did not influence colony forming capacities of *Kras* cells (Figure 15B). On the other hand downregulation of Atg5 in different dosages did not alter basal autophagic flux determined by *LC3* levels in western blot (Figure 15A).

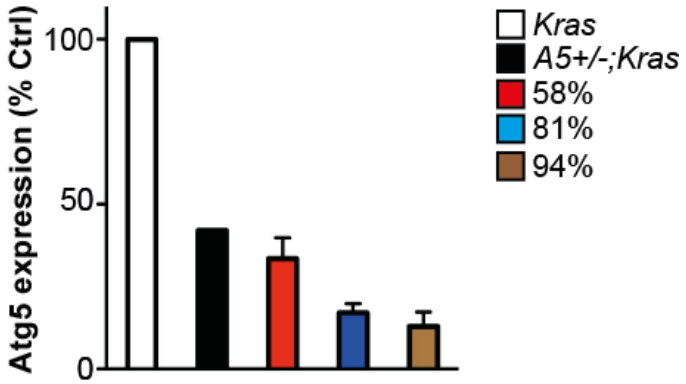

Figure 14: qRT-PCR of *Atg5* normalized to *cyclophilin*. Depicted are *Kras* cell lines transfected with shRNA against *Atg5*. The percentages refer to the percentage of knockdown efficiency for each shRNA (58%, 81%, 94%). The y-axis shows % *Atg5*-mRNA detected in comparison to *Kras* control cell lines (set to 100%) (n=2). Mean±SD.

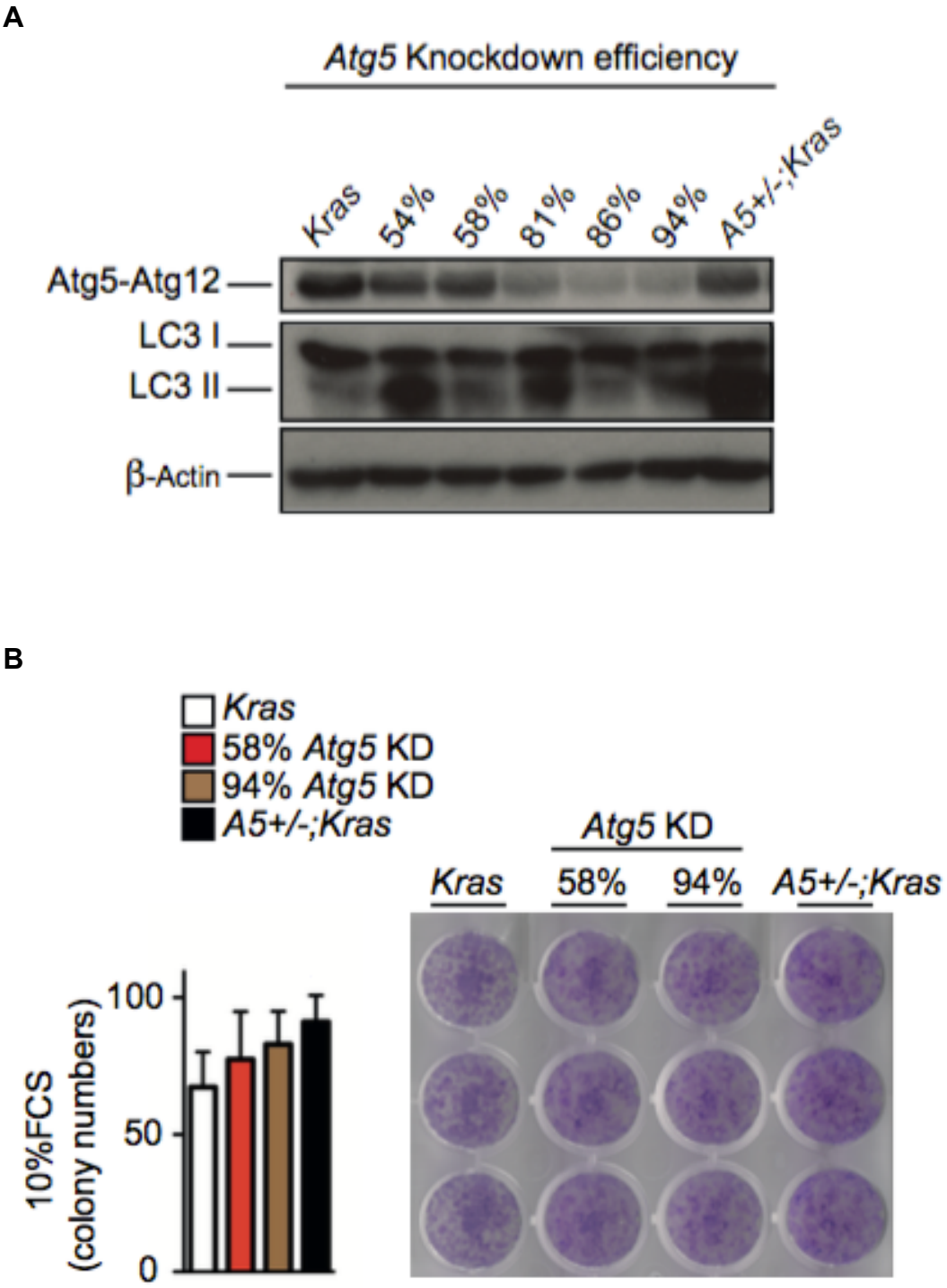

Figure 15: Downregulation of Atg5 does not alter basal autophagic flux and colony forming capacities of cancer cells. (A) Western blot of Atg5-Atg12 and LC3I/II in *Kras, A5+/-;Kras* and *Kras* cells after 54, 58, 81, 86, 94% shRNA-mediated knockdown of *Atg5*. **(B)** Colony formation assay in *Kras, A5+/-;Kras*, and *Kras* cells after 58, 94% knockdown (KD) of Atg5 (n>3) (left); representative pictures are shown (right); cells were cultivated in medium with 10% FCS. Mean±SD (n>3).

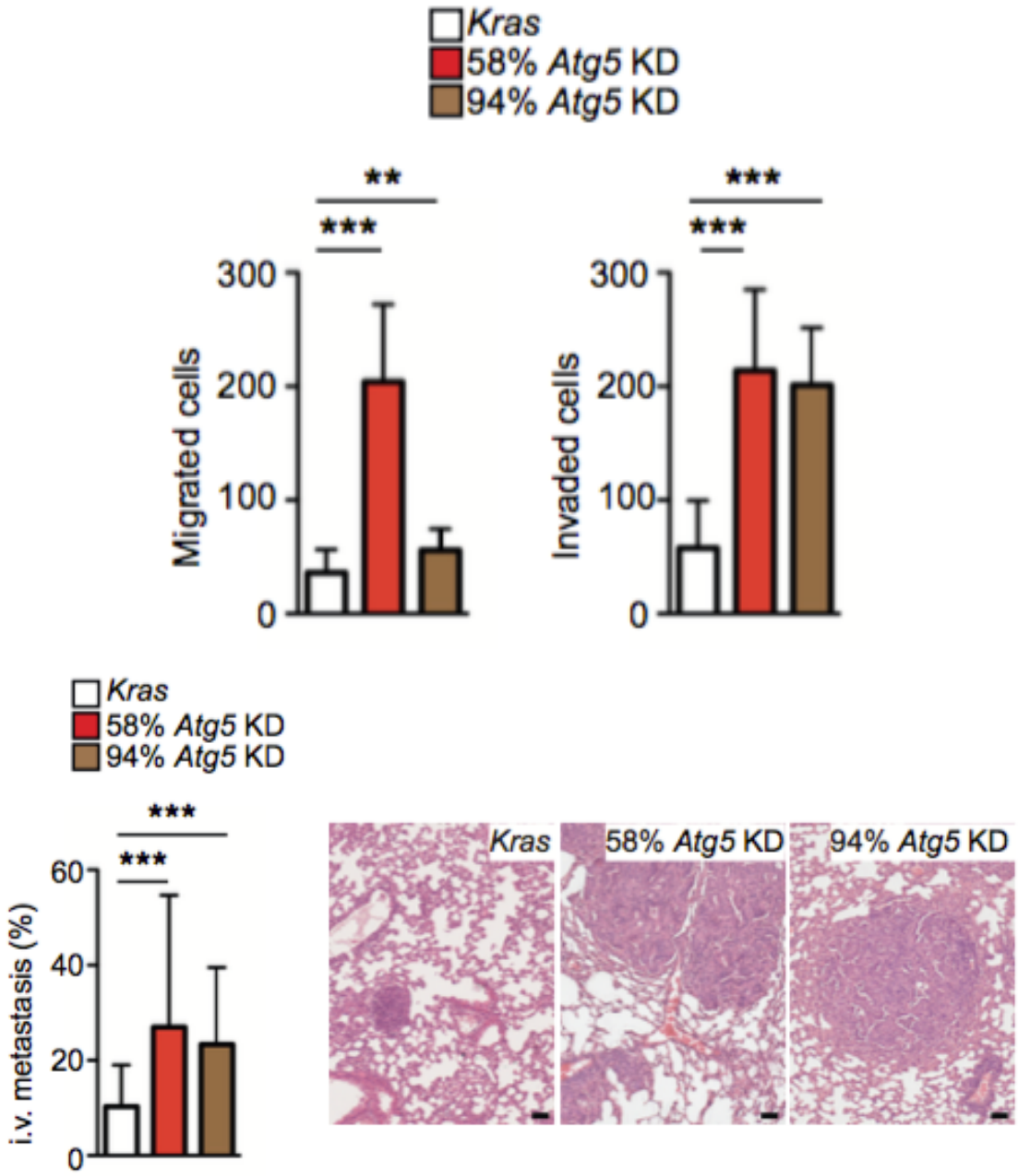

Figure 16: Downregulation of Atg5 increases metastatic properties of cancer cells *in vitro* and *in vivo*. (A) Migration (left), invasion (right) of *Kras* versus *Kras* cells with 58, 94% knockdown (KD) of *Atg5*. **(B)** Quantification of lung tumor formation after tail vein injection (i.v.) of *Kras* and *Kras* cells with 58, 94% knockdown (KD) of *Atg5* (% area); representative H&E pictures are included. Mean±SD (n>3), ****P<0.001, **P<0.01*. Scale bars equal 50µm.

5.2.4 Monoallelic loss of Atg5 enhances weight loss of intravenously cancer cells injected mice.

Pancreatic cancer aggressiveness is associated with weight loss. Due to this feature, weight loss was analyzed after intra-tail vein injection of cancer cells. Body weight of mice, as a sign of cachexia, was also decreased more after injection with *A5+/-;Kras* cells compared to *Kras* cells (Figure 17).

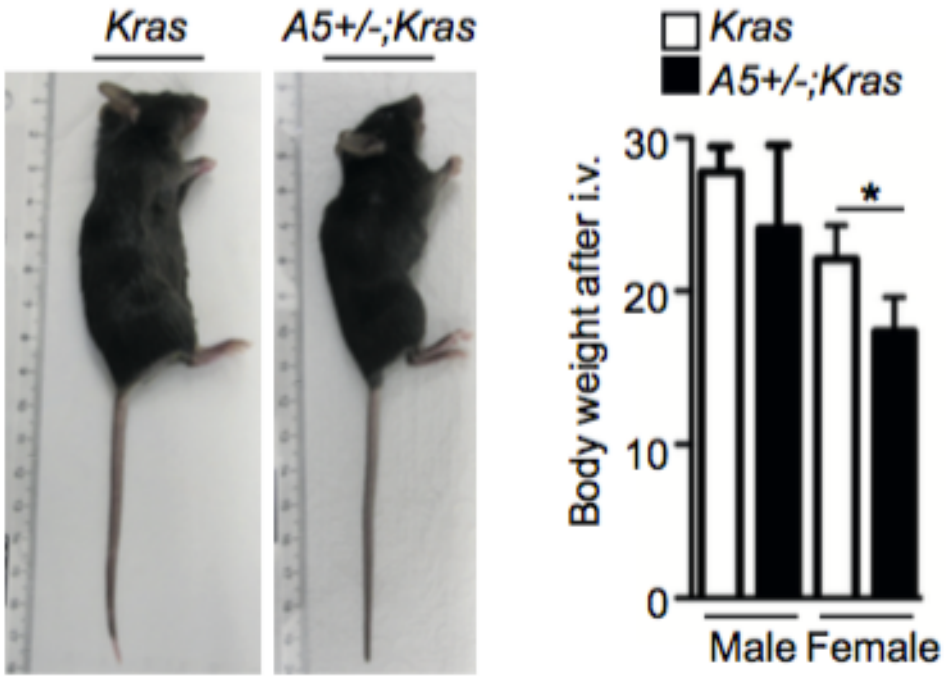

Figure 17: Monoallelic loss of Atg5 heighten weight loss after metastasis. Representative macroscopic picture of wildtype mice after tail vein (i.v.) injection of *Kras* and *A5+/-;Kras* cells (left), and quantification of body weight in male and females (n≥3) (right). Mean±SD (n>3), ****P<0.001, **P<0.01*.

5.3 Role of Atg5 in Transcriptional and Metabolic Status of Cancer Cells

5.3.1 Monoallelic loss of Atg5 induces transcriptional changes.

Autophagy is very well established to regulate transcription [124]. Moreover, the autophagy-lysosomal pathway is controlled on a transcriptional level in PDAC [126]. To interrogate how monoallelic loss of Atg5 redounds tumor cell metastasis and aggressiveness, transcriptomic analyses in *Kras* and *A5+/-;Kras* pancreatic tumor cells were performed. Remarkably, loss of one allele of Atg5 was adequate to change transcriptomic pathway regulation on a large scale. Gene enrichment analysis unveiled that loss of one allele of Atg5 led to a decline in the number of upregulated pathways by half (Figure 18).

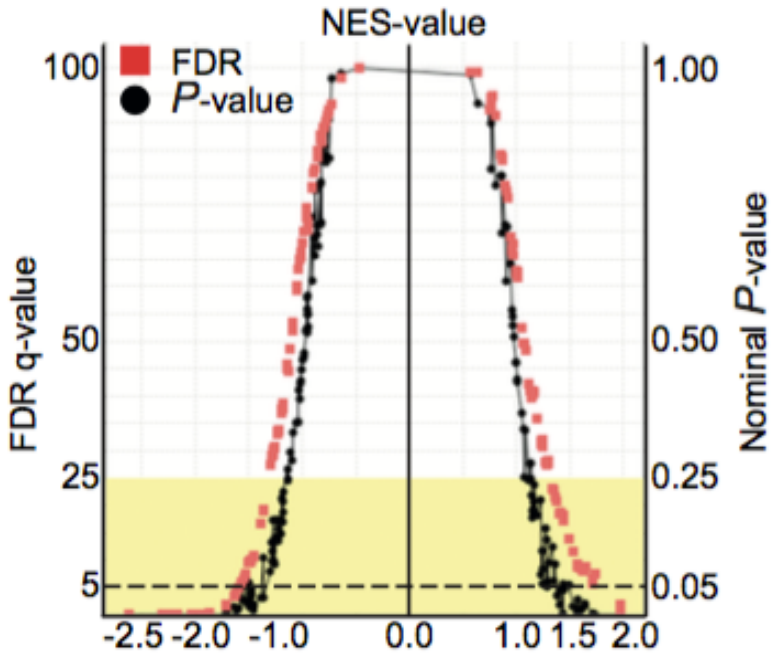

Kras	*A5+/-;Kras*
104 upregulated	69 upregulated
32 (*P*<5%, NES≤-1.4)	17 (*P*<5%, NES≥1.4)

Figure 18: Monoallelic loss of Atg5 changes enrichment of upregulated pathways. Normalized enrichment score (NES) versus significance plot illustrating gene sets, identified by GSEA, enriched in either *Kras* or *A5+/-;Kras* pancreatic tumor cells (n=3); enriched pathways are localized beneath dotted line.

Functional classification of the most significantly regulated genes established multiple cellular functions influenced by monoallelic loss of Atg5. Essentially, an increment was spotted in metabolism, immunity, development, and vesicular trafficking/homeostasis associated cellular functions; a decline was spotted in adhesion and cell cycle associated cellular functions (Figure 19).

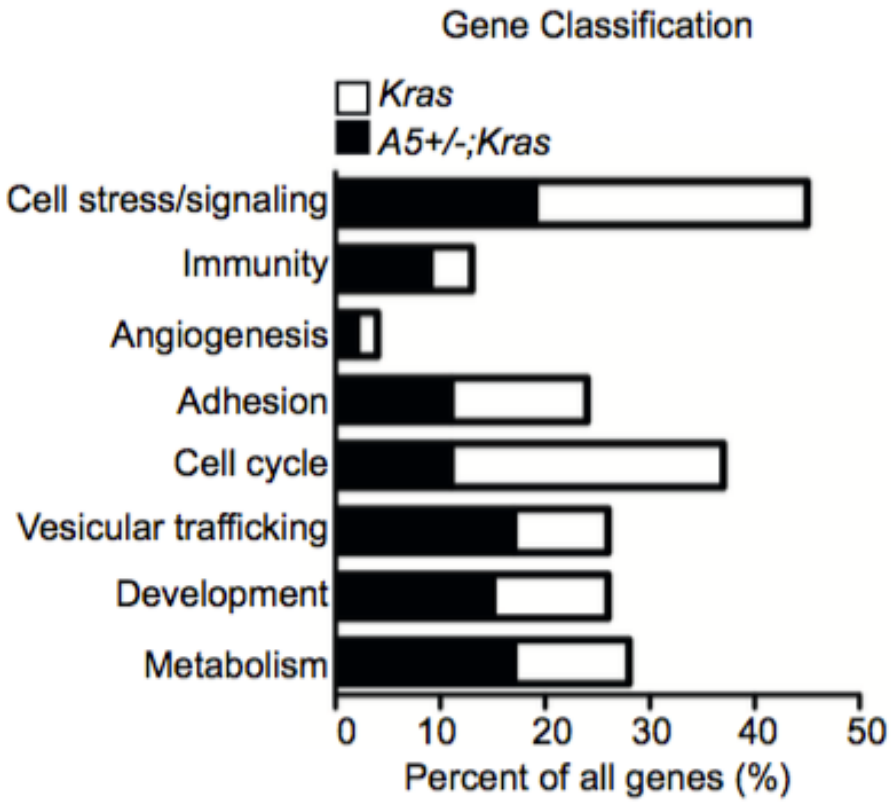

Figure 19: Monoallelic loss of Atg5 alters multiple cellular functions. Functional classification of most highly regulated genes identified by GSEA in *Kras* and *A5+/-;Kras* cells.

Classification of KEGG-pathways confirmed the increase in inflammation and the decrease in proliferation/ synthesis-associated pathways in *A5+/-;Kras* cells (Figure 20 and Figure 21). Intriguingly, the gene set associated with lysosomal function was enriched in *A5+/-;Kras* cells further supporting a deregulation in vesicular homeostasis (Figure 20 and Figure 21). Of note, gene enrichment analysis using the Transcription Factor Binding Motif database further supported the enrichment of development and inflammation-associated gene sets and the downregulation of proliferation-associated gene sets in *A5+/-;Kras* cells (Figure 20B).

A

KEGG *Kras*

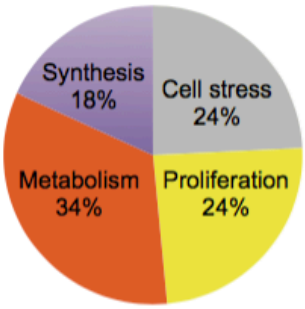

KEGG_Pathway	NES	*P*
Spliceosome	2.62	0.0
DNA_Replication	2,31	0.0
Pyrimidine_Metabolism	2.29	0.0
Proteasome	1.85	0.0

KEGG *A5+/-;Kras*

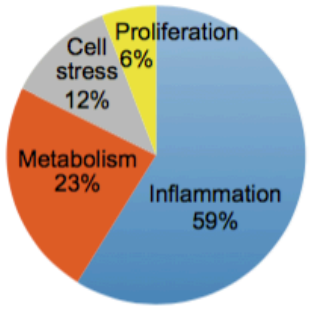

KEGG_Pathway	NES	*P*
Cytokine_Cytokine_Receptor_Interaction	1.73	0.0
Lysosome	1.96	0.0
Galactose_Metabolism	1.71	0.0
Basal_Cell_Carcinoma	1.56	0.005

B

Transcription factors *Kras*

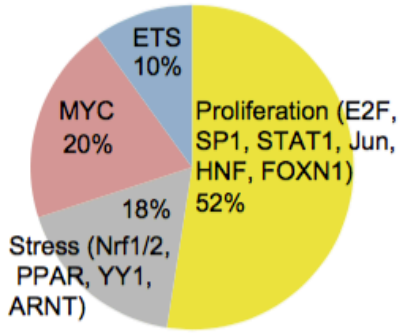

Transcription_Factor_Pathway	NES	*P*
E2F1_Q6_01	2.20	0.0
MYC_Q2	1.77	0.0
Nrf2_01	1.97	0.0
ELK1_02	2.16	0.0

Transcription factors *A5+/-;Kras*

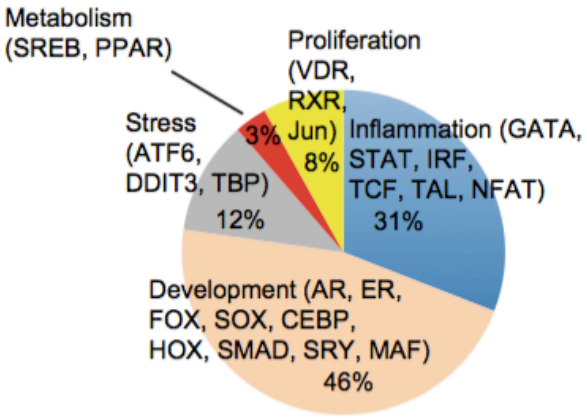

Transcription_Factor_Pathway	NES	*P*
ISRE_01 (STAT1)	1.65	0.0
ATF6_01	1.46	0.003
SREBP1_02	1.58	0.009
AP2ALPHA_01 (TFAP2A)	1.67	0.0
AP1_C (Jun)	1.46	0.004

Figure 20: Monoallelic loss of Atg5 leads comprehensive changes in transcriptomics. (A) Classification of significantly enriched gene sets into categories for *Kras* (left) and *A5+/-;Kras* (right) cells (P value 0.0 indicates *P<0.001*). **(B)** Classification of significantly enriched gene sets into categories, based on Transcription Factor Binding Motif database for *Kras* (left) and *A5+/-;Kras* (right) cells; pie charts show classification and tables highlight examples of enriched pathways (NES≥1.0, *P<0.05; P* value 0.0 indicates *P<0.001*).

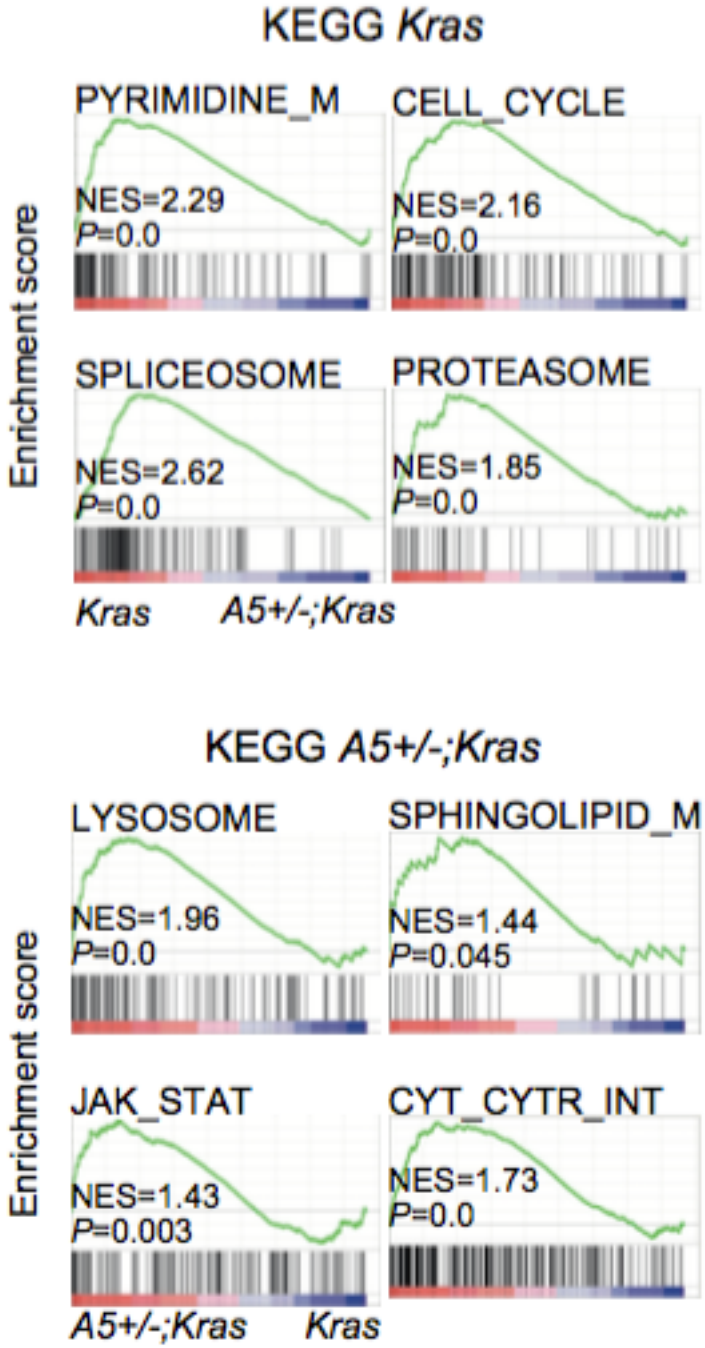

Figure 21: Monoallelic loss of Atg5 influences enriched KEGG pathways. GSEA diagrams of significantly enriched KEGG pathways found in *Kras* (top) and *A5+/-;Kras* (bottom) cells.

5.3.2 Monoallelic loss of Atg5 induces metabolic changes.

Autophagy is an important cellular process in terms of metabolic pathways. Therefore non-targeted metabolic profiling was performed in *Kras* and *A5+/-;Kras* cell lines and their supernatants (Figure 22). Importantly, *A5+/-;Kras* cells contained elevated amounts of nucleotides and spermidine, corresponding to deregulated proliferation, elevated amounts of oxidative and cell stress-associated metabolites (e.g., S-nitrosoglutathione, hypotaurine, S-lactoylglutathione, involved in oxidative stress, and ADP-ribose connected with cell stress), increased 3/2-phosphoglycerate compromised in glucose metabolism, and changes in the amounts of fatty acids engaged in energy metabolism (e.g., myristoylcarnitine, valerylcarnitine) (Figure 22). Supernatants of *A5+/-;Kras* cells depicted alterations in lysolipids (e.g., 1-Stearoyl-GPE) and other lipids (e.g., polyunsaturated fatty acids), sign of changes in membrane composition/signaling; arginine, suggesting an inducer of the immune microenvironment (especially M2 macrophages); and 6-phosphogluconate, a metabolite associated with the pentose phosphate pathway (Figure 22).

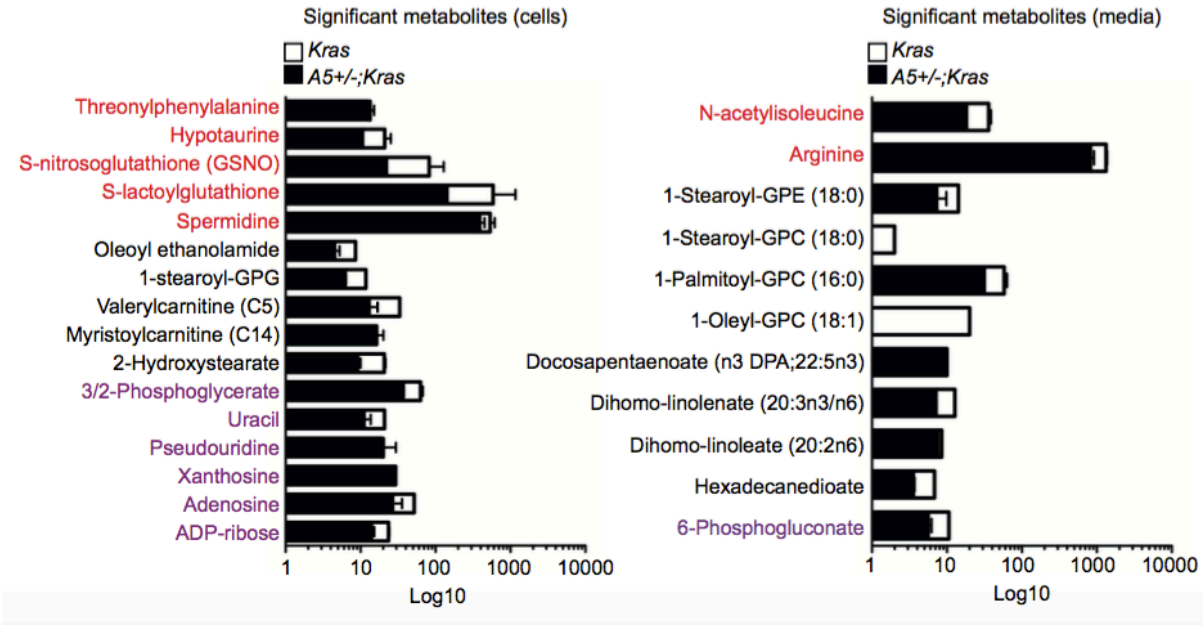

Figure 22: Monoallelic loss of Atg5 changes metabolic profile. Classification of significantly upregulated metabolites in *Kras* and *A5+/-;Kras* cells (left) and their supernatants (media, right); amino acids/ peptides=red, lipids=black, nucleotides/ carbohydrates=purple; Mean±SD (n=3).

5.3.3 Monoallelic loss of Atg5 reduces mitochondrial functionality.

A series of experiments were performed related to mitochondrial functionality and cell stress to reveal the effect of monoallelic Atg5-loss on metabolism. Electron microscopy depicted changes in mitochondrial morphology. Especially, there was an increase in mitochondrial fission and differences in cristae stacking between *Kras* and *A5+/- ;Kras* cells (Figure 23).

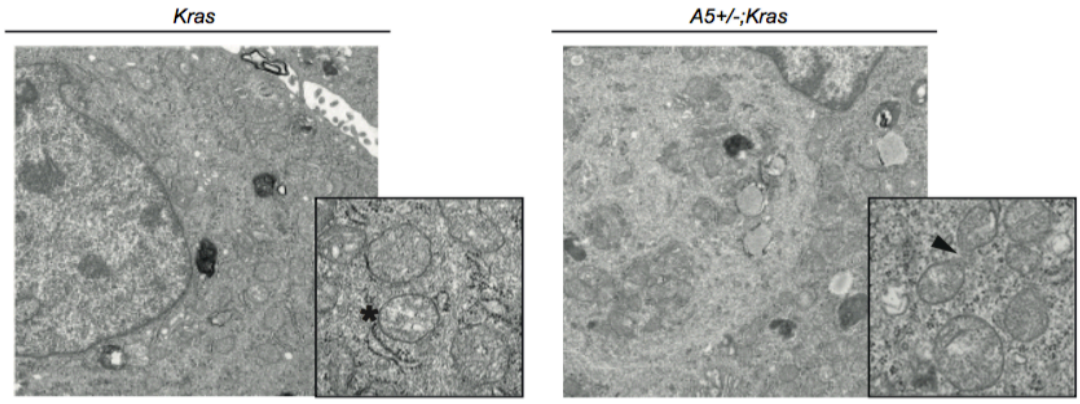

Figure 23: Monoallelic loss of Atg5 changes mitochondrial morphology. TEM pictures of *Kras* and *A5+/-;Kras* cells (4000x, 20000x); asterisk/ black arrowhead indicate mitochondria/ mitochondrial fission.

Mitochondrial function was further assessed by detailed comparison of oxidative and glycolytic capacities in *Kras* and *A5+/-;Kras* cell lines (Figure 24-27).

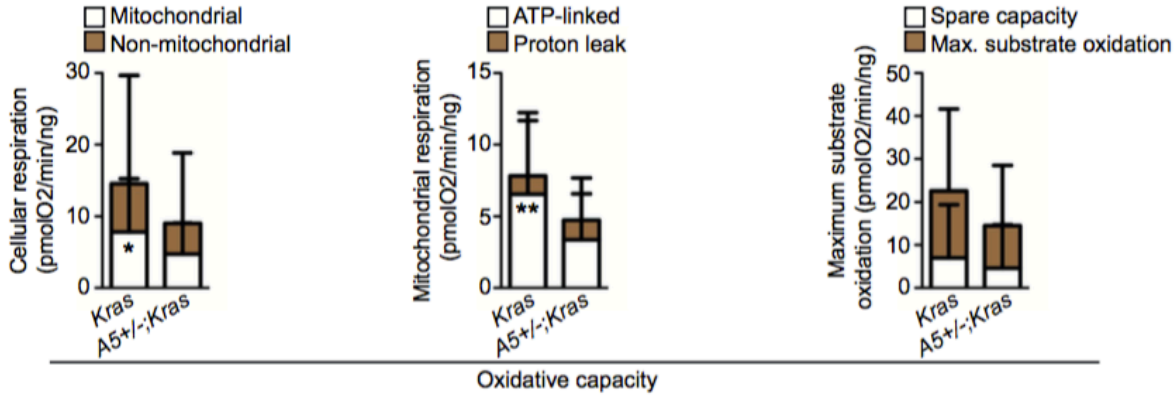

Figure 24: Monoallelic loss of Atg5 decreases oxidative capacity. Oxidative capacity (pmolO2/min) of *Kras* and *A5+/-;Kras* cells normalized to protein or DNA (ng) (n≥30). Mean±SD, **P<0.05, **P<0.01*.

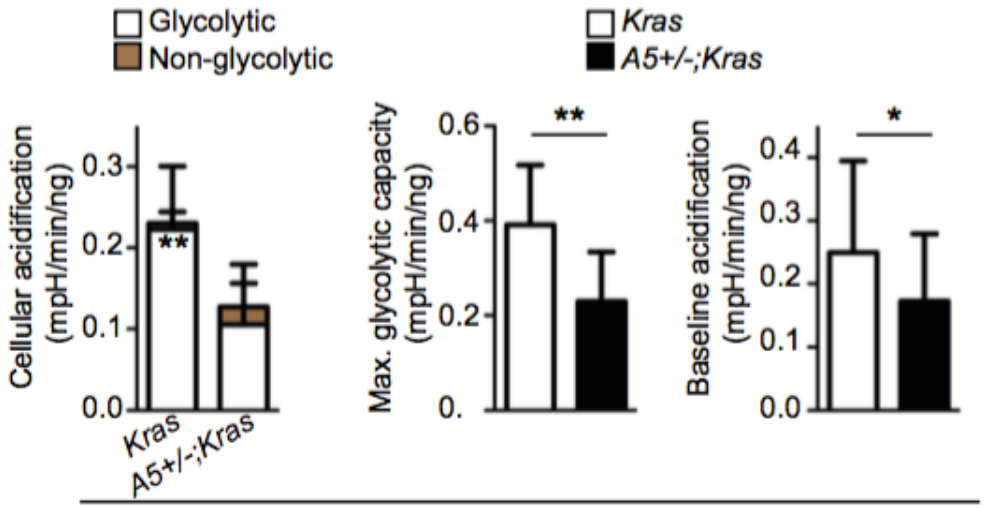

Figure 25: Monoallelic loss of Atg5 decreases glycolytic capacity. Glycolytic capacity (mpH/min) of *Kras* and *A5+/-;Kras* cells normalized to protein or DNA (ng) (n=9). Mean±SD, **P<0.05, **P<0.01*.

A decrease was detected in oxidative capacity, as evidenced by cellular respiration rate, mitochondrial respiration rate, and maximum substrate oxidation rate, at the consumption of mitochondrial ATP production (Figure 24). More than that *A5+/-;Kras* cells depicted a reduction in glycolysis, as indicated by decreased cellular acidification rates, maximum glycolytic capacity, and baseline acidification rate (Figure 25). Mitochondrial coupling efficiency did not show any significant difference (Figure 26). An oxygen consumption rate versus extracellular acidification plot (OCR/ECAR) corroborates these results showing an attenuation in metabolic activity in *A5+/-;Kras* cells (Figure 27A). This is depicted by the movement of the *A5+/-;Kras* cell line measurements fronting both, lower OCR and lower ECAR, demonstrating reduced ATP turnover (Figure 27A).

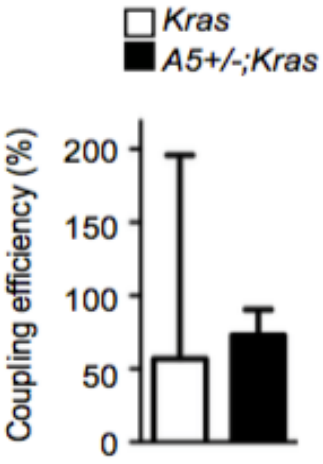

Figure 26: Monoallelic loss of Atg5 does not influence mitochondrial coupling. Coupling efficiency (%) of mitochondria in *Kras* and *A5+/-;Kras* cells as measured by seahorse (n≥30). Mean±SD, **P<0.05, **P<0.01*.

Curiously, cellular fractionation experiments revealed a deracination in the mitochondrial fraction as detected by GLDH-activity. Exceptionally, mitochondria were shifted towards the autophagosomal fraction, depicting deteriorated integrity of mitochondria (Figure 27B).

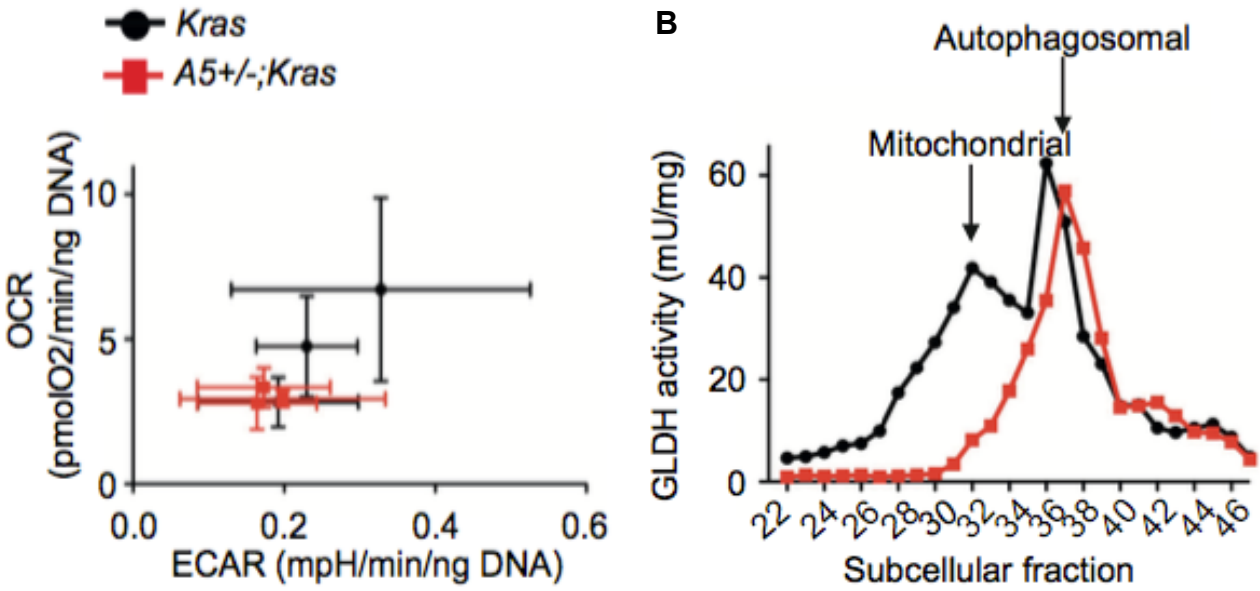

Figure 27: Monoallelic loss of Atg5 decreases metabolic activitiy. (A) Oxygen consumption rate (pmolO2/min/ng DNA) versus extracellular acidification rate (mpH/min/ng DNA) for *Kras* and *A5+/-;Kras* cells. **(B)** Mean glutamate dehydrogenase activity (GLDH, mU/mg protein) distribution into density fractions (with decreasing density from 22 to 46) in *Kras* and *A5+/-;Kras* cell extracts (n=4).

Protein expression analyses embellished slight elevations in oxidative phosphorylation associated mitochondrial proteins (COX II/ IV, ATP Core 2), in mitochondrial stress-associated SOD2, and in endoplasmic reticulum (ER)-stress associated BiP. ER-stress was also shown by an increase in the spliced form of Xbp1 (Figure 28A). mRNA expression levels of Nrf1 and mitochondrial Sod2 were increased validating the elevated mitochondrial stress (Figure 28B); Nrf2 and cytosolic Sod1 were not changed (Figure 28C).

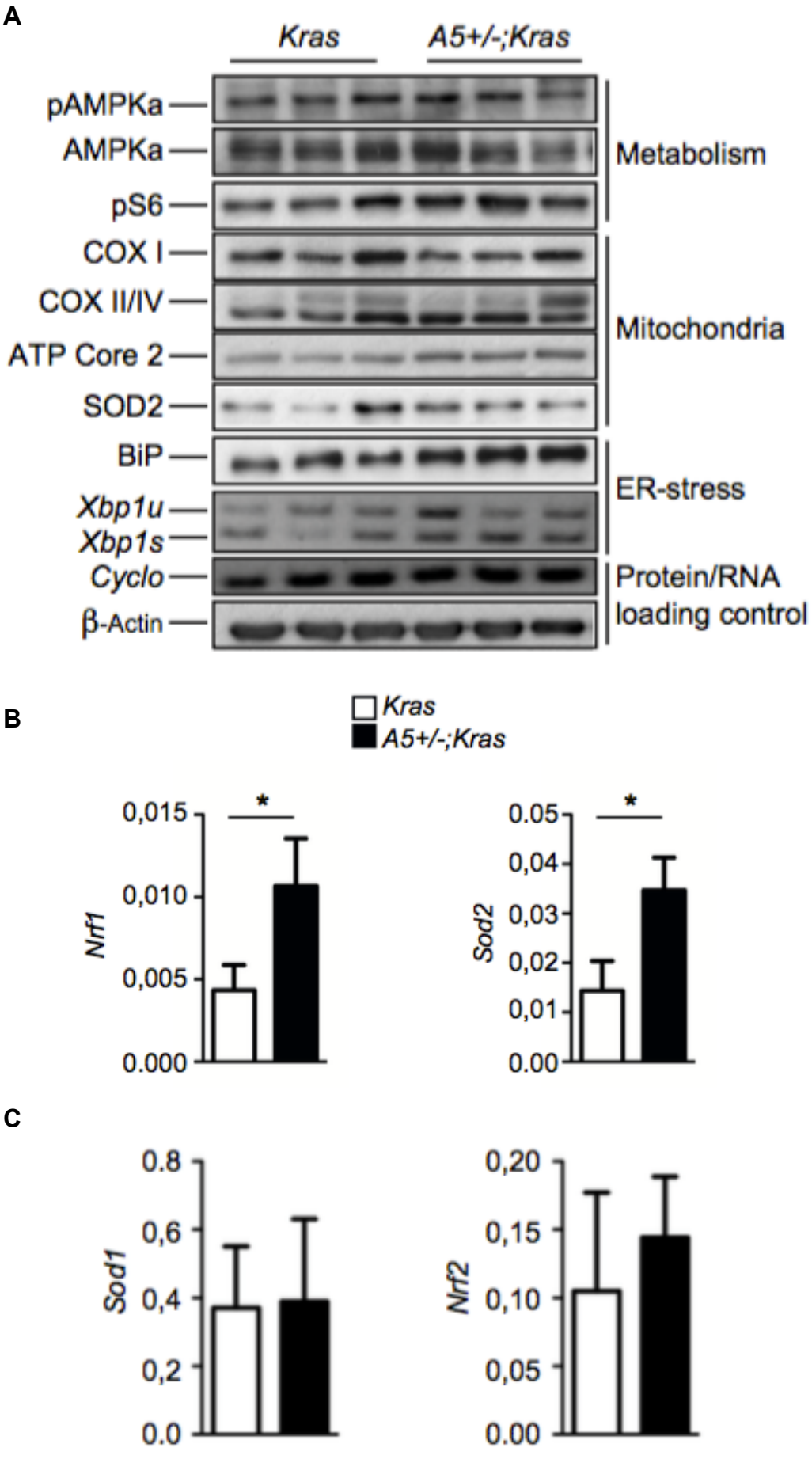
A
Kras
A5+/-;Kras
pAMPKa
AMPKa
pS6
COX I
COX II/IV
ATP Core 2
SOD2
BiP
Xbp1u
Xbp1s
Cyclo
β-Actin
Metabolism
Mitochondria
ER-stress
Protein/RNA loading control
B
Kras
A5+/-;Kras
Nrf1
0,015
0,010
0,005
0.000
*
Sod2
0.05
0,04
0,03
0,02
0,01
0.00
*
C
Sod1
0.8
0,6
0,4
0,2
0.0
Nrf2
0,20
0,15
0,10
0,05
0.00

Figure 28: Monoallelic loss of Atg5 decreases metabolic activitiy. (A) Analysis of phospho-AMPKa, AMPKa, phospho-S6, mitochondrial complexes (COX I, COX II/IV, ATP Core 2), SOD2, and BiP in protein lysates and Xbp1 splicing (Xbp1u=unspliced, Xbp1s=spliced) in RNA-preparations from *Kras* and *A5+/-;Kras* cells; β-Actin and cyclophilin were used as loading controls. **(B)** qRT-PCR of Sod1 and Nrf2 in mRNA extracts from *Kras* and *A5+/-;Kras* cells; data are normalized to cyclophilin (n=3). **(C)** qRT-PCR of Nrf1 and Sod2 normalized to cyclophilin (n=3). Mean±SD, **P<0.05, **P<0.01*. (previous page)

5.3.4 P53 status is not altered by monoallelic loss of Atg5 in pancreatic cancer cells.

Another important player that can modulate the effects of autophagy on pancreatic cancer is p53. Either presence or absence of p53 can reverse the effects of autophagy on PDAC. It is known that both oncogenic Kras and autophagy inhibition can activate p53. For this reason, p53 levels were analyzed in *Kras* and *A5+/-;Kras* pancreata and cancer cells. To compare p53 levels, p53 immunohistochemistry in *Kras* and *A5+/-;Kras* tumors and p53 western blot in the corresponding cell lines (Figure 29-30). As clearly visible there is no difference in the expression level of p53 in tumor structures (black asterisk) or the tumor microenvironment (black arrowhead) in the mouse tissues of *Kras* and *A5+/-;Kras* (Figure 29). In fact, p53 can be readily detected in both mouse models in the tumor microenvironment (Figure 29).

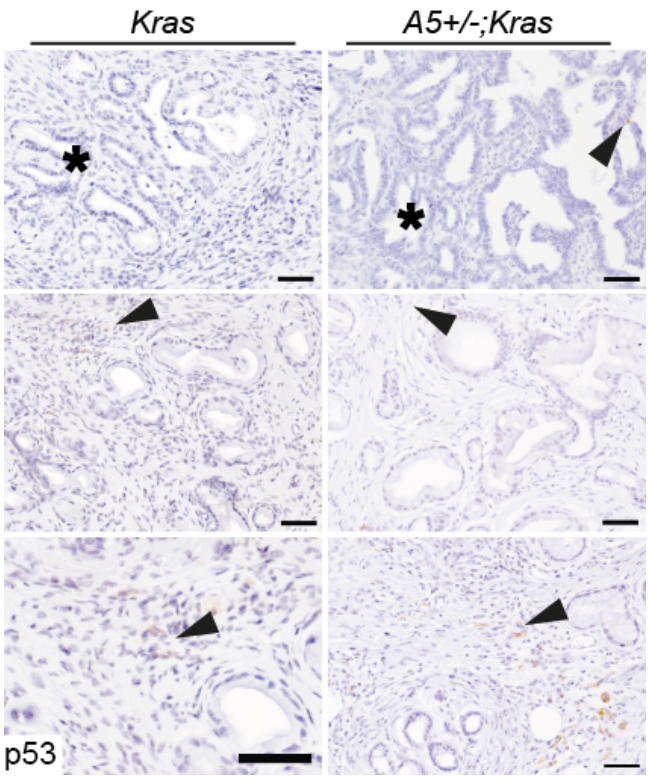

Figure 29: Monoallelic loss of Atg5 does not alter p53 levels in cancer structures. Immunohistochemistry of p53 in *Kras* and *A5+/-;Kras* mouse tissues; positive cells of the tumor microenvironment are indicated by the black arrowhead; tumor structures are shown by the black asterisks. Scale bars equal 50 µm.

As it is mentioned above, p53 levels were also analyzed in Kras and A5+/-;Kras cells by western blot. It showed no difference in between the cell lines (Figure 30).

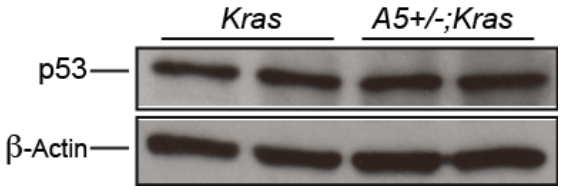

Figure 30: Monoallelic loss of Atg5 does not change p53 levels in cancer cells. Representative western blot of p53 in *Kras* and *A5+/-;Kras* mouse cell lines; β -Actin was used as loading control (n=4 per group).

Thus, p53 is expressed at a similar level between *Kras* and *A5+/-;Kras* mouse tumors *in vivo* and *in vitro*, indicating that p53 is not a key player in this model.

5.4 Role of Atg5 in Cell Autonomous Mechanisms of Mestastasis

5.4.1 Atg5 level influences Ca^{2+} flux in the cancer cells.

Mitochondria and lysosomes play an important role in buffering intracellular Ca^{2+} levels and are hence jointly related to Ca^{2+} fluctuations. Additionally, Ca^{2+} responses impact mitochondrial function/ morphology, gene transcription [41,127,128], vesicle trafficking, cellular migration, and lamellipodia formation at the front of migrating cells [129]. Accordingly, cellular Ca^{2+} responses were analyzed in more detail as a presumptive mechanism linking our observations. Supportively, Ca^{2+} responses of *Kras* and *A5+/-;Kras* cells after treatment with 0.01 or 0.05% FBS were significantly different (Figure 31A). Cytosolic Ca^{2+} responses in *A5+/-;Kras* cells were characterized by superior amplitudes and merely one peak of Ca^{2+} elevation. Furthermore, the number of FBS-responding cells was slightly elevated in *A5+/-;Kras* versus *Kras* cells (Figure 31B)

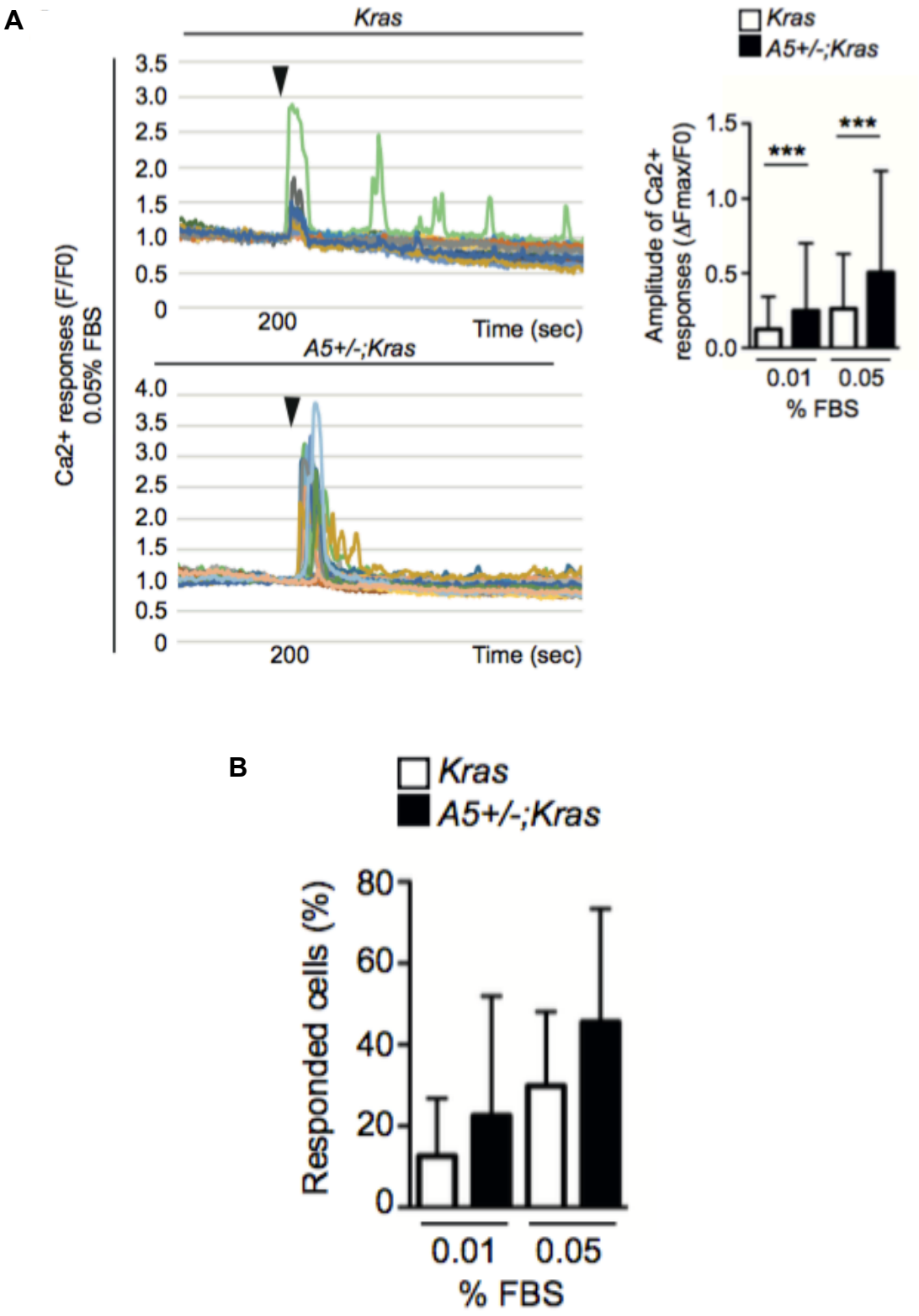

Figure 31: Monoallelic loss of Atg5 does not change p53 levels in cancer cells. **(A)** Representative recordings (left) and amplitude (right) of cytosolic Ca^{2+} responses in *Kras* and *A5+/-;Kras* cells after FBS-stimulation (at 200sec, marked with black arrowhead) (n>170). **(B)** Proportions of *Kras* and *A5+/-;Kras* cells producing Ca^{2+} responses after stimulation with 0.01% or 0.05% FBS (n>170). Mean±SD, **P<0.05, **P<0.01, ***P<0.001*.

S100a4, a Ca^{2+} - binding protein associated with increased metastatic capacities, was found highly expressed in *A5+/-;Kras* tumors compared to only slight expression in *Kras* tumors. The higher PanIN orders and established PDAC- structures were particularly positive for S100a4 expression (Figure 32).

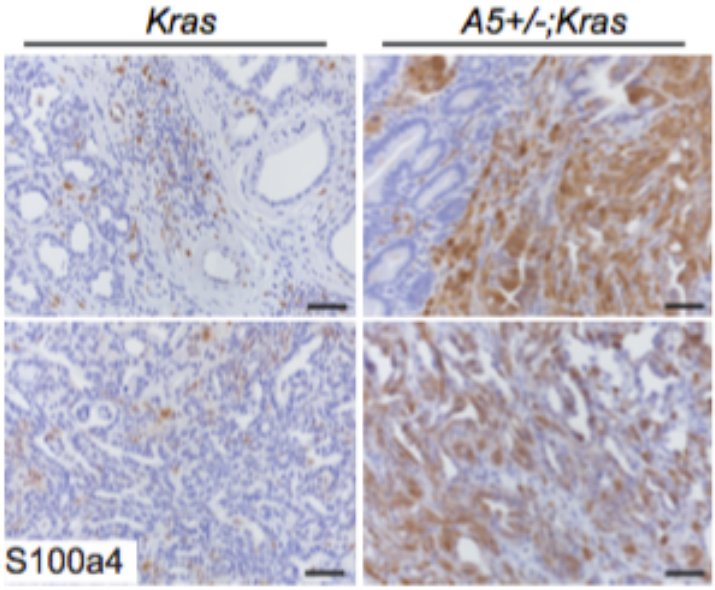

Figure 32: Monoallelic loss of Atg5 increases S100a4 in pancreatic tumor. S100a4 immunohistochemistry in *Kras* and *A5+/-;Kras* mice. Scale bars equal 50µm.

5.4.2 Atg5 level influences extracellular cathepsin activity and filopodia formation in the cancer cells.

Lysosomal trafficking and exocytosis of lysosomal cathepsins is regulated by intracellular Ca^{2+} fluctuations as well [130]. Measurement of lysosomal cathepsin activities in cell culture supernatants depicted a significantly higher activity of cathepsin L and cathepsin D (Figure 33A), although cathepsin B was not changed (Figure 33B). Protein levels of the corresponding pro-cathepsins also displayed an inclination towards heightened amounts in *A5+/-;Kras* cells (Figure 33C). Furthermore copy number of genes associated with lysosomes indicated a difference in regulation between normal pancreas and pancreatic cancer samples (Figure 34).

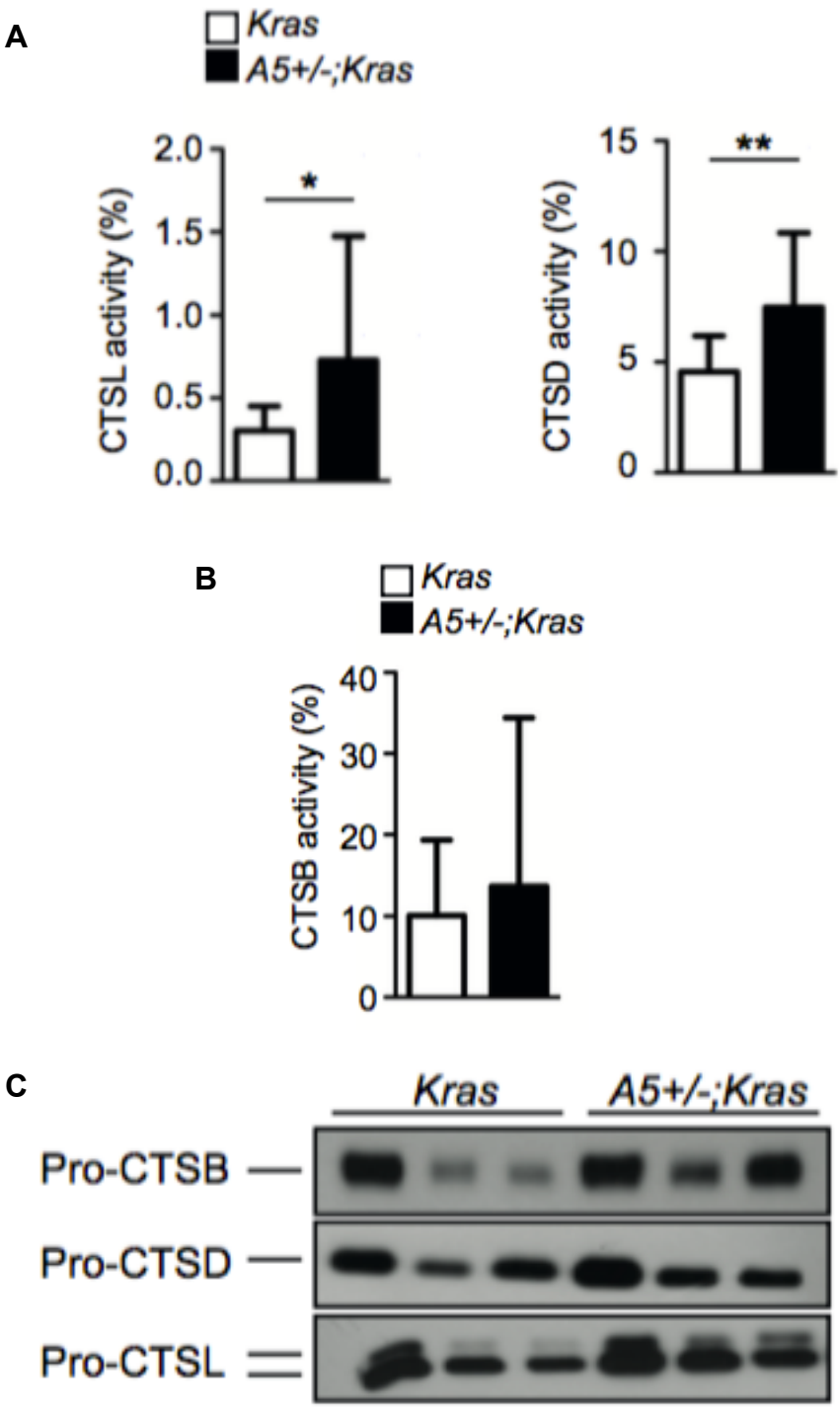

Figure 33: Monoallelic loss of Atg5 escalates extracellular cathepsin activites. (A) Cathepsin L (CTSL) and Cathepsin D (CTSD) extracellular activity (% extracellular activity versus total activity) as measured from supernatants of *Kras* and *A5+/-;Kras* cells (n=15). **(B)** Cathepsin B (CTSB) extracellular activity (% extracellular activity versus total activity) as measured from supernatants of *Kras* and *A5+/-;Kras* cells (n=15). **(C)** Western blot analysis of Pro-cathepsin B (Pro-CTSB), Pro-cathepsin D (CTSD), and Pro-cathepsin L (Pro-CTSL) in supernatants of *Kras* and *A5+/-;Kras* cells. Mean±SD, **P<0.05, **P<0.01, ***P<0.001.*

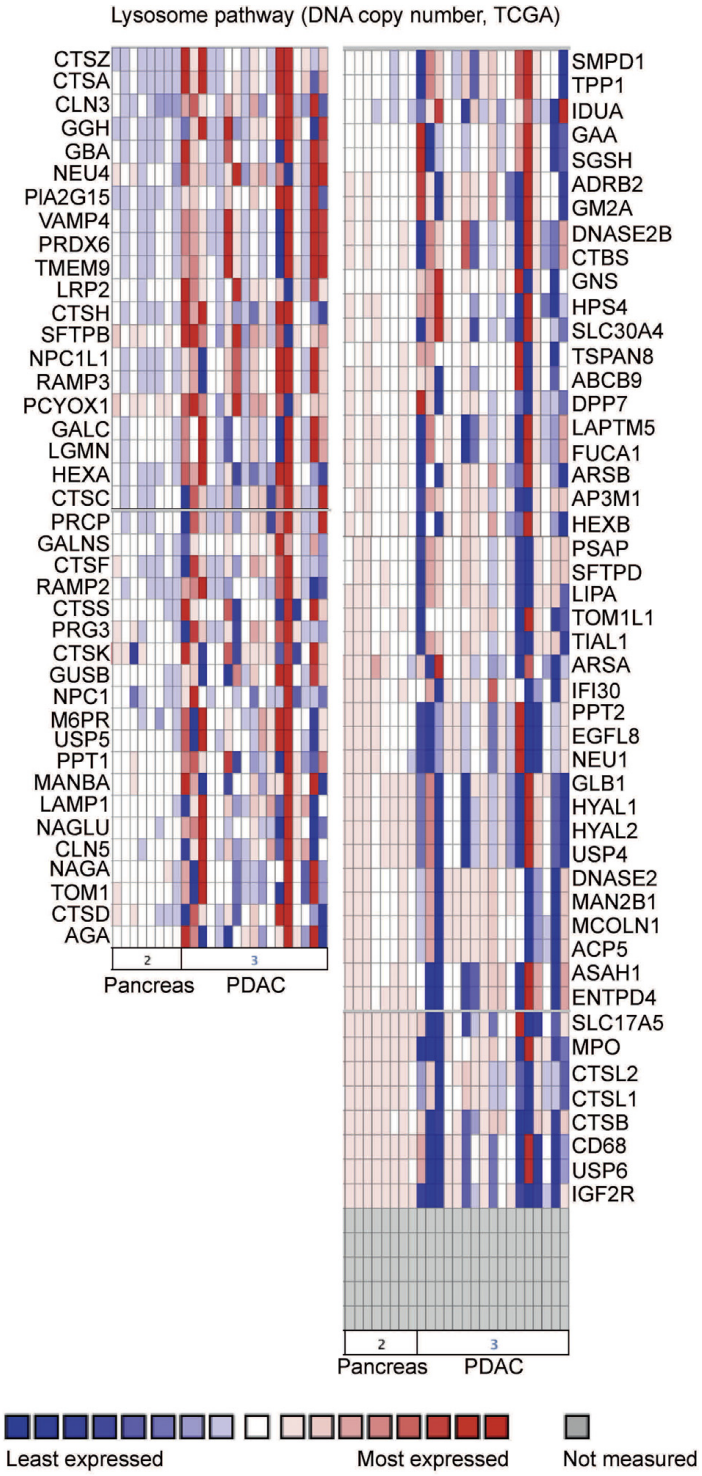

Figure 34: Lysosome-associated DNA copies differ between normal pancreas and PDAC. Illustration of lysosome-associated DNA copy number gain (red) or loss (blue) (TCGA data) in normal pancreas versus pancreatic ductal adenocarcinoma (PDAC) samples (log2 copy number units).

Moreover, the relevance of extracellular cathepsin activity in cell spreading and invasion was functionall analyzed. For this reason, Kras and A5+/-;Kras cells were treated with the cathepsin inhibitor E64d. The amount of colonies formed by Kras and A5+/-;Kras cells did not alter after E64d treatment (Figure 35). After the cathepsin inhibitor E64d treatment, the number of filopodia per sphere (Figure 36A) and the number of matrigel invaded cells were quantified (Figure 36B). Cell spreading and invasive capacities were significantly inhibited in A5+/-;Kras cells (Figure 36A-B). Of note, E64d did not affect filopodia formation and invasive capacities of Kras cells.

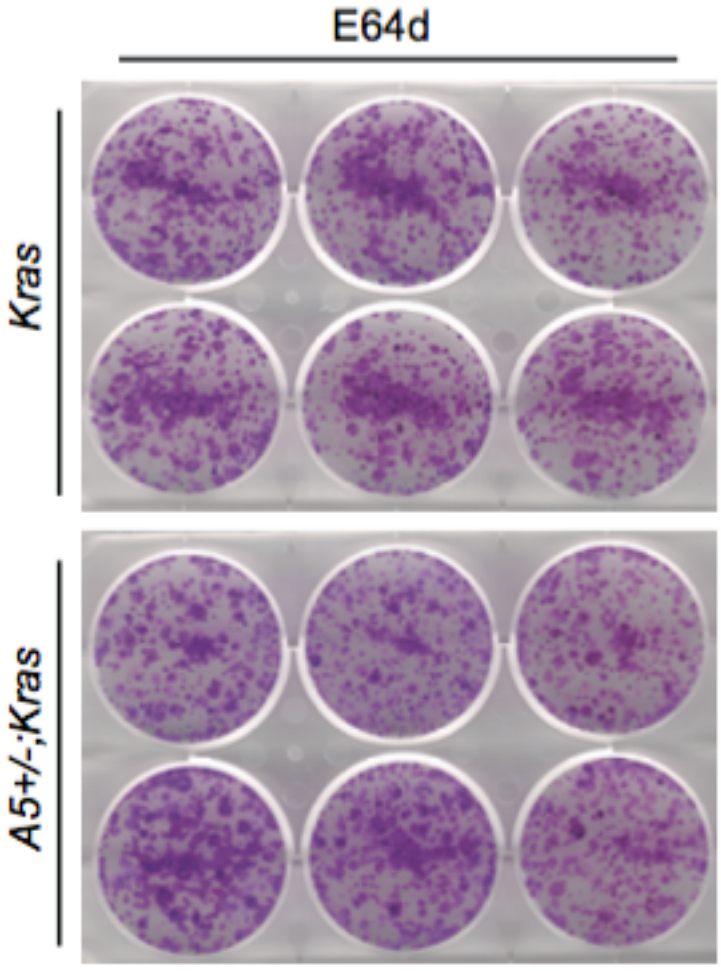

Figure 35: Cathepsin inhibitor does not influence colony forming capacities of *Kras* and *A5+/-;Kras* cells. Colony formation assay in *Kras* and *A5+/-;Kras* cells after cultivation with E64d.

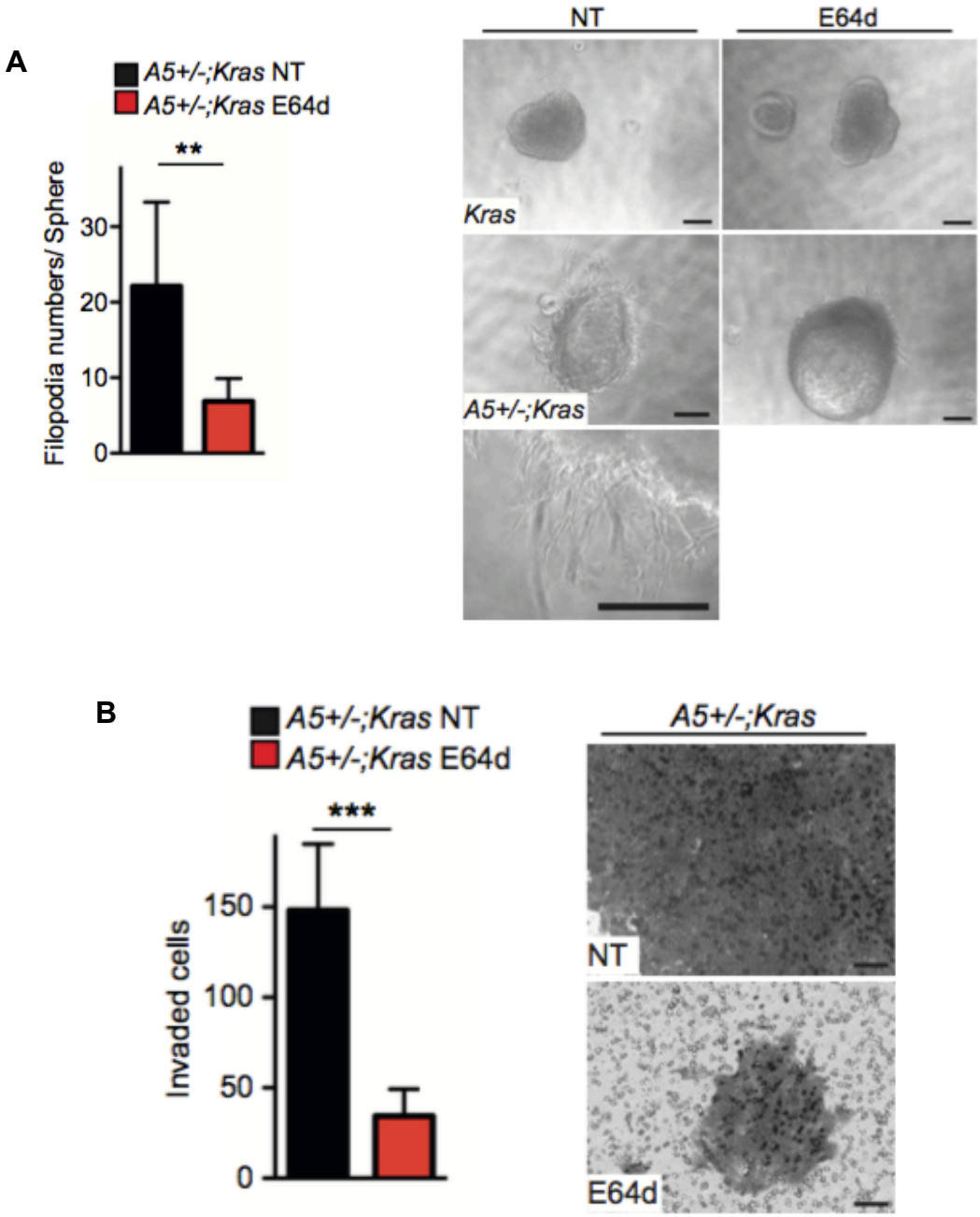

Figure 36: Cathepsin inhibitor decreases cell spreading and invasive capacities of *A5+/-;Kras* cells. (A) Quantification of filopodia numbers/ sphere in *A5+/-;Kras* cells after E64d treatment compared to no treatment (NT) (n>3) (left); representative bright field picture of cell spreading and filopodia (right). **(B)** Quantification of invaded *A5+/-;Kras* cells after E64d treatment or no treatment (NT) (n>3) (left); representative picture of invaded cells (right). Mean±SD, **P<0.05, **P<0.01, ***P<0.001*. Scale bars equal 50µm.

In a nutshell levels of Atg5 significantly determine cellular Ca^{2+} responses and lysosomal enzyme activities, which are prerequisite for increased cell spreading and invasion.

5.5 Effect of Atg5 levels in Non Cell-Autonomous Mechanisms of Metastasis

5.5.1 Atg5 level influences cytokine profile of cancer cells.

Alterations in inflammation have been shown to boost tumorigenesis and cancer cell invasion/ metastasis. Our transcriptomic results classified changes in inflammatory pathways. Furthermore, extracellular arginine levels, known to induce pro-tumorigenic- versus pro-inflammatory M1-macrophages, were increased in *A5+/-;Kras* versus Kras cells. Hence, the effect of Atg5-monoallelic loss on macrophage-mediated inflammation is elucidated. Firstly, the cytokine/ chemokine profile of *Kras* and *A5+/-;Kras* cells in cell culture supernatants were analyzed (Figure 37).

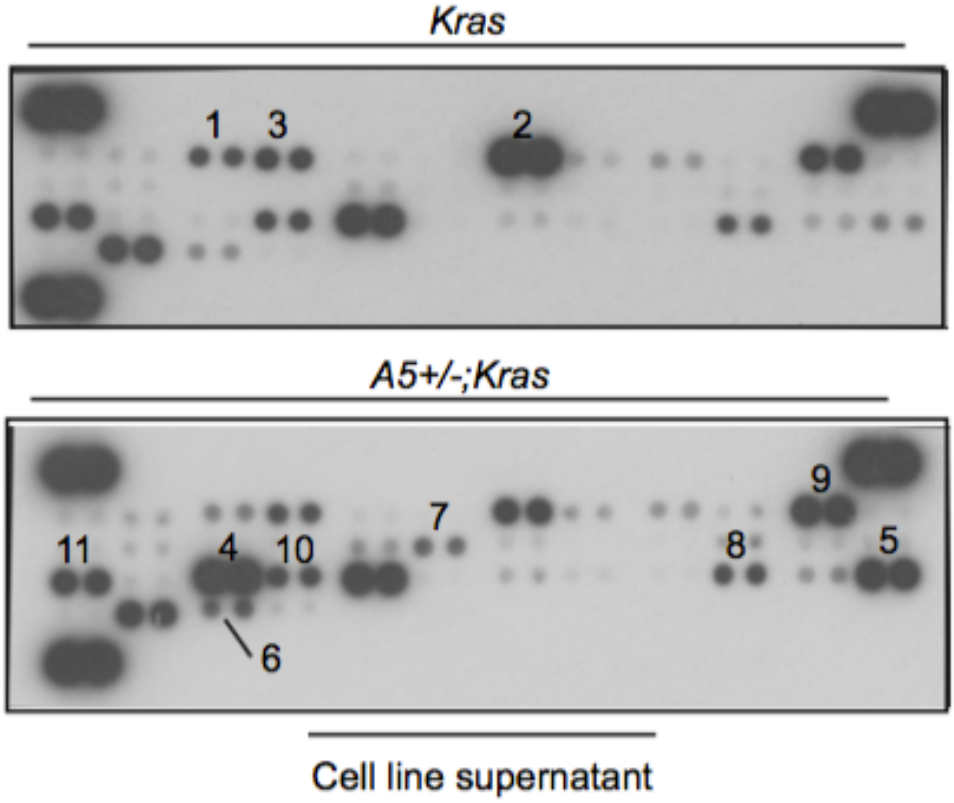

Figure 37: Monoallelic loss of Atg5 alters the profile of cytokines released from the cancer cells. Cytokine profile expression shown by immunoblotting of protein lysates from *Kras* and *A5+/-;Kras* supernatants (n=1)

Quantification of dot plot-pixel intensity showed upregulation of cytokines involved in macrophage chemoattraction (CXCL1, CXCL12), M2- polarization (M-CSF, CXCL12, IL-10, CXCL2, IL1a, CXCL10), and tumor progression/metastasis (TNFa) in A5+/-;Kras versus Kras cells, whereas cytokines important for M1-polarization (GM-CSF), M1- chemoattraction (sICAM-1), and granulocyte attraction (G-CSF) were downregulated (Figure 38).

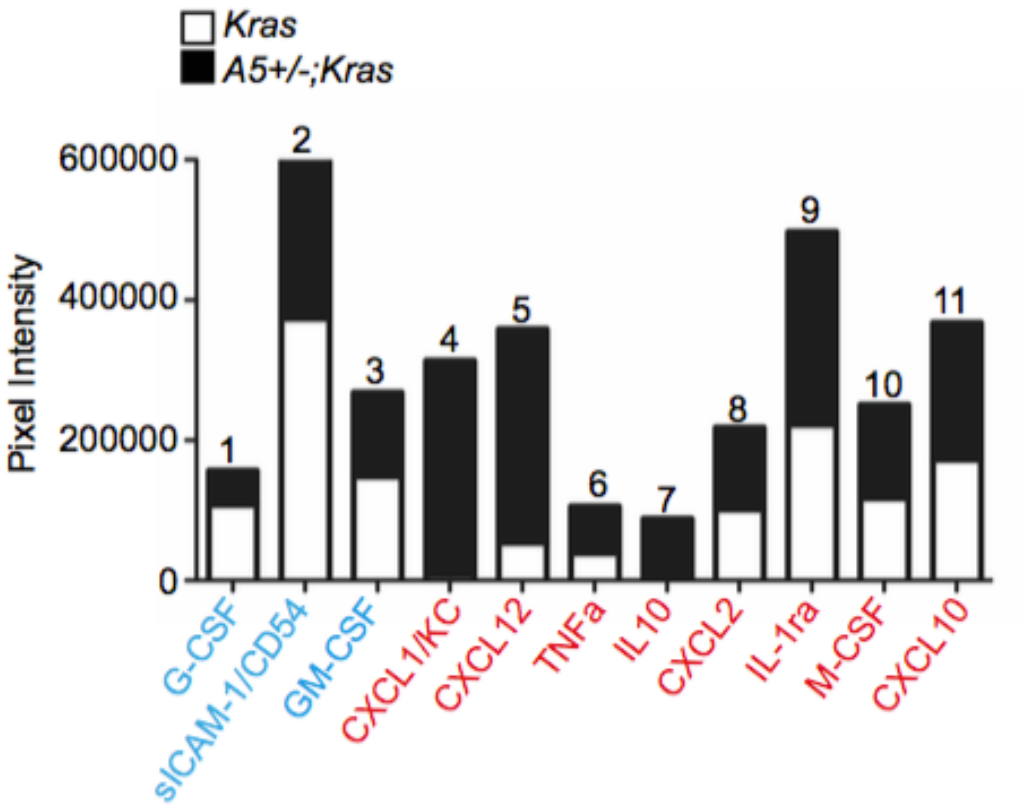

Figure 38: Monoallelic loss of Atg5 increases several pro-tumorigenic cytokines. Quantification of average pixel intensity between two dots corresponding to the same cytokines; numbers above graph (Figure 36) correspond to dot-position in plot (n=1).

5.5.2 Atg5 level influences cytokine profile of cancer cells.

To analyze in more detail the effect of *Kras* and *A5+/-;Kras* cells on the inflammatory microenvironment, we cultured undifferentiated Raw macrophages with the cell culture supernatants of *Kras* and *A5+/-;Kras* cells and defined the alterations in macrophage morphology, as described previously [123].

Supernatants from Kras cells induced macrophage polarization into the M1-subtype; supernatants from *A5+/-;Kras* cells elseways switched polarization towards the M2-subtype by presenting increased cell elongation, (Figure 39A), confirmed by elevated

levels of Arginase 1 expression (Figure 39B).

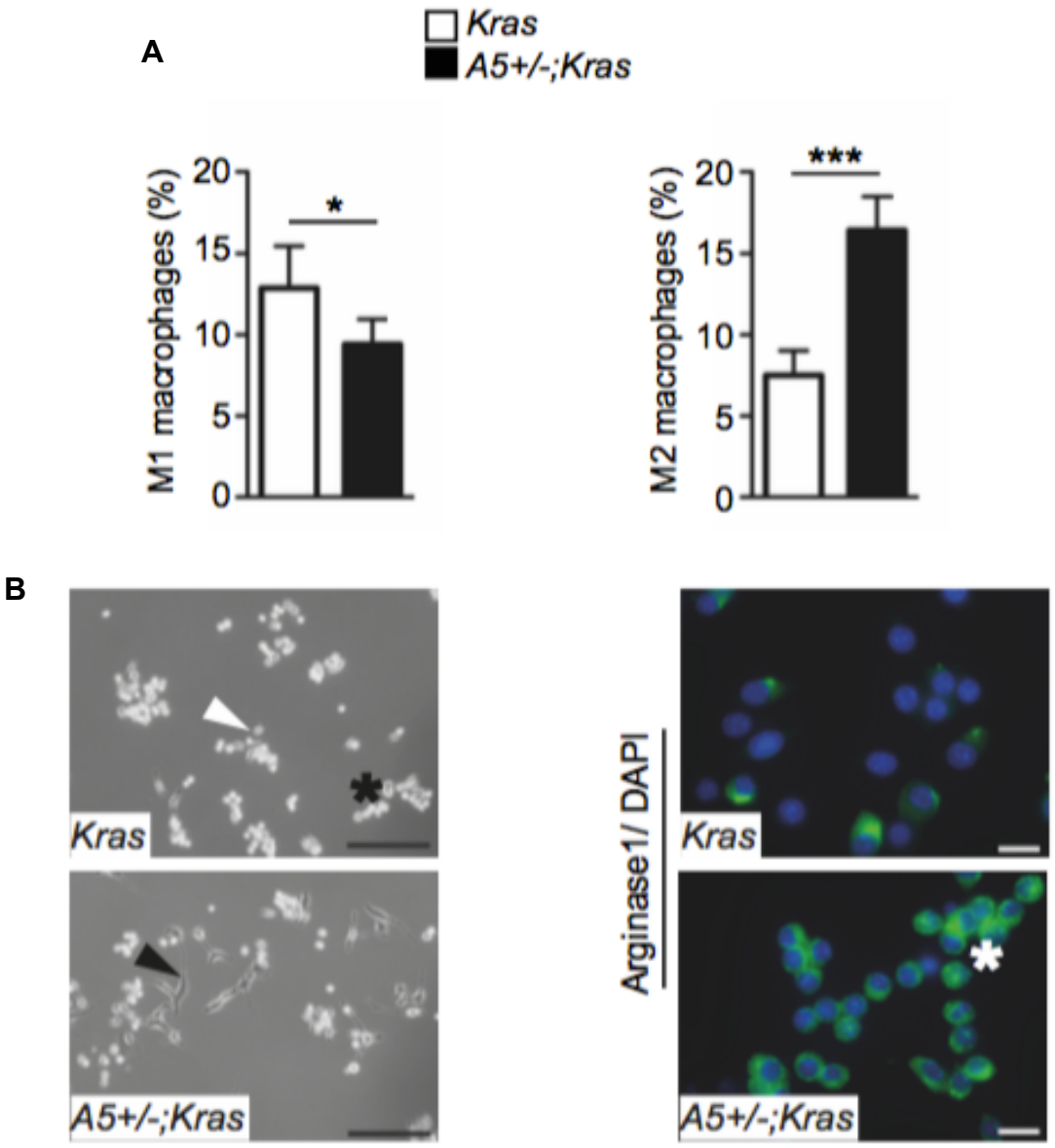

Figure 39: Monoallelic loss of Atg5 increases polarization of M2 macrophages via several cytokines and arginine. (A) Quantification of M1 and M2 macrophages (% of all macrophages) according to their morphology after stimulation with supernatants from *Kras* and *A5+/-;Kras* cells (n≥3); representative bright field pictures are shown indicating morphology of undifferentiated (asterisk), M1 (white arrowhead), and M2 (black arrowhead) macrophages. **(B)** Arginase-1 immunofluorescence in macrophages after stimulation with supernatants from *Kras* and *A5+/-;Kras* cells; nuclei are detected with DAPI. Mean±SD, **P<0.05, **P<0.01, ***P<0.001*. Scale bars equal 50µm.

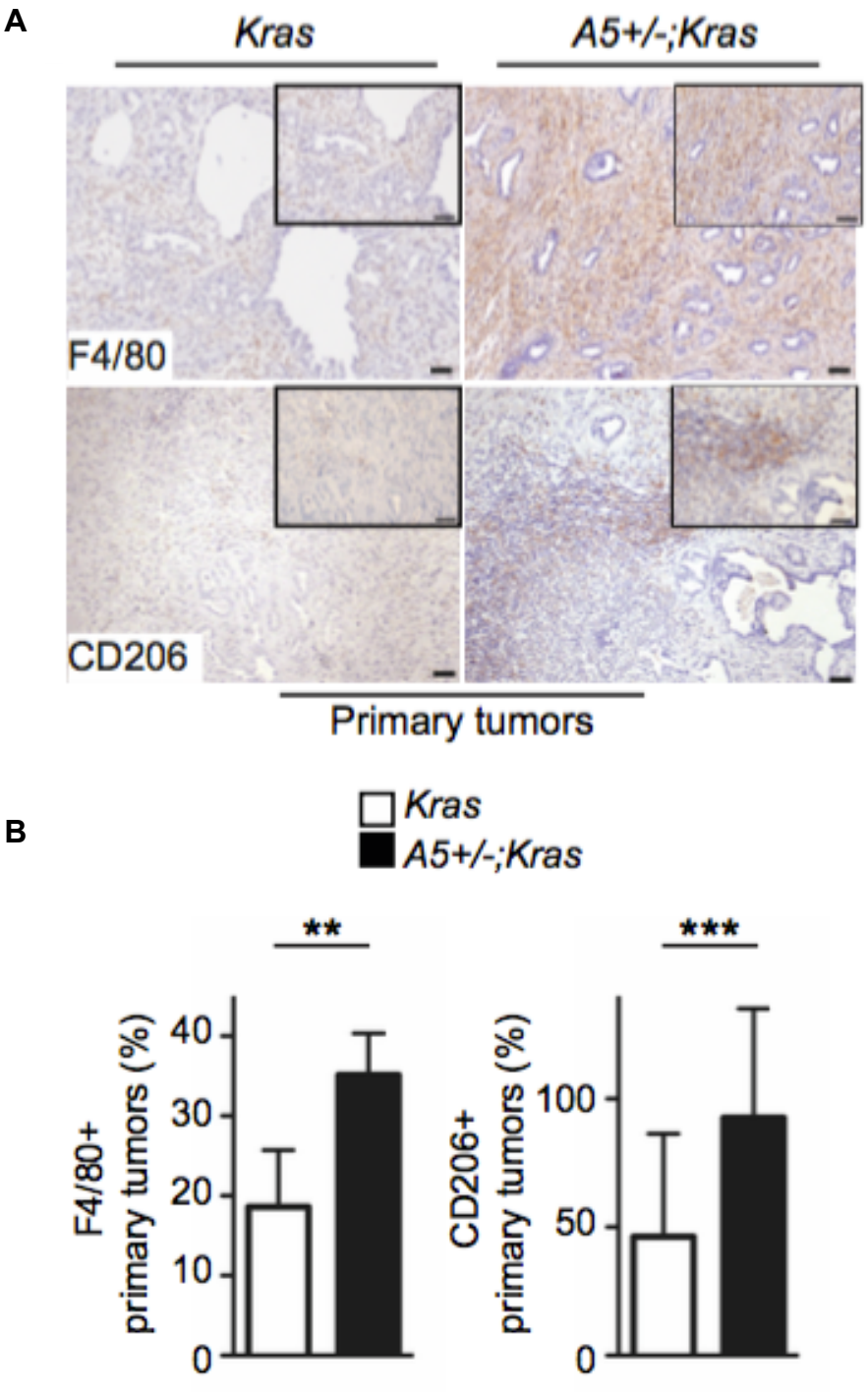

Figure 40: Monoallelic loss of Atg5 increases infiltration of macrophages and polarization of M2 macrophages *in vivo*. (A) Representative immunohistochemistry pictures of F4/80 and CD206 in primary tumors from *Kras* and *A5+/-;Kras* mice. **(B)** Quantification of F4/80 and CD206-positive macrophages (% positive nuclei) in *Kras* and *A5+/-;Kras* primary tumors (n>3). Mean±SD, **P<0.05, **P<0.01, ***P<0.001*. Scale bars equal 50µm.

Furthermore, the in vivo ability of *Kras* and *A5+/-;Kras* cells to attract macrophages is evaluated by quantifying F4/80 and CD206 in the original pancreatic tumor tissues of these mice (Figure 41A). Predominantly, F4/80- and CD206-macrophage numbers were clearly elevated in *A5+/-;Kras* tumors, indicating more CD206 and thus M2-macrophages after monoallelic loss of Atg5 (Figure 41B).

Additionally, F4/80 and Arginase-1 positive M2-macrophages were also called into the lungs of mice after tail vein injection of *A5+/-;Kras* compared to *Kras* cells (Figure 41), farther shielding the *in vitro* and *in vivo* findings (Figure 39- 40).

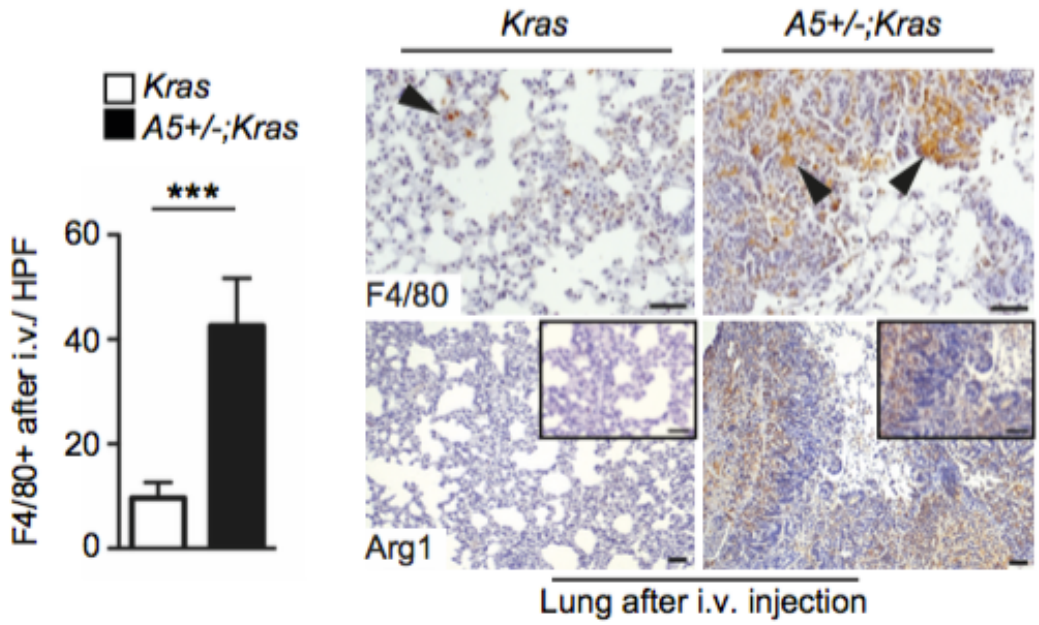

Figure 41: Monoallelic loss of Atg5 increases infiltration of macrophages and polarization of M2 macrophages in the lungs after IV injection. (A) Immunohistochemical quantification of F4/80-positive cells per high power field (HPF) in the lungs of mice after i.v. with *Kras* and *A5+/-;Kras* cells (n=20) (left); representative F4/80 and Arginase 1 (Arg1) immunohistochemistry in tissue sections from the lungs of mice after tail vein injection (i.v.) with *Kras* and *A5+/-;Kras* cells; black arrowheads indicate F4/80-positive macrophages (right). Mean±SD, **P<0.05, **P<0.01, ***P<0.001*. Scale bars equal 50µm.

5.5.3 Depletion of macrophages decreases metastatic capacity of A5+/-;Kras cells.

To reveal if macrophages critically prompt the metastatic capabilities of *A5+/-;Kras* cells, macrophages in wildtype mice were depleted by using liposomal- clodronate. Afterwards, tail vein injection of *A5+/-;Kras* cells was performed and then analyzed metastatic colonization in the lungs. Clodronate treatment was able to deplete most of the macrophages, as depicted by F4/80 immunohistochemistry (Figure 42, right). Interestingly, macrophage depletion significantly decreased metastasis of A5+/-;Kras cells compared to control liposome-treated mice, headlining the significance of infiltrating macrophages in potentiating metastasis. Consequently, monoallelic loss of Atg5 promotes changes in cytokine/ chemokine secretion from tumor cells arising in accumulation of M2-macrophages eventually shaping the inflammatory microenvironment to critically facilitate tumor aggressiveness and promote tumor metastasis.

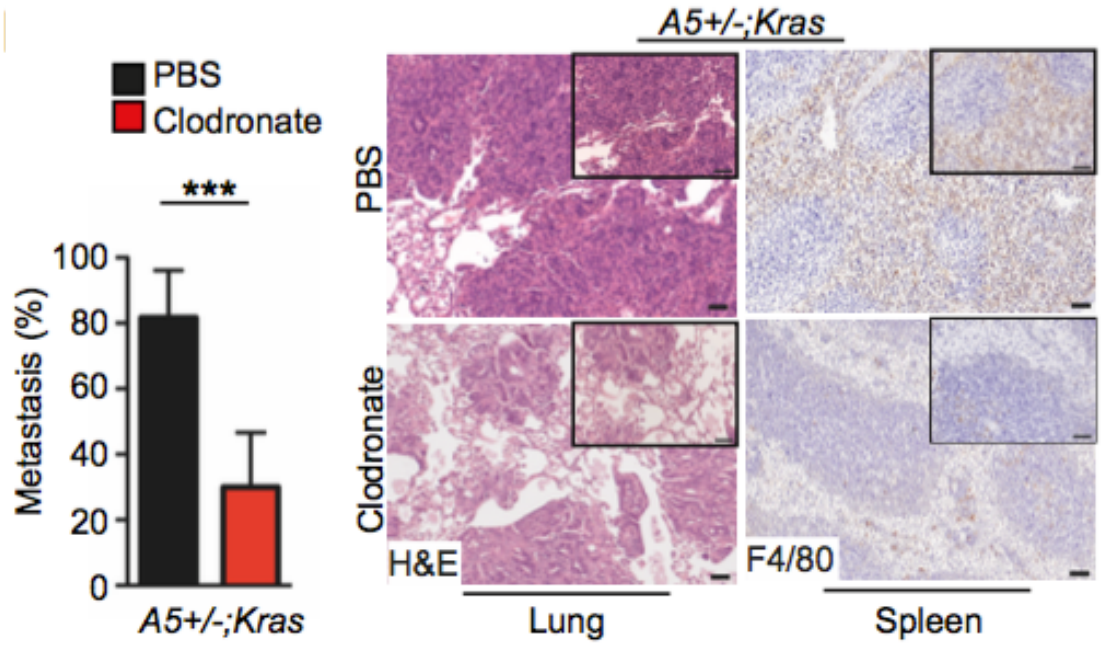

Figure 42: Metastasis of *A5+/-;Kras* cells can be reversed by macrophages depletion. Quantification of lung metastasis (% area) after tail vein injection of *A5+/-;Kras* cells into PBS or clodronate-treated wildtype mice (n>3) (left); representative H&E pictures of the lung and F4/80 immunohistochemistry pictures of the spleen after the respective treatments. Mean±SD, **P<0.05, **P<0.01, ***P<0.001*. Scale bars equal 50µm.

5.6 Levels of Atg5 are correlated to human pancreatic cancer aggressiveness.

To reveal a connection between the mouse model results and human pancreatic cancer ATG5 protein levels were analyzed in three independent patient cohorts (Tables 13, 14, 15). ATG5-ATG12 protein expression in lysates from pancreatic tumor patients (Cohort 1) was different between the samples (Figure 43, top). Grouping the patients into ATG5 high versus ATG5 low-moderate expression depicted a tendecy towards decreased survival in the low-moderate ATG5-expression group (Figure 43, bottom).

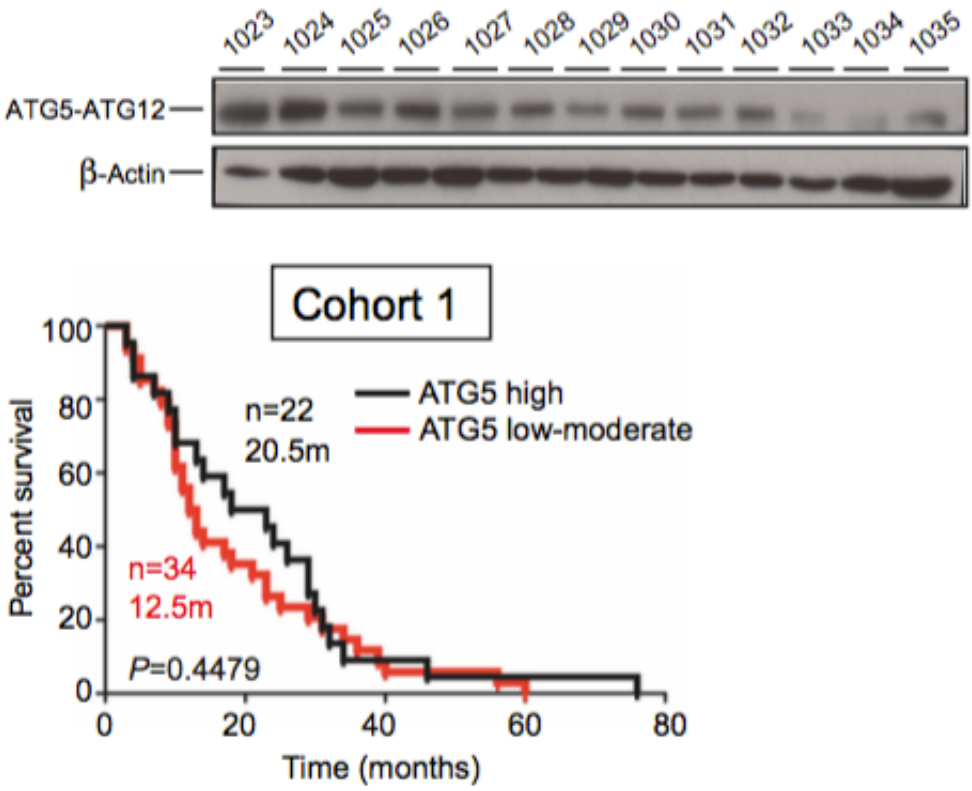

Figure 43: Low-Moderate levels of Atg5 protein levels in the human cancer tissues show tendency towards pancreatic cancer aggressiveness. ATG5-ATG12 protein levels in human pancreatic cancer samples (top); Kaplan-Meier survival analysis (months) with Cohort 1 patients separated into high (ATG5/ β-Actin ratio equal/ above 0,5; n=22, median survival 20,5 months) versus low-moderate (ATG5/ β-Actin ratio below 0,5; n=34, median survival 12,5 months) ATG5 expression groups (*P=0.4479*).

As a results of the variations in tumor cellularity and the restraints of western blotting, ATG5 immunohistochemistry was performed (Cohort 2 and Cohort 3). As anticipated

and already described (ProteinAtlas), ATG5 is expressed not only in the pancreatic epithelial tumor structures but also in other cell types (e.g., endothelial and islet cells) in the tissue (Figure 44).

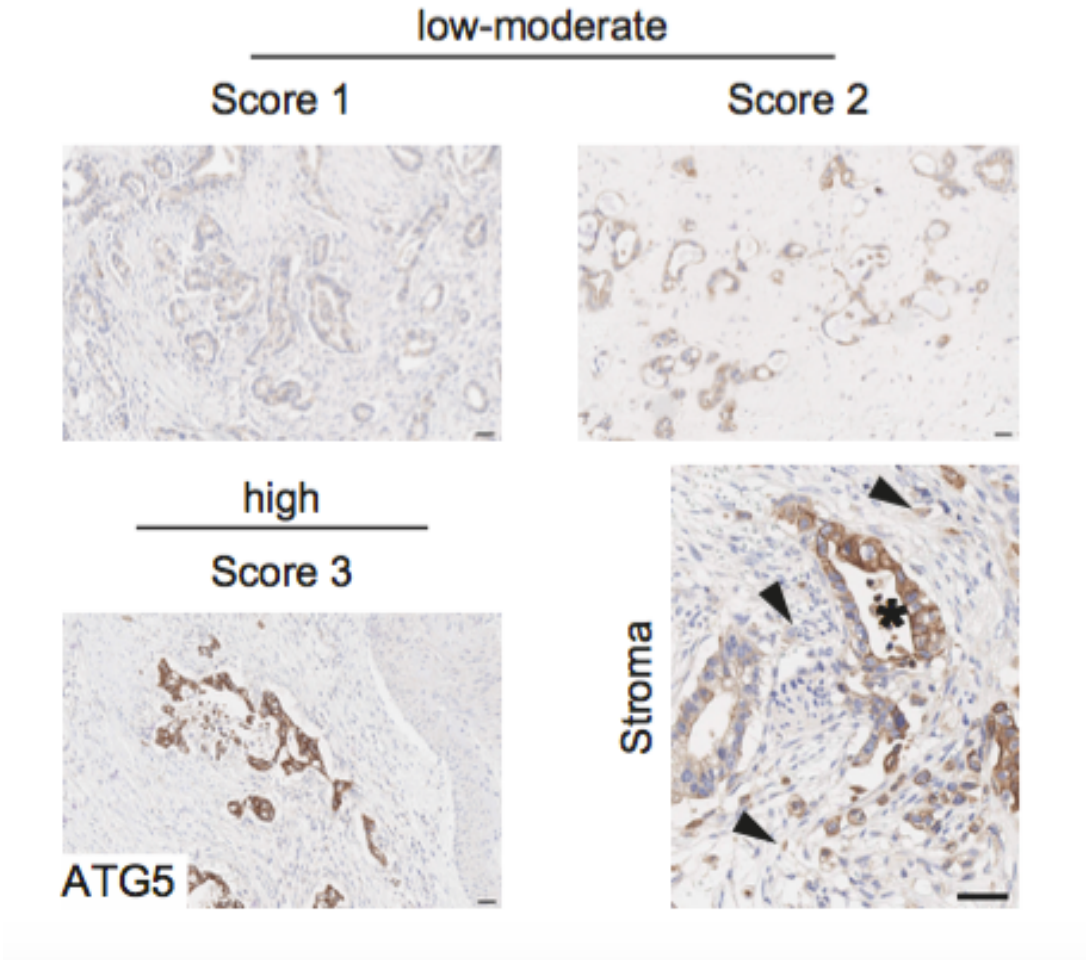

Figure 44: Atg5 is expressed in the tumor stroma and pancreatic islets, not only in the pancreatic cancer structures. Representative ATG5 immunohistochemistry in primary human PDAC tissues separated into Score 1/ 2 (low-moderate) and Score 3 (high); asterisk/ arrowhead/ circle mark epithelial cancer/ endothelial/ islet cells. Scale bars equal 50µm.

After determining an ATG5-expression score (Score 1, Score 2, Score 3), the patients were subdivided into low-moderate (Score 1, Score 2) and high (Score 3) ATG5 expression (Figure 44). Implementing this analysis on a small distant metastatic patient cohort (Cohort 2) depicted a higher metastasis incidence in the low-moderate ATG5 expressing patients (Figure 45).

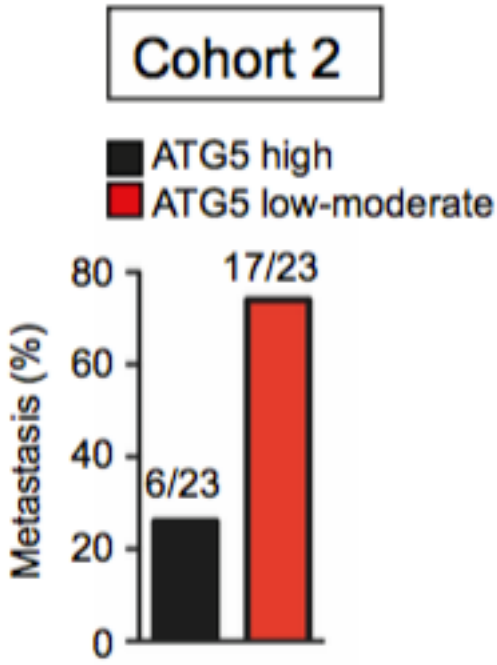

Figure 45: Low-moderate Atg5 expressing patients have more distant metastasis incidence. Distant metastasis incidence (%) in n=23 Cohort 2 patients separated into high (n=6) versus low-moderate (n=17) ATG5 expression groups according to Figure 43.

Moreover, reduced survival with lower ATG5 expression in a larger cohort of patients undergoing pancreatic cancer resection was significantly correlated (Cohort 3, Figure 46B). Because of no difference between the groups in terms of lymph node and resection status, excluding important confounding factors (Figure 46A), these analyses conceivably represent the re- occurrence of metastases and hereby aggressiveness of the tumors. Substantially, metastatic relapse in resected patients specifies survival. Finally, TCGA-databank analysis identified a reduction in ATG5 copy numbers between pancreatic cancer samples and normal human pancreas (Figure 47). In this way, lower levels of ATG5 are associated with increased pancreatic cancer metastasis and patient survival.

A

Cohort 3				
ATG5 level	pN0 (%)	pN1 (%)	R0 (%)	R1 (%)
low-moderate	21	79	66	30
high	17	83	65	30

B

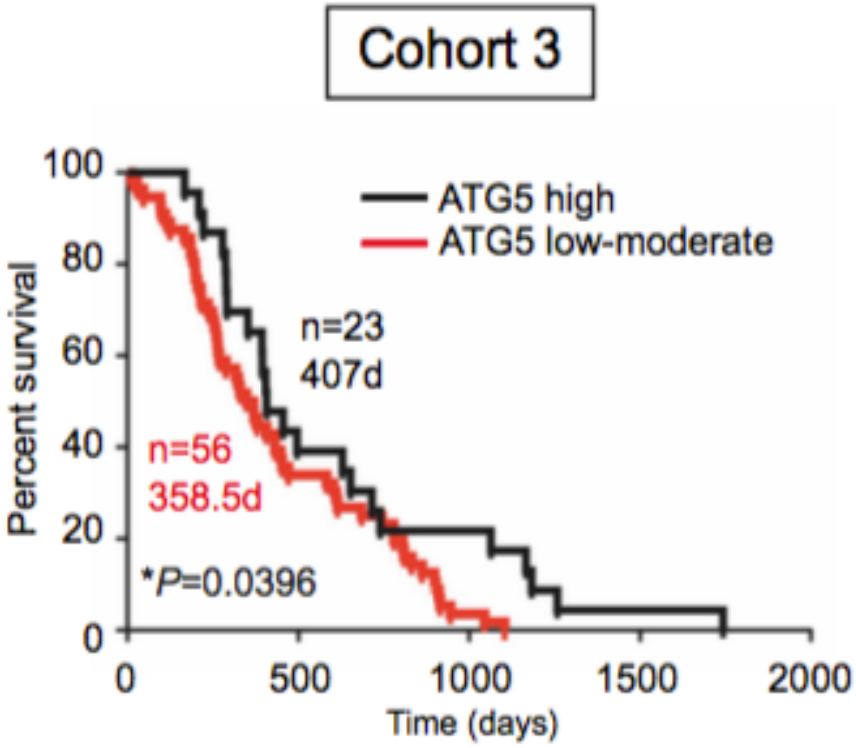

Figure 46: Low-moderate Atg5 expressing patients have shorter survival compared to high Atg5 expressing tumor patients. (A) Table shows lymph node infiltration (%, pN0, pN1) and resection status (%, R0, R1). **(B)** Kaplan-Meier survival analysis (days) with Cohort 3 patients separated into high (n=23, median survival 407 days) versus low-moderate (n=56, median survival 358,5 days) ATG5 expression groups according to Figure 41 (**P=0.0396*).

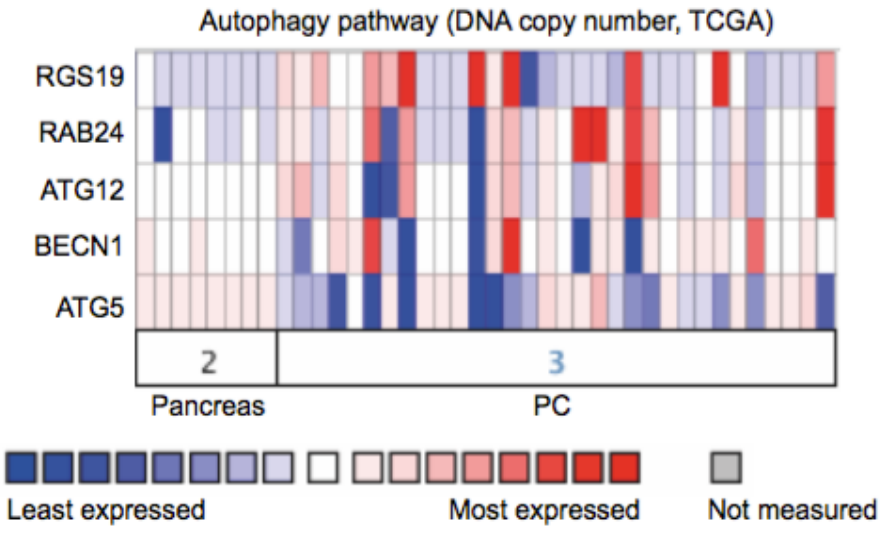

Figure 47: Pancreatic cancer samples express reduced Atg5 copy numbers compared to normal human pancreas in TCGA-databank. Illustration of autophagy-associated DNA copy number gain (red) or loss (blue) (TCGA data) in normal versus pancreatic cancer (PC) samples; blue bars correlate to less than hemizygous, white to hemizygous, and red to more than hemizygous levels.

Tables of Results

Table 12: PDAC and Metastasis in *A5+/-;Kras* mice. List of *A5+/-;Kras* mice that were used for Pancreatic Adenocarcinoma (PDAC) and metastasis quantification; mouse number (ID), Gender, Age (days), PDAC incidence, Histology, liver/ lung/ diaphragm metastasis, ascites incidence, and other abnormalities are presented; Male=M, Female=F, Yes=Y, No=N, Ductal=D, Undifferentiated=U, lymph node infiltration=LN, Spleen infiltration=Spl, Kidney infiltration=Kd.

ID	Gender	Age	PDAC	Histology	Liver	Lung	Diaphragm	Ascites	Others
7135	F	698	Y	D	N	N	N	N	
9138	F	293	Y	D	Y	N	N	N	LN
9137	F	340	Y	D	Y	Y	Y	Y	LN
9384	F	453	Y	D	Y	Y	Y	Y	Spl
2835	M	389	Y	U	N	N	N	N	
M5683	M	133	N	N	N	N	N	N	
M5681	M	346	Y	D	Y	Y	Y	Y	LN
M5617	F	385	Y	D	N	Y	N	N	
M5618	M	451	Y	D	N	Y	Y	N	
M5551	M	578	Y	D	Y	Y	N	Y	LN
P642	M	673	Y	D	Y	N	Y	Y	LN/Spl/Kd
M6215	F	451	N	N	N	N	N	N	

Table 13: Human pancreatic cancer patient cohort (Cohort 1). List of the analyzed human pancreatic cancer samples for ATG5-western blot (n=67). Patient ID, Histology (Pancreatic Ductal Adenocarcinoma (PDAC)), extent of primary tumor (T), lymph node infiltration (N), metastasis (M), tumor differentiation grade (G), survival (months), ATG5 protein expression normalized to b-Actin and quantified by ImageJ (ATG5 protein), and Tumor stage are shown. Samples marked with red or containing an X were not used in the analysis. The last 4 samples did not have patient data and were excluded from the study.

ID	Histology	T	N	M	G	Survival	ATG5 protein	Tumor stage
M374	PDAC	4	1	1	3	13	1,0351	IV
M758	PDAC	3	1	1	3	12	0,3039	IV
M604	PDAC	3	1	1	3	9	0,4598	IV
1021	PDAC	3	1	1	3	11	0,030	IV
1020	PDAC	3	1	1	2	7	0,000	IV
M247	PDAC	4	1	0	3	9	0,4715	III
M603	PDAC	4	1	0	3	12	0,1439	III
M060	PDAC	4	1	x	2	17	0,3686	III
M762	PDAC	4	1	x	2	5	0,2938	III
1009	PDAC	3	1	0	4	13	0,529	III
M704	PDAC	3	1	0	3	26	0,6242	IIB
M312	PDAC	3	1	x	3	10	0,5538	IIB
M606	PDAC	3	1	x	3	29	0,6852	IIB
M607	PDAC	3	1	x	3	29	0,6982	IIB
M440	PDAC	3	1	0	3	7	0,8726	IIB
M713	PDAC	3	1	0	3	4	0,7694	IIB
M190	PDAC	3	1	0	3	5	0,0162	IIB
1001	PDAC	3	1	0	3	3	0,488	IIB
1006	PDAC	3	1	0	3	lost to FU	0,621	IIB
1008	PDAC	3	1	0	3	10	0,491	IIB
1007	PDAC	3	1	0	3	4	0,526	IIB
1014	PDAC	3	1	0	3	14	1,308	IIB
1015	PDAC	3	1	0	3	9	0,966	IIB
1016	PDAC	3	1	0	3	17	1,005	IIB
1022	PDAC	3	1	0	3	11	0,428	IIB
1026	PDAC	3	1	0	3	lost to FU	0,838	IIB
1034	PDAC	3	1	0	3	lost to FU	0,042	IIB
1002	PDAC	3	1	0	2	3	0,380	IIB
1003	PDAC	3	1	0	2	29	0,382	IIB
1004	PDAC	3	1	0	2	25	0,350	IIB
1010	PDAC	3	1	0	2	34	0,649	IIB
1011	PDAC	3	1	0	2	46	0,548	IIB
1012	PDAC	3	1	0	2	31	0,758	IIB
1033	PDAC	3	1	0	2	lost to FU	0,167	IIB
M680	PDAC	3	1	0	2	10	0,1150	IIB
M214	PDAC	3	1	0	2	40	0,1565	IIB

M111	PDAC	3	1	0	2	3	0,9639	IIB
M324	PDAC	3	1	x	2	13	0,2582	IIB
M724	PDAC	3	1	x	2	10	0,2548	IIB
M584	PDAC	3	1	0	1	24	0,7767	IIB
1018	PDAC	3	1	0	1	56	0,210	IIB
1032	PDAC	3	1	X		14	0,535	IIB
M287	PDAC	2	1	0	1	23	0,1014	IIB
1017	PDAC	1	1	0	3	60	0,047	IIB
M510	PDAC	3	0	0	3	4	0,8050	IIA
M234	PDAC	3	0	0	3	31	0,4605	IIA
M109	PDAC	3	0	x	3	18	0,4859	IIA
M539	PDAC	3	0	x	3	8	0,5386	IIA
1023	PDAC	3	0	0	3	76	2,504	IIA
1025	PDAC	3	0	0	3	10	0,653	IIA
1030	PDAC	3	0	0	3	lost to FU	0,502	IIA
M598	PDAC	3	0	0	2	32	0,9114	IIA
M270	PDAC	3	0	x	2	21	0,3028	IIA
M732	PDAC	3	0	0	2	10	0,0518	IIA
M119	PDAC	3	0	x	2	39	0,3881	IIA
1005	PDAC	3	0	0	2	36	0,298	IIA
1024	PDAC	3	0	0	2	30	1,674	IIA
1028	PDAC	3	0	0	2	18	0,572	IIA
1029	PDAC	3	0	0	2	lost to FU	0,405	IIA
M211	PDAC	3	0	x	1	23	0,7472	IIA
M303	PDAC	3	0	x	1	34	0,1806	IIA
1031	PDAC	2	0	0	3	lost to FU	0,533	IB
M669	PDAC	2	0	0	2	23	0,0983	IB
1013	PDAC						0,848	
1019	PDAC						0,006	
1035	PDAC						0,312	
1027	PDAC						0,493	

Table 14: Human pancreatic cancer patient cohort (palliative/ metastatic, Cohort 2).
List of the analyzed human pancreatic cancer samples for ATG5-immunohistochemistry (n=26). Each row represents one individual diagnosed with PDAC and exhibiting distant metastasis (M1, i.e., HEP=hepatic, PER=peritoneal, SKI=skin, ADR=adrenal). Patients were resected between 2008 and 2013 at the University Hospital Heidelberg. ATG5 protein was detected by immunohistochemistry; membranous ATG5 was scored according to the percentage and intensity of positive cells on a 0 to 3+ scale (negative as score 0, faint expression as score 1+, moderate expression as score 2+ and strong expression as score 3+). The sum score is provided in the second column. Patients without ATG5 score were excluded from the analysis.

Histology	ATG5	M1
PDAC	2.3	HEP, PER
PDAC	3	HEP
PDAC		HEP
PDAC	2.8	HEP
PDAC	1	HEP
PDAC		HEP, PER, ADR
PDAC		HEP
PDAC	2.9	HEP
PDAC		HEP
PDAC	2	PER
PDAC	2	PER
PDAC	2.8	PER
PDAC	3	HEP
PDAC	2.1	HEP
PDAC	1.8	HEP
PDAC	2.5	HEP
PDAC	2	SKI
PDAC	2.9	HEP
PDAC	1.9	HEP
PDAC		HEP
PDAC		HEP
PDAC	3	HEP
PDAC	2.1	HEP
PDAC		SKI
PDAC	3	HEP
PDAC	3	HEP

Table 15: Human pancreatic cancer patient cohort (Cohort 3).
List of the analyzed human pancreatic cancer samples for ATG5-immunohistochemistry (n=134). Each row represents one individual diagnosed with PDAC (Pancreatic Ductal Adenocarcinoma) at the Charité University Hospital Berlin. Event of death (yes=1, no=0), Survival (days), lymph node status (pN), metastasis status (pM), tumor stage (pT), patient characteristics (gender, age), UICC tumor staging, and resection margin (R) are shown. ATG5 protein was detected by immunohistochemistry; membranous ATG5 was scored according to the percentage and intensity of positive cells on a 0 to 3+ scale (negative as score 0, faint expression as score 1+, moderate expression as score 2+ and strong expression as score 3+). The sum score is provided in the first column. Patients without death event and no registered survival were removed from the analysis.

ATG5	Death	Survival	pN	pM	pT	Gender	Age	Stage	R
2.7	1	431	0	0	2	w	74	Stage I	0
2	1	898	1	0	2	w	75	Stage IIB	0
1	0		0	0	3	w	64	Stage IIA	0
2.7	0	5748	1	0	3	w	56	Stage IIB	1
3	1	278	1	0	3	m	47	Stage IIB	0
1	1	780	1	0	2	m	67	Stage IIB	0
3	1	407	1	0	3	w	62	Stage IIB	0
2.4	1	452	1	1	3	m	31	Stage IV	1
3	1	1166	1	0	2	w	63	Stage IIB	0
2.5	1	215	0	0	2	w	58	Stage I	0
3	1	629	1	0	2	m	53	Stage IIB	1
2.8	1	329	1	0	3	w	62	Stage IIB	0
2.8	1	46	0	0	2	w	61	Stage I	0
2.9	1	406	1	0	3	m	69	Stage IIB	0
2.1	1	236	0	0	2	w	70	Stage I	1
2.6	0	2459	0	0	2	w	71	Stage I	
2.6			1	0	2	m	64	Stage IIB	0
2.2	1	862	1	0	2	w	64	Stage IIB	0
2.3	1	448	1	0	2	m	71	Stage IIB	0
2.5	0	2302	1	0	2	m	64	Stage IIB	
3	1	287	1	0	3	w	47	Stage IIB	1
3	0	305	1	0	3	m	62	Stage IIB	
1.3	1	945	1	0	3	w	75	Stage IIB	0
2.2	1	832	1	0	3	w	62	Stage IIB	0
2.9	1	685	0	0	3	w	59	Stage IIA	
1.2			1	0	3	m	50	Stage IIB	0
2	1		1	0	2	m	60	Stage IIB	
1.3	0	2049	0	0	3	m	63	Stage IIA	0
2.2			1	0	3	m	66	Stage IIB	0
2.9	1	1045	1	0	3	w	49	Stage IIB	0
2.9	0	2104	0	0	2	w	64	Stage I	0
3	1	1743	1	0	2	m	71	Stage IIB	0
2.2			1	0	3	w	59	Stage IIB	0
1.2	0		0	0	3	m	59	Stage IIA	0
2.9	1	744	1	0	3	w	73	Stage IIB	1
3	1	740	1	0	3	m	50	Stage IIB	0
3	1	1258	0	0	3	w	62	Stage IIA	0
2.5	1	809	1	0	3	w	61	Stage IIB	0
3	1	167	1	0	3	m	66	Stage IIB	0

2	1	348	1	0	3	w	59	Stage IIB	1
2.2	1	911	1	0	3	m	64	Stage IIB	0
2.5	1	779	0	0	3	w	69	Stage IIA	0
2.9	1	471	0	0	2	w	76	Stage I	0
2.3	1	125	1	0	3	m	63	Stage IIB	0
2.2	0	1427	0	0	3	m	65	Stage IIA	1
3	1	395	0	0	3	m	60	Stage IIA	0
1.2	1		1	0	2	w	77	Stage IIB	
3	1		1	0	3	m	38	Stage IIB	
2	1		1	0	3	w	76	Stage IIB	1
3	0		1	0	3	m	63	Stage IIB	1
3			1	0	3	w	65	Stage IIB	0
2.6	1	432	0	0	2	w	69	Stage I	0
2.7	1	805	1	0	3	m		Stage IIB	
2.2	0	2644	0	0	3	w	62	Stage IIA	
3	1	496	1	0	3	w	79	Stage IIB	
2.8	1	198	1	0	3	m	49	Stage IIB	0
3	1		1	0	3	m	70	Stage IIB	
3	1	404	1	0	3	m	73	Stage IIB	
2.8	1		0	0	3	w	77	Stage IIA	
2	1	902	1	0	3	w	73	Stage IIB	
2.8	1	112	1	1	3	m	55	Stage IV	0
3	1	715	1	0	3	m	64	Stage IIB	0
3	1	209	1	0	3	w	51	Stage IIB	0
2.8	1	260	1	0	3	m	51	Stage IIB	0
3	1	353	1	0	3	w	67	Stage IIB	0
3	0		1	0	3	m	48	Stage IIB	
1.8	1	611	1	0	3	w	78	Stage IIB	0
2.9	1	98	1	0	3	w	63	Stage IIB	0
2.7	1	28	0	0	3	w	74	Stage IIA	1
2.7	0	2645	1	0	2	m	53	Stage IIB	0
2	0		0	0	2	w	59	Stage I	0
3	0	2609	1	0	3	m	69	Stage IIB	0
2.8	1		1	0	3	m	72	Stage IIB	0
2.8	1	255	1	0	3	m	74	Stage IIB	0
3	1		0	0	3	m	78	Stage IIA	0
2.9	1	184	0	0	4	w	72	Stage III	0
3	1	291	1	0	3	w	69	Stage IIB	0
3	0	1273	0	0	3	m	56	Stage IIA	0
3	1	1183	0	0	3	m	50	Stage IIA	0
2.6	1	96	1	0	3	w	75	Stage IIB	1
3	1		1	0	3	m	57	Stage IIB	0
0.7	1		1	0	4	w	70	Stage III	0
3	1	1064	1	0	3	m	72	Stage IIB	1
2	1	288	1	0	3	w	61	Stage IIB	0
2.8	1	192	1	0	4	m	57	Stage III	1
2.8	1	370	1	0	3	w	74	Stage IIB	0
2.9	1	1186	1	0	3	w	72	Stage IIB	0
3	1	394	0	0	3	m	69	Stage IIA	1
3	0	17	1	0	3	w	68	Stage IIB	1
1	1	369	0	0	3	w	79	Stage IIA	1
2.8			1	0	3	w	62	Stage IIB	1
2.8	0	7	1	0	3	m	60	Stage IIB	1
3	1	59	1	0	3	w	61	Stage IIB	1

3	1	289	1	0	4	m	60	Stage III	1
3			1	0	3	m	70	Stage IIB	0
2.2			0	0	1	m	66	Stage I	0
3	1	222	1	0	3	m	61	Stage IIB	1
2.05	0	415	0	0	3	w	81	Stage IIA	0
3	1	653	1	1	3	w	46	Stage IV	0
2	1	12	1	0	4	m	69	Stage III	1
3			1	0	3	m	59	Stage IIB	1
2.8	0	12	1	0	3	m	67	Stage IIB	0
2.8	1	205	1	0	3	m	69	Stage IIB	1
3			1	0	4	m	73	Stage III	0
2.5	1	615	1	0	3	m	54	Stage IIB	1
2.3	1	263	1	0	3	m	67	Stage IIB	1
2.7			0	0	3	m	65	Stage IIA	0
2	1	915	0	0	3	m	68	Stage IIA	0
3			1	0	3	m	75	Stage IIB	0
2	1	316	1	0	3	m	64	Stage IIB	0
3	1		1	0	2	m	73	Stage IIB	0
1.8	0	1079	1	0	3	w	59	Stage IIB	0
3	1	455	1	0	3	m	56	Stage IIB	0
2.7	0	210	1	0	3	m	43	Stage IIB	1
1.2	1	603	1	0	3	w	58	Stage IIB	1
2.8	0	865	1	0	3	w	57	Stage IIB	0
2.3			1	0	3	m	77	Stage IIB	1
3	0	311	1	0	3	m	61	Stage IIB	0
2.3	1	199	1	1	3	m	41	Stage IV	0
2.9	0	866	0	0	3	m	75	Stage IIA	0
2.2	1	582	1	0	3	m	75	Stage IIB	0
2.1			1	0	3	w	75	Stage IIB	1
2.3	1	265	1	0	4	m	74	Stage III	1
2	0	696	1	0	3	w	66	Stage IIB	0
2.2	1	185	1	0	3	m	51	Stage IIB	1
2.1	1	268	1	0	3	w	81	Stage IIB	0
2.9	0	586	0	0	3	m	69	Stage IIA	0
1.5	0	5	0	0	3	w	69	Stage IIA	0
2.2	1	1104	1	0	3	w	68	Stage IIB	0
2.6	1	324	1	0	3	w	68	Stage IIB	1
2.2	1	380	1	0	3	m	58	Stage IIB	0
2.3	1	249	1	0	3	w	63	Stage IIB	0
2.3	1	166	1	0	3	m	72	Stage IIB	0
2.8	1	216	1	0	3	m	55	Stage IIB	1

6 DISCUSSION

Autophagy has been shown to play a dual role in tumorigenesis of different tissue types [131,132]. Specifically, autophagy appears to accelerate tumor initiation whilst hindering progression of pre-neoplastic lesions, as demonstrated in PDAC [64,133]. Studies have primarily exploited models with complete loss of autophagic function, which is usually not seen in human patients. Herewith, the effect of varying levels of Atg5 on PDAC-development was analyzed. Stunningly, bi-allelic loss of Atg5 blocks tumorigenesis, while monoallelic loss of Atg5 boosts tumorigenesis and metastasis. Cell intrinsic changes in mitochondrial homeostasis, cytoplasmic Ca2+ responses, autophagy regulation, extracellular activities of lysosomal cathepsins, and tumor promoting changes in the inflammatory microenvironment were pivotal for the heightened PDAC-aggressiveness. Importantly, shRNA-mediated *Atg5*-dosage regulation also enhanced metastatic capabilities of pancreatic cancer cells, showing that a smooth decrease in *Atg5*-levels is sufficient to impact PDAC-metastasis. The clinical importance of this observation is supported by the analysis of three independent human pancreatic cancer cohorts corroborating the connection between Atg5-levels, PDAC-metastasis, and patient survival.

6.1 Levels of Atg5 determine PDAC-aggressiveness but do not influence canonical autophagy

Autophagy is tightly linked with PDAC and multiple pathways determine this interaction, e.g., ER-stress, ROS-levels, mitochondrial metabolism, hypoxia, and the surrounding tumor microenvironment [63,64,134]. Past studies have shown that the interaction between autophagy and oncogenic *Kras* during PDAC-development and progression is also controlled by other genetic alterations, but conflicting results could not provide clear answers [63,64]. Our preceding analysis of consecutive pancreatic cancer stages (ADM, PanIN, tumor, metastasis) implied targeted induction of autophagy during PDAC-development, confirming previous results on steady elevation of threshold autophagy during pancreatic tumorigenesis. The significance of autophagy in pancreatic cancer progression was further verified by homozygous deletion of Atg5, confirming results from past publications [63,64]. Along the same line, whole-body inhibition of autophagy by Atg4B in a reversible and irreversible manner

was recently shown to control pancreatic tumor growth via intrinsic and extrinsic mechanisms in mice [134]. Unlike biallelic loss of Atg5 however, monoallelic loss of Atg5 yielded higher tumor incidence and metastasis occurrence. *Atg5*-dosage regulation via shRNA-mediated knockdown also boosted metastatic capacities of pancreatic cancer cells, showing that despite the clear phenotypic difference between complete existence of Atg5, partial presence, and complete absence of Atg5, the phenotypic effect pursues *Atg5*-dosage in a non-linear trend. Monoallelic loss of autophagy related proteins holds an importance for several cancer types. Especially, the *Beclin 1* autophagy gene is monoallelically deleted in 40–75% of cases of human ovarian, prostate and breast cancers [135–14]. However, monoallelic inactivation of Atg5 has not been demonstrated in human cancers in depth. Heretofore, only one published study has revealed a connection between monoallelic deletion of Atg5, increased metastasis, and therapeutic resistance in melanoma supporting our results [143]. Underlying mechanisms for the phenotype in melanoma continued to be undefined in detail.

Atg5 as one of the important members of the Atg-conjugation system is required for autophagic stream. Atg-mediated closure of inner autophagosomal membrane components is necessary for lysosomal degradation and recycling [144]. Consequent to complete loss of Atg5 in the pancreas, autophagosomes accumulate in acinar cells and autophagic degradation is hindered by showing a significant accumulation of *p62* [124]. Nevertheless, the influence of *Atg5*-monoallelic loss on autophagic flux is unclear. During evaluation of the effects of *Atg5*-monoallelic loss on autophagy in isolated murine pancreatic cancer cells, decreased Atg5-protein levels were observed. Curiously, attenuated protein amounts did not result in an apparent negative consequence on autophagy as *A5+/-;Kras* cells were more resistant to autophagy inhibitors or activators by maintaining a constant level of autophagy. Additionally, *A5+/-;Kras* cells were functionally not affected by manipulation of autophagy. Therefore, monoallelic loss of Atg5 enhanced autophagy levels in a cell-intrinsic manner, showing active adaptation of pancreatic cancer cells. Atg5 is considered to be one of the crucial molecules for the induction of macroautophagy. But autophagy can take place via several pathways which are the *Atg5*-dependent, and the *Atg5*-independent alternative pathways [145–147].

6.2 Monoallelic loss of Atg5 increases aggressiveness of pancreatic cancer.

Loss of one allele of Atg5 predominantly changed not only autophagic induction, but also tumor cell aggressiveness by augmenting migration and invasion. Importantly, *Atg5*-heterozygous cell lines could form tumors in hosts and give rise to more distant metastases. Metastasis to distant tissues involves a multiple-step cascade starting with invasion [148,149]. To promote survival and metastatic outgrowth, cancer cells have to traverse through a set of cellular adaptations including phenotypic and metabolic adaptations [96].

Mitochondrial changes [150], intracellular Ca^{2+} amplitudes [151], extracellular matrix degradation by lysosomal cathepsins [152], and the pro-metastatic tumor microenvironment [153] have been shown to determine tumor progression and aggressiveness. Loss of one allele of Atg5 was able to alter mitochondrial dynamics in cancer cells. Particularly, mitochondrial function was decreased, while specific mitochondrial stress markers were increased. Mitochondrial turnover was also altered as more fission events could be observed coupled with an increase of mitochondrial mass in the autophagosomal fraction, depicting ingestion of damaged, superfluous, and effete mitochondria. Recent studies have shown that increased mitochondrial fission and fragmentation promote tumor cell growth, migration, and invasion [150]. Furthermore, mitochondrial metabolism is essential to patronize cancer cell dissemination, during which a particular degree of cell stress is required to switch mitochondrial programming and contribute to cellular adaptation [77,154,155]. Mitochondria are also important adjusters of cytoplasmic Ca^{2+} by sequestrating and releasing it [83]. Especially in the pancreas, Ca^{2+} signaling controls secretion of fluids and enzymes from pancreatic acinar cells under physiological conditions and its translocation on cytoskeletal proteins as a messenger regulates migratory activities [156,157]. Interestingly, intracellular Ca^{2+} oscillations are involved in tumor cell dissemination determining migration and vesicle trafficking. Calcium dependent regulation of S100a4 determines interaction with cytoskeletal proteins, e.g., myosin heavy chain IIa to increase lamellipodial structures required for migration and invasion [91,93]. Previous studies have shown that S100a4 has tight connections with motility, invasion, and chemoresistance in pancreatic cancer [157–160]. Along the same lines, monoallelic loss of Atg5 increased FBS-mediated migration/ invasion, FBS-

induced Ca^{2+} responses as well as expression of Ca^{2+} binding proteins (S100a4). In support, *Atg5*-expression was recently linked to heightened tumor cell metastasis via disrupting the V_1V_0-ATPase, which is closely connected to cytosolic Ca^{2+} , indicating a pathway through which a autophagy-related gene can promote metastasis in an autophagy-independent manner. Consequently, monoallelic loss of Atg5 establishes an intermediate stress level in tumor cells characterized by defective mitochondrial homeostasis and Ca^{2+} signaling, which intensifies their aggressive and metastatic potential.

Increased activity of lysosomal cathepsins has an inevitable role in the cascade of invasion and metastasis [152]. Lysosomes are also one of the specific organelles handling Ca^{2+} homeostasis via expression of Ca^{2+} channels [161]. A calcium-permeable channel namely transient receptor potential melastatin 2 (TRPM2) is specifically activated by intracellular adenosine diphosphoribose (ADPR) metabolite [88,162]. ADPR was increased in *A5+/-;Kras* compared to *Kras* cells postulating a first hint of the involvement of lysosomes in the metastatic cascade. Lysosomal Ca^{2+} signaling regulates cellular homeostasis via autophagic induction [86,163]. In addition, lysosomes contain cysteine cathepsins, which are not only in charge of degradation, but also execute a role in autophagy, stress signaling, metabolism, and lysosome-mediated cell death to maintain cellular homeostasis. Cathepsins control the amount of autophagosomes and lysosomes [164]. Additionally, increased lysosomal cathepsin D contributes to metastatic spread of pancreatic cancer cells with the overexpression of S100P, a member of the calcium-binding protein family [165]. Therefore, lysosomal Ca^{2+} signaling constitutes an important regulator of migration and invasion. *A5+/-;Kras* cells showed heightened extracellular cathepsin activation. Importantly, cathepsin activation in the extracellular medium was essential and sufficient to allow invasion of cancer cells. Monoallelic loss of Atg5 may in this scenario trigger multiple cellular changes starting with mitochondrial, lysosomal, and Ca^{2+} homeostasis. Feedback between Ca^{2+} signaling and lysosomes may impinge lysosomal homeostasis and fusions with autophagosomes, deteriorated even further by the direct effects of Atg5 on autophagy levels. Therewithal, it was shown that the interaction of Atg5-Atg12 with the tethering factor TECPR1 (Tectonin Beta-Propeller Repeat Containing 1) is crucially involved in the initiation of autophagosomal/ lysosomal fusion to promote autophagic flux [166]. Consequently, monoallelic loss of Atg5 could be closely associated to impaired lysosomal biogenesis and fusion. A

penurious autolysosomal maturation process may thus lead to an accidental activation of pro-cathepsins and subsequently their leakage via lysosomal exocytosis into the extracellular medium eventually mediating migration, invasion, and metastasis.

6.3 Loss of one Atg5-allele induces a pro-tumorigenic tumor microenvironment by stimulating M2 macrophages

The inflammatory response, cytokine maturation, and cytokine secretion can be coordinated by lysosomal pathways and homeostasis [167,168]. The inflammatory tumor microenvironment has a pivotal role in promoting spontaneous PDAC-development and augmenting the metastatic cascade. PDAC-promoting immune microenvironment comprises many cell types like M2-macrophages, lymphocytes, and neutrophils [169,170]. Interestingly, the cytokine profile of *A5+/-;Kras* but not *Kras* cells could be specified as M2 macrophage-promoting. The cytokines included in the profile were CXCL1/ CXCL12 known to affect macrophages, M-CSF/ CXCL12/ IL10/ CXCL2/ IL1ra/ CXCL10 crucial for M2-polarization, and TNFa known to premediate tumor progression and metastasis [171]. Contrastingly GM-CSF, an M1-polarizing factor [172] and sICAM-1, an M1-chemoattractant [173], were downregulated. In addition to that, one of the most significantly increased metabolites in *A5+/-;Kras* cells was Arginine. Tumor associated macrophages, polarizing to the M2-phenotype, require Arginine for their metabolism [174–177]. In support of all these data increased M2-macrophages were observed in the *A5+/-;Kras* original pancreatic tumors as well as in the lung metastases formed after tail vein injection of *A5+/-;Kras* cell lines. Remarkably, depleting macrophages via liposomal clodronate significantly decreased *A5+/-;Kras* cell metastasis *in vivo*, highlighting the significance of macrophages in redounding metastasis. Consequentially, monoallelic loss of *Atg5* enkindles cell-intrinsic changes, which ultimately alter the tumor microenvironment favoring metastatic spread to distant organs (Figure 48).

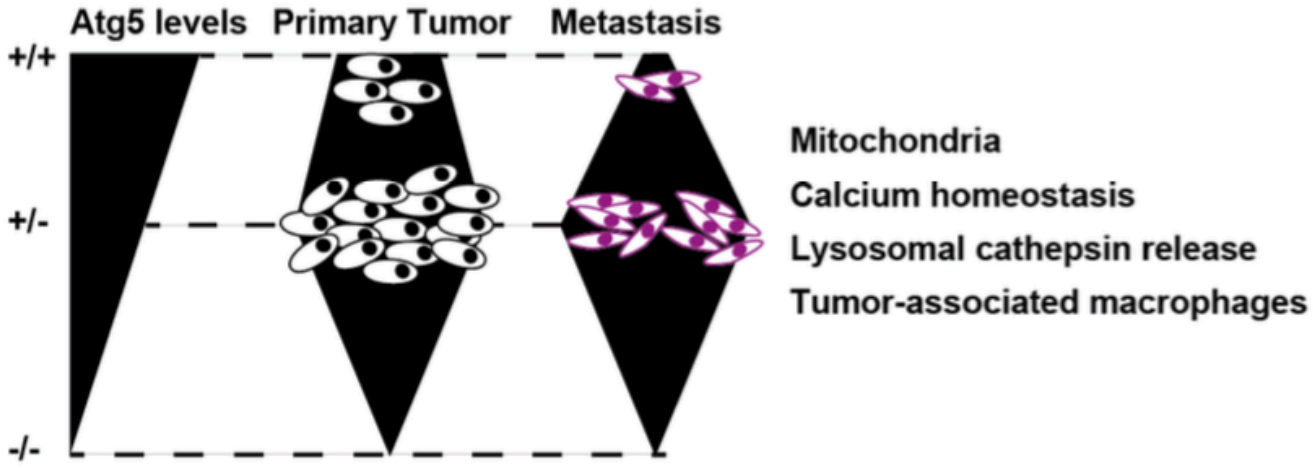

Figure 48: Monoallelic loss of Atg5 initiates autonomous and non-autonomous cellular changes in terms of mitochondria, calcium homeostasis, lysosomal cathepsin release and tumor associated macrophages. See text for details. White and purple cells represent primary tumor cells and metastatic cells, respectively. Cellular adaptations were classified as mitochondrial stress, calcium homeostasis, lysosomal cathepsin release and tumor associated macrophages. Each geometric shape approximates primary tumor and metastasis occurrence at various expression levels of Atg5.

6.4 Decreased levels of Atg5 are correlated to human pancreatic cancer aggressiveness.

As it is mentioned above only the autophagy protein Beclin-1 has been found monoallelically deleted in a variety of cancer types, such as breast, ovarian, and prostate cancer. In favor of these findings *Beclin-1* heterozygous mice presented with frequent spontaneous malignancies [135]. The correlation of Atg5-protein expression with metastasis and survival in three independent human pancreatic cancer cohorts expands the spectrum of monoallelically affected autophagy genes to Atg5. Clinical trials on pancreatic cancer patients are currently evaluating the efficacy of autophagy inhibitors such as chloroquine in adjuvant therapies combined with gemcitabine (NCT01777477) [178,179]. Nevertheless, autophagy inhibitors are not only less specific, but most probably only incompletely hinder autophagic flux [180]. As it is depicted that monoallelic loss of Atg5 elicits chloroquine resistance and higher metastatic dissemination, administration of chloroquine may herewith lead to the production of resistant cancer cell subclones with heightened aggressiveness. In addition, when applying autophagy inhibitors in clinical trials for pancreatic cancer patients,

increased awareness is needed for their systemic effects on patients. Cytotoxic chemotherapeutic regimens may accelerate aging [181]. It is known that autophagy acts as a promoter of longevity [182]. Therefore, using autophagy inhibitors as adjuvant therapies with chemotherapeutic regimens may fasten aging of other organs. Consequently, side effects of chemotherapeutic regimens would increase on patients while simultaneously treating them with autophagy inhibitors. Dosages of several genes and oncogenes influence tumor development and aggressiveness [183,184]. Atg5-dosage may alter response against chemotherapeutics and influence tumor aggressiveness. Therapeutic strategies to manipulate autophagy in PDAC should consider the effects of Atg5 to prevent the expansion of resistant and highly aggressive cancer cells.

7 SUMMARY

The main focus of the present study was to analyze the role of autophagy related gene Atg5 in pancreatic cancer development and progression. Autophagy has a pivotal role to maintain cellular homeostasis in terms of cell growth, proliferation, and metabolism. Inhibition of autophagy has been suggested to act against to tumor growth in pancreatic cancer. But the autophagy-independent roles of autophagy-related proteins have not been analyzed in pancreatic cancer yet.

To exemplify, the significance of autophagy-related 5 protein in pancreatic cancer development and progression, pancreas-specific Atg5 monoallelic and biallelic deleted Kras mutation harboring mice were generated and characterized in detail. Addition to *in vivo* mouse models, isolated murine pancreatic cancer cells were used to analyze the effect of Atg5 *in vitro*. Finally, metastatic status, survival, and Atg5 levels were analyzed in human PDAC patients.

Pancreas specific monoallelic loss of Atg5 in *Kras* mutation harboring cancer model resulted in significantly higher cancer and metastasis incidence compared to *Kras* model. Decreased levels of Atg5 enabled murine pancreatic cancer cells resistant to induction and inhibiton of autophagy. Altered mitochondrial morphology, compromised mitochondrial function, amendments in intracellular Ca^{2+} flux, and increased activity of extracellular cathepsin L and D were observerd in *A5+/-;Kras* tumor cells. In *A5+/-;Kras* tumors, tumor microenvironment had increased amount of type 2 macrophages compared *Kras* tumors. Cytokine profile of *A5+/-;Kras* tumor cells was changed compared to control tumor cells in terms of macrophage chemoattraction and differentiation into M2 macrophage. Knockdown of Atg5 in murine pancreatic cancer cell lines also increased migratory and invasive capacities, and metastatic dissemination following injection into littermate mice. In human PDAC tissues, lower levels of Atg5 correlated with tumor metastasis and shorter survival time.

In mice that harbor oncogenic *Kras* in pancreatic cells, heterozygous obliteration of Atg5 and decreased protein levels enchange tumor development, whereas homozygous deletion of Atg5 blocks pancreatic tumorigenesis. Therapeutic approaches to manipulate autophagy in PDAC should take in consideration the

effects of Atg5 levels to prohibit the expansion of resistant and highly aggressive cells.

8 REFERENCES

1. Levy JMM, Towers CG, Thorburn A. Targeting autophagy in cancer. *Nat Rev Cancer*. 2017;17(9):528-542. doi:10.1038/nrc.2017.53
2. Novikoff AB, Beaufay H, De Duve C. Electron microscopy of lysosome-rich fractions from rat liver. *J Cell Biol*. 1956. doi:10.1083/jcb.2.4.179
3. Klionsky DJ, Abdelmohsen K, Abe A, et al. Guidelines for the use and interpretation of assays for monitoring autophagy (3rd edition). 8627. doi:10.1080/15548627.2015.1100356
4. Mizushima N. Autophagy: Process and function. *Genes Dev*. 2007. doi:10.1101/gad.1599207
5. Mizushima N, Yoshimori T, Ohsumi Y. The Role of Atg Proteins in Autophagosome Formation. *Annu Rev Cell Dev Biol*. 2011;27(1):107-132. doi:10.1146/annurev-cellbio-092910-154005
6. Sica V, Galluzzi L, Bravo-San Pedro JM, Izzo V, Maiuri MC, Kroemer G. Organelle-Specific Initiation of Autophagy. *Mol Cell*. 2015. doi:10.1016/j.molcel.2015.07.021
7. Cecconi F, Levine B. The Role of Autophagy in Mammalian Development: Cell Makeover Rather than Cell Death. *Dev Cell*. 2008. doi:10.1016/j.devcel.2008.08.012
8. Deretic V, Levine B. Autophagy, Immunity, and Microbial Adaptations. *Cell Host Microbe*. 2009;5(6):527-549. doi:10.1016/j.chom.2009.05.016
9. Levine B, Kroemer G. Autophagy in the Pathogenesis of Disease. *Cell*. 2008. doi:10.1016/j.cell.2007.12.018
10. Menzies FM, Moreau K, Rubinsztein DC. Protein misfolding disorders and macroautophagy. *Curr Opin Cell Biol*. 2011. doi:10.1016/j.ceb.2010.10.010
11. Mizushima N, Yoshimori T, Levine B. Primer Methods in Mammalian Autophagy Research. 2010:313-326. doi:10.1016/j.cell.2010.01.028
12. Mizushima N, Levine B, Cuervo AM, Klionsky DJ. Autophagy fights disease through cellular self-digestion. *Nature*. 2008. doi:10.1038/nature06639
13. Virgin HW, Levine B. Autophagy genes in immunity. *Nat Immunol*. 2009. doi:10.1038/ni.1726
14. White E, Karp C, Strohecker AM, Guo Y, Mathew R. Role of autophagy in suppression of inflammation and cancer. *Curr Opin Cell Biol*. 2010.

doi:10.1016/j.ceb.2009.12.008

15. Wong E, Cuervo AM. Autophagy gone awry in neurodegenerative diseases. *Nat Neurosci*. 2010. doi:10.1038/nn.2575
16. Yang Z, Klionsky DJ. Mammalian autophagy: Core molecular machinery and signaling regulation. *Curr Opin Cell Biol*. 2010. doi:10.1016/j.ceb.2009.11.014
17. Mari M, Tooze S a, Reggiori F. The puzzling origin of the autophagosomal membrane. *F1000 Biol Rep*. 2011. doi:10.3410/B3-25
18. Orsi A, Razi M, Dooley HC, et al. Dynamic and transient interactions of Atg9 with autophagosomes, but not membrane integration, are required for autophagy. *Mol Biol Cell*. 2012. doi:10.1091/mbc.E11-09-0746
19. Shpilka T, Mizushima N, Elazar Z. Ubiquitin-like proteins and autophagy at a glance. *J Cell Sci*. 2012. doi:10.1242/jcs.093757
20. Monastyrska I, Rieter E, Klionsky DJ, Reggiori F. Multiple roles of the cytoskeleton in autophagy. *Biol Rev*. 2009. doi:10.1111/j.1469-185X.2009.00082.x
21. Wild P, McEwan DG, Dikic I. The LC3 interactome at a glance. *J Cell Sci*. 2014;127(1):3-9. doi:10.1242/jcs.140426
22. Li WW, Li J, Bao JK. Microautophagy: Lesser-known self-eating. *Cell Mol Life Sci*. 2012. doi:10.1007/s00018-011-0865-5
23. Cuervo AM, Wong E. Chaperone-mediated autophagy: Roles in disease and aging. *Cell Res*. 2014. doi:10.1038/cr.2013.153
24. Guo JY, White E. Autophagy, metabolism, and cancer. *Cold Spring Harb Symp Quant Biol*. 2016. doi:10.1101/sqb.2016.81.030981
25. Green DR, Levine B. To be or not to be? How selective autophagy and cell death govern cell fate. *Cell*. 2014. doi:10.1016/j.cell.2014.02.049
26. Kaur J, Debnath J. Autophagy at the crossroads of catabolism and anabolism. *Nat Rev Mol Cell Biol*. 2015. doi:10.1038/nrm4024
27. Mukherjee A, Patel B, Koga H, Cuervo AM, Jenny A. Selective endosomal microautophagy is starvation-inducible in Drosophila. *Autophagy*. 2016. doi:10.1080/15548627.2016.1208887
28. Tasset I, Cuervo AM. Role of chaperone-mediated autophagy in metabolism. *FEBS J*. 2016. doi:10.1111/febs.13677
29. Boya P, González-Polo R-A, Casares N, et al. Inhibition of macroautophagy triggers apoptosis. *Mol Cell Biol*. 2005. doi:10.1128/MCB.25.3.1025-1040.2005

30. Mizushima N. The role of the Atg1/ULK1 complex in autophagy regulation. *Curr Opin Cell Biol*. 2010. doi:10.1016/j.ceb.2009.12.004
31. Kim YC, Guan K. mTOR : a pharmacologic target for autophagy regulation. 2015;125(1):25-32. doi:10.1172/JCI73939.such
32. Mihaylova MM, Shaw RJ. The AMPK signalling pathway coordinates cell growth , autophagy and metabolism. *Nat Publ Gr*. 2011;13(9):1016-1023. doi:10.1038/ncb2329
33. Lee IH, Cao L, Mostoslavsky R, et al. A role for the NAD-dependent deacetylase Sirt1 in the regulation of autophagy. *Proc Natl Acad Sci*. 2008. doi:10.1073/pnas.0712145105
34. Hayashi-Nishino M, Fujita N, Noda T, Yamaguchi A, Yoshimori T, Yamamoto A. A subdomain of the endoplasmic reticulum forms a cradle for autophagosome formation. *Nat Cell Biol*. 2009. doi:10.1038/ncb1991
35. Buchberger A, Bukau B, Sommer T. Protein Quality Control in the Cytosol and the Endoplasmic Reticulum: Brothers in Arms. *Mol Cell*. 2010. doi:10.1016/j.molcel.2010.10.001
36. Rouschop KMA, Van Den Beucken T, Dubois L, et al. The unfolded protein response protects human tumor cells during hypoxia through regulation of the autophagy genes MAP1LC3B and ATG5. *J Clin Invest*. 2010. doi:10.1172/JCI40027
37. Liu L, Wise DR, Diehl JA, Simon MC. Hypoxic reactive oxygen species regulate the integrated stress response and cell survival. *J Biol Chem*. 2008. doi:10.1074/jbc.M805056200
38. Scherz-Shouval R, Shvets E, Fass E, Shorer H, Gil L, Elazar Z. Reactive oxygen species are essential for autophagy and specifically regulate the activity of Atg4. *EMBO J*. 2007. doi:10.1038/sj.emboj.7601623
39. Wong CH, Iskandar KB, Yadav SK, Hirpara JL, Loh T, Pervaiz S. Simultaneous induction of non-canonical autophagy and apoptosis in cancer cells by ROS-dependent ERK and JNK activation. *PLoS One*. 2010;5(4). doi:10.1371/journal.pone.0009996
40. Green DR, Kroemer G. Cytoplasmic functions of the tumour suppressor p53. *Nature*. 2009. doi:10.1038/nature07986
41. Gomes LC, Scorrano L. Mitochondrial morphology in mitophagy and macroautophagy. *Biochim Biophys Acta - Mol Cell Res*. 2013;1833(1):205-212.

doi:10.1016/j.bbamcr.2012.02.012

42. Drake LE, Springer MZ, Poole LP, Kim CJ, Macleod KF. Expanding perspectives on the significance of mitophagy in cancer. *Semin Cancer Biol*. 2017;47(February):110-124. doi:10.1016/j.semcancer.2017.04.008
43. Galluzzi L, Kepp O, Trojel-Hansen C, Kroemer G. Mitochondrial control of cellular life, stress, and death. *Circ Res*. 2012. doi:10.1161/CIRCRESAHA.112.268946
44. Jin SM, Lazarou M, Wang C, Kane LA, Narendra DP, Youle RJ. Mitochondrial membrane potential regulates PINK1 import and proteolytic destabilization by PARL. *J Cell Biol*. 2010. doi:10.1083/jcb.201008084
45. Pandol SJ. Normal Pancreatic Function. *Pancreapedia*. 2015. doi:10.3998/panc.2015.17
46. Grendell JH. Structure and function of the exocrine pancreas. In: *Gastrointestinal Anatomy and Physiology: The Essentials*. ; 2014. doi:10.1002/9781118833001.ch6
47. Lankisch PG, Apte M, Banks PA. Seminar Acute pancreatitis. *Lancet*. 2015. doi:10.1016/S0140-6736(14)60649-8
48. Chiari H. Über die Selbstverdauung des menschlichen Pankreas. *Zeitschrift für Heilkd*. 1896. doi:10.1016/j.psychres.2014.12.028
49. Dawra R, Sah RP, Dudeja V, et al. Intra-acinar trypsinogen activation mediates early stages of pancreatic injury but not inflammation in mice with acute pancreatitis. *Gastroenterology*. 2011. doi:10.1053/j.gastro.2011.08.033
50. Capurso G, Zerboni G, Signoretti M, et al. Role of the gut barrier in acute pancreatitis. *J Clin Gastroenterol*. 2012. doi:10.1097/MCG.0b013e3182652096
51. Kleeff J, Whitcomb DC, Shimosegawa T, et al. Chronic pancreatitis. *Nat Rev Dis Prim*. 2017. doi:10.1038/nrdp.2017.60
52. Yadav D, Lowenfels AB. The epidemiology of pancreatitis and pancreatic cancer. *Gastroenterology*. 2013. doi:10.1053/j.gastro.2013.01.068
53. Whitcomb DC, Frulloni L, Garg P, et al. Chronic pancreatitis: An international draft consensus proposal for a new mechanistic definition. *Pancreatology*. 2016. doi:10.1016/j.pan.2016.02.001
54. Siegel RLRL, Miller DK, Jemal A, Miller KD, Jemal A. Cancer Statistics, 2016. CA Cancer J Clin. doi:10.3322/caac.21332.
55. Rahib L, Smith BD, Aizenberg R, Rosenzweig AB, Fleshman JM, Matrisian LM.

Projecting cancer incidence and deaths to 2030: The unexpected burden of thyroid, liver, and pancreas cancers in the united states. *Cancer Res*. 2014. doi:10.1158/0008-5472.CAN-14-0155

56. Freed-Pastor WA, Prives C. Mutant p53: One name, many proteins. *Genes Dev*. 2012. doi:10.1101/gad.190678.112
57. Kleeff J, Korc M, Apte M, et al. Pancreatic cancer. *Nat Rev Dis Prim*. 2016;2(May):1-23. doi:10.1038/nrdp.2016.22
58. Biankin A V., Waddell N, Kassahn KS, et al. Pancreatic cancer genomes reveal aberrations in axon guidance pathway genes. *Nature*. 2012. doi:10.1038/nature11547
59. Bailey P, Chang DK, Nones K, et al. Genomic analyses identify molecular subtypes of pancreatic cancer. *Nature*. 2016. doi:10.1038/nature16965
60. Yang S, Wang X, Contino G, et al. Pancreatic cancers require autophagy for tumor growth Pancreatic cancers require autophagy for tumor growth. 2011:717-729. doi:10.1101/gad.2016111
61. Commisso C, Davidson SM, Soydaner-Azeloglu RG, et al. Macropinocytosis of protein is an amino acid supply route in Ras-transformed cells. *Nature*. 2013. doi:10.1038/nature12138
62. Hutcheson J, Balaji U, Porembka MR, et al. Immunologic and metabolic features of pancreatic ductal adenocarcinoma define prognostic subtypes of disease. *Clin Cancer Res*. 2016. doi:10.1158/1078-0432.CCR-15-1883
63. Yang A, Rajeshkumar N V., Wang X, et al. Autophagy is critical for pancreatic tumor growth and progression in tumors with p53 alterations. *Cancer Discov*. 2014. doi:10.1158/2159-8290.CD-14-0362
64. Rosenfeldt MT, O'Prey J, Morton JP, et al. p53 status determines the role of autophagy in pancreatic tumour development. *Nature*. 2013;504:296. http://dx.doi.org/10.1038/nature12865.
65. Samaras P, Tusup M, Nguyen-Kim TDL, et al. Phase I study of a chloroquine–gemcitabine combination in patients with metastatic or unresectable pancreatic cancer. *Cancer Chemother Pharmacol*. 2017. doi:10.1007/s00280-017-3446-y
66. Halbrook CJ, Lyssiotis CA. Review Employing Metabolism to Improve the Diagnosis and Treatment of Pancreatic Cancer. *Cancer Cell*. 2017;31(1):5-19. doi:10.1016/j.ccell.2016.12.006
67. Lunt SY, Vander Heiden MG. Aerobic Glycolysis: Meeting the Metabolic

Requirements of Cell Proliferation. *Annu Rev Cell Dev Biol*. 2011. doi:10.1146/annurev-cellbio-092910-154237

68. Hensley CT, Wasti AT, DeBerardinis RJ. Glutamine and cancer: Cell biology, physiology, and clinical opportunities. *J Clin Invest*. 2013. doi:10.1172/JCI69600
69. Lyssiotis CA, Son J, Cantley LC, Kimmelman AC. Pancreatic cancers rely on a novel glutamine metabolism pathway to maintain redox balance. *Cell Cycle*. 2013. doi:10.4161/cc.25307
70. Deberardinis RJ, Cheng T. Q's next: The diverse functions of glutamine in metabolism, cell biology and cancer. *Oncogene*. 2010. doi:10.1038/onc.2009.358
71. DeBerardinis RJ, Sayed N, Ditsworth D, Thompson CB. Brick by brick: metabolism and tumor cell growth. *Curr Opin Genet Dev*. 2008. doi:10.1016/j.gde.2008.02.003
72. Zu XL, Guppy M. Cancer metabolism: Facts, fantasy, and fiction. *Biochem Biophys Res Commun*. 2004. doi:10.1016/j.bbrc.2003.11.136
73. Heiden MG Vander, Cantley LC, Thompson CB. Understanding the warburg effect: The metabolic requirements of cell proliferation. *Science (80-)*. 2009. doi:10.1126/science.1160809
74. Chan DC. Fusion and Fission: Interlinked Processes Critical for Mitochondrial Health. *Annu Rev Genet*. 2012. doi:10.1146/annurev-genet-110410-132529
75. Mishra P, Chan DC. Metabolic regulation of mitochondrial dynamics. *J Cell Biol*. 2016. doi:10.1083/jcb.201511036
76. van der Bliek A, Shen Q, Kawajiri S. Mechanisms of mitochondrial fission and fusion. *Cold Spring Harb Perspect Biol*. 2013;5(6):1-16. doi:10.1101/cshperspect.a011072
77. Altieri DC. Mitochondria on the move: Emerging paradigms of organelle trafficking in tumour plasticity and metastasis. *Br J Cancer*. 2017. doi:10.1038/bjc.2017.201
78. Galluzzi L, Kepp O, Kroemer G. Mitochondria : master regulators of danger signalling. 2012;13(December):3-7. doi:10.1038/nrm3479
79. Lee JE, Westrate LM, Wu H, Page C, Voeltz GK. Multiple dynamin family members collaborate to drive mitochondrial division. *Nature*. 2016. doi:10.1038/nature20555

80. Kashatus JA, Nascimento A, Myers LJ, et al. Erk2 phosphorylation of Drp1 promotes mitochondrial fission and MAPK-driven tumor growth. *Mol Cell*. 2015. doi:10.1016/j.molcel.2015.01.002
81. Serasinghe MN, Wieder SY, Renault TT, et al. Mitochondrial division is requisite to RAS-induced transformation and targeted by oncogenic MAPK pathway inhibitors. *Mol Cell*. 2015. doi:10.1016/j.molcel.2015.01.003
82. Xie Q, Wu Q, Horbinski CM, et al. Mitochondrial control by DRP1 in brain tumor initiating cells. *Nat Neurosci*. 2015. doi:10.1038/nn.3960
83. Giorgi C, Marchi S, Pinton P. The machineries, regulation and cellular functions of mitochondrial calcium. *Nat Rev Mol Cell Biol*. 2018. doi:10.1038/s41580-018-0052-8
84. Prevarskaya N, Skryma R, Shuba Y. Calcium in tumour metastasis: New roles for known actors. *Nat Rev Cancer*. 2011. doi:10.1038/nrc3105
85. Giorgi C, Danese A, Missiroli S, Patergnani S, Pinton P. Calcium Dynamics as a Machine for Decoding Signals. *Trends Cell Biol*. 2018. doi:10.1016/j.tcb.2018.01.002
86. Medina DL, Di Paola S, Peluso I, et al. Lysosomal calcium signalling regulates autophagy through calcineurin and TFEB. *Nat Cell Biol*. 2015. doi:10.1038/ncb3114
87. Perraud AL, Fleig A, Dunn CA, et al. ADP-ribose gating of the calcium-permeable LTRPC2 channel revealed by Nudix motif homology. *Nature*. 2001. doi:10.1038/35079100
88. Lange I, Yamamoto S, Partida-Sanchez S, Mori Y, Fleig A, Penner R. TRPM2 functions as a lysosomal Ca2+-release channel in β cells. *Sci Signal*. 2009. doi:10.1126/scisignal.2000278
89. Brundage RA, Fogarty KE, Tuft RA, Fay FS. Calcium gradients underlying polarization and chemotaxis of eosinophils. *Science (80-)*. 1991. doi:10.1126/science.1948048
90. Hahn K, Debiasio R, Taylor DL. Patterns of elevated free calcium and calmodulin activation in living cells. *Nature*. 1992. doi:10.1038/359736a0
91. Boye K, Mælandsmo GM. S100A4 and metastasis: A small actor playing many roles. *Am J Pathol*. 2010;176(2):528-535. doi:10.2353/ajpath.2010.090526
92. Bresnick AR, Weber DJ, Zimmer DB. S100 proteins in cancer. *Nat Rev Cancer*. 2015. doi:10.1038/nrc3893

93. Kim EJ, Helfman DM. Characterization of the metastasis-associated protein, S100A4: Roles of calcium binding and dimerization in cellular localization and interaction with myosin. *J Biol Chem*. 2003. doi:10.1074/jbc.M304909200
94. Bjørnland K, Winberg JO, Ødegaard OT, et al. S100A4 involvement in metastasis: Deregulation of matrix metalloproteinases and tissue inhibitors of matrix metalloproteinases in osteosarcoma cells transfected with an anti-S100A4 ribozyme. *Cancer Res*. 1999. doi:10.1002/jcb.240560106
95. Saleem M, Kweon M-H, Johnson JJ, et al. S100A4 accelerates tumorigenesis and invasion of human prostate cancer through the transcriptional regulation of matrix metalloproteinase 9. *Proc Natl Acad Sci*. 2006. doi:10.1073/pnas.0606747103
96. Lambert AW, Pattabiraman DR, Weinberg RA. Emerging Biological Principles of Metastasis. *Cell*. 2017;168(4):670-691. doi:10.1016/j.cell.2016.11.037
97. Del Monte U. Does the cell number 109still really fit one gram of tumor tissue? *Cell Cycle*. 2009. doi:10.4161/cc.8.3.7608
98. Talmadge JE, Fidler IJ. AACR centennial series: The biology of cancer metastasis: Historical perspective. *Cancer Res*. 2010;70(14):5649-5669. doi:10.1158/0008-5472.CAN-10-1040
99. Kozlowski JM, Hart IR, Fidler IJ, Hanna N. A human melanoma line heterogeneous with respect to metastatic capacity in athymic nude mice. *J Natl Cancer Inst*. 1984. doi:10.1093/jnci/72.4.913
100. Bronsert P, Enderle-Ammour K, Bader M, et al. Cancer cell invasion and EMT marker expression: a three-dimensional study of the human cancer-host interface. *J Pathol*. 2014. doi:10.1002/path.4416
101. Olson OC, Joyce JA. Cysteine cathepsin proteases: Regulators of cancer progression and therapeutic response. *Nat Rev Cancer*. 2015. doi:10.1038/nrc4027
102. Kurz T, Terman A, Gustafsson B, Brunk UT. Lysosomes and oxidative stress in aging and apoptosis. *Biochim Biophys Acta - Gen Subj*. 2008. doi:10.1016/j.bbagen.2008.01.009
103. Boya P, Andreau K, Poncet D, et al. Lysosomal Membrane Permeabilization Induces Cell Death in a Mitochondrion-dependent Fashion. *J Exp Med*. 2003. doi:10.1084/jem.20021952
104. Fonović M, Turk B. Cysteine cathepsins and extracellular matrix degradation.

Biochim Biophys Acta - Gen Subj. 2014. doi:10.1002/wsb.858

105. Niedergethmann M, Wostbrock B, Sturm JW, Willeke F, Post S, Hildenbrand R. Prognostic impact of cysteine proteases cathepsin B and cathepsin L in pancreatic adenocarcinoma. *Pancreas*. 2004. doi:10.1021/ie50268a021
106. Kitamura T, Qian BZ, Pollard JW. Immune cell promotion of metastasis. *Nat Rev Immunol*. 2015. doi:10.1038/nri3789
107. Aras S, Raza Zaidi M. TAMeless traitors: Macrophages in cancer progression and metastasis. *Br J Cancer*. 2017. doi:10.1038/bjc.2017.356
108. Gocheva V, Wang HW, Gadea BB, et al. IL-4 induces cathepsin protease activity in tumor-associated macrophages to promote cancer growth and invasion. *Genes Dev*. 2010. doi:10.1101/gad.1874010
109. Kamoshida G, Ogawa T, Oyanagi J, et al. Modulation of matrix metalloproteinase-9 secretion from tumor-associated macrophage-like cells by proteolytically processed laminin-332 (laminin-5). *Clin Exp Metastasis*. 2014. doi:10.1007/s10585-013-9627-0
110. Wang D, Sun H, Wei J, Cen B, DuBois RN. CXCL1 is critical for premetastatic niche formation and metastasis in colorectal cancer. *Cancer Res*. 2017. doi:10.1158/0008-5472.CAN-16-3199
111. Lee CC, Lin JC, Hwang WL, et al. Macrophage-secreted interleukin-35 regulates cancer cell plasticity to facilitate metastatic colonization. *Nat Commun*. 2018. doi:10.1038/s41467-018-06268-0
112. Kale S, Raja R, Thorat D, Soundararajan G, Patil T V., Kundu GC. Osteopontin signaling upregulates cyclooxygenase-2 expression in tumor-associated macrophages leading to enhanced angiogenesis and melanoma growth via α9β1 integrin. *Oncogene*. 2014. doi:10.1038/onc.2013.184
113. Hara T, Nakamura K, Matsui M, et al. Suppression of basal autophagy in neural cells causes neurodegenerative disease in mice. *Nature*. 2006. doi:10.1038/nature04724
114. Nakhai H, Sel S, Favor J, et al. Ptf1a is essential for the differentiation of GABAergic and glycinergic amacrine cells and horizontal cells in the mouse retina. *Development*. 2007. doi:10.1242/dev.02781
115. Mizushima N. In Vivo Analysis of Autophagy in Response to Nutrient Starvation Using Transgenic Mice Expressing a Fluorescent Autophagosome Marker. *Mol Biol Cell*. 2003. doi:10.1091/mbc.E03-09-0704

116. Jackson EL, Willis N, Mercer K, et al. Analysis of lung tumor initiation and progression using conditional expression of oncogenic K-ras. *Genes Dev*. 2001. doi:10.1101/gad.943001
117. Noll EM, Eisen C, Stenzinger A, et al. CYP3A5 mediates basal and acquired therapy resistance in different subtypes of pancreatic ductal adenocarcinoma. *Nat Med*. 2016. doi:10.1038/nm.4038
118. Schlitter AM, Jesinghaus M, Jäger C, et al. pT but not pN stage of the 8th TNM classification significantly improves prognostication in pancreatic ductal adenocarcinoma. *Eur J Cancer*. 2017. doi:10.1016/j.ejca.2017.06.034
119. Muckenhuber A, Berger AK, Schlitter AM, et al. Pancreatic ductal adenocarcinoma subtyping using the biomarkers hepatocyte nuclear factor-1A and cytokeratin-81 correlates with outcome and treatment response. *Clin Cancer Res*. 2018. doi:10.1158/1078-0432.CCR-17-2180
120. Stenzinger A, Endris V, Klauschen F, et al. High SIRT1 expression is a negative prognosticator in pancreatic ductal adenocarcinoma. *BMC Cancer*. 2013. doi:10.1186/1471-2407-13-450
121. Seubert W. *Methods of Enzymatic Analysis*.; 1965. doi:10.1016/B978-0-12-395630-9.50134-1
122. Palade GE. A STUDY OF FIXATION FOR ELECTRON MICROSCOPY. *J Exp Med*. 1952. doi:10.1084/jem.95.3.285
123. Mcwhorter FY, Wang T, Nguyen P, Chung T, Liu WF. Modulation of macrophage phenotype by cell shape. 2013;110(43):17253-17258. doi:10.1073/pnas.1308887110
124. Diakopoulos KN, Lesina M, Wörmann S, et al. Impaired autophagy induces chronic atrophic pancreatitis in mice via sex- and nutrition-dependent processes. *Gastroenterology*. 2015. doi:10.1053/j.gastro.2014.12.003
125. Lahiri V, Klionsky DJ. CCPG1 is a noncanonical autophagy cargo receptor essential for reticulophagy and pancreatic ER proteostasis. *Autophagy*. 2018. doi:10.1080/15548627.2018.1467199
126. Perera RM, Stoykova S, Nicolay BN, et al. Transcriptional control of autophagy-lysosome function drives pancreatic cancer metabolism. *Nature*. 2015. doi:10.1038/nature14587
127. Gunter TE, Yule DI, Gunter KK, Eliseev RA, Salter JD. Calcium and mitochondria. In: *FEBS Letters*. ; 2004. doi:10.1016/j.febslet.2004.03.071

128. Brandon M, Baldi P, Wallace DC, et al. Mitochondrial mutations in cancer. *Oncogene*. 2006. doi:10.1038/sj.onc.1209607
129. Tsai FC, Meyer T. Ca 2+ pulses control local cycles of lamellipodia retraction and adhesion along the front of migrating cells. *Curr Biol*. 2012. doi:10.1016/j.cub.2012.03.037
130. Settembre C, Fraldi A, Medina DL, Ballabio A. Signals from the lysosome: A control centre for cellular clearance and energy metabolism. *Nat Rev Mol Cell Biol*. 2013. doi:10.1038/nrm3565
131. White E, DiPaola RS. The Double-Edged Sword of Autophagy Modulation in Cancer. *Clin Cancer Res*. 2009;15(17):5308 LP-5316. http://clincancerres.aacrjournals.org/content/15/17/5308.abstract.
132. Kenific CM, Thorburn A, Debnath J. Autophagy and metastasis: Another double-edged sword. *Curr Opin Cell Biol*. 2010;22(2):241-245. doi:10.1016/j.ceb.2009.10.008
133. Yang A, Kimmelman AC. Inhibition of autophagy attenuates pancreatic cancer growth independent of TP53/TRP53 status. *Autophagy*. 2014;10(9):1683-1684. doi:10.1158/2159-8290.CD-14-0362
134. Yang A, Herter-Sprie G, Zhang H, et al. Autophagy sustains pancreatic cancer growth through both cell-autonomous and nonautonomous mechanisms. *Cancer Discov*. 2018. doi:10.1158/2159-8290.CD-17-0952
135. Qu X, Yu J, Bhagat G, et al. Promotion of tumorigenesis by heterozygous disruption of the beclin 1 autophagy gene. *J Clin Invest*. 2003. doi:10.1172/JCI20039
136. Russell SE, Hickey GI, Lowry WS, White P, Atkinson RJ. Allele loss from chromosome 17 in ovarian cancer. *Oncogene*. 1990.
137. Eccles DM, Russell SE, Haites NE, et al. Early loss of heterozygosity on 17q in ovarian cancer. The Abe Ovarian Cancer Genetics Group. *Oncogene*. 1992.
138. Cliby W, Ritland S, Hartmann L, et al. Human Epithelial Ovarian Cancer Allelotype. *Cancer Res*. 1993. doi:10.1101/ps.840101.)
139. Tangir J, Muto MG, Berkowitz RS, Welch WR, Bell DA, Mok SC. A 400 kb novel deletion unit centromeric to the BRCA1 gene in sporadic epithelial ovarian cancer. *Oncogene*. 1996.
140. Futreal PA, Barrett JC, Cochran C, Barrett JC, Wiseman RW. Detection of Frequent Allelic Loss on Proximal Chromosome 17q in Sporadic Breast

Carcinoma Using Microsatellite Length Polymorphisms. *Cancer Res*. 1992.

141. Saito H, Inazawa J, Saito S, et al. Detailed Deletion Mapping of Chromosome 17q in Ovarian and Breast Cancers: 2-cM Region on 17q21.3 Often and Commonly Deleted in Tumors. *Cancer Res*. 1993.
142. Gao X, Zacharek A, Salkowski A, et al. Loss of Heterozygosity of the BRCA1 and Other Loci on Chromosome 17q in Human Prostate Cancer. *Cancer Res*. 1995.
143. García-Fernández M, Karras P, Checinska A, et al. Metastatic risk and resistance to BRAF inhibitors in melanoma defined by selective allelic loss of ATG5. *Autophagy*. 2016;12(10):1776-1790. doi:10.1080/15548627.2016.1199301
144. Koyama-Honda I, Tsuboyama K, Mizushima N. ATG conjugation-dependent degradation of the inner autophagosomal membrane is a key step for autophagosome maturation. *Autophagy*. 2017. doi:10.1080/15548627.2017.1319041
145. Ma T, Li J, Xu Y, et al. Atg5-independent autophagy regulates mitochondrial clearance and is essential for iPSC reprogramming. *Nat Cell Biol*. 2015. doi:10.1038/ncb3256
146. Nishida Y, Arakawa S, Fujitani K, et al. Discovery of Atg5 / Atg7-independent alternative macroautophagy. *Nature*. 2009;461(7264):654-658. doi:10.1038/nature08455
147. Honda S, Arakawa S, Nishida Y, Yamaguchi H, Ishii E, Shimizu S. Ulk1-mediated Atg5-independent macroautophagy mediates elimination of mitochondria from embryonic reticulocytes. *Nat Commun*. 2014. doi:10.1038/ncomms5004
148. Fidler IJ. The pathogenesis of cancer metastasis: The “seed and soil” hypothesis revisited. *Nat Rev Cancer*. 2003. doi:10.1038/nrc1098
149. Fidler IJ, Poste G. The “seed and soil” hypothesis revisited. *Lancet Oncol*. 2008. doi:10.1016/S1470-2045(08)70201-8
150. Chen H, Chan DC. Mitochondrial Dynamics in Regulating the Unique Phenotypes of Cancer and Stem Cells. *Cell Metab*. 2017. doi:10.1016/j.cmet.2017.05.016
151. Prevarskaya N, Skryma R, Shuba Y. Calcium in tumour metastasis : new roles for known actors. 2011;11(August):609-618. doi:10.1038/nrc3105

152. Olson OC, Joyce JA. Cysteine cathepsin proteases : regulators of cancer progression and therapeutic response. *Nat Publ Gr*. 2015;15(12):712-729. doi:10.1038/nrc4027
153. Guerriero JL. Macrophages: The Road Less Traveled, Changing Anticancer Therapy. *Trends Mol Med*. 2018. doi:10.1016/j.molmed.2018.03.006
154. Amoedo ND, Rodrigues MF, Rumjanek FD. Mitochondria: Are mitochondria accessory to metastasis? *Int J Biochem Cell Biol*. 2014. doi:10.1016/j.biocel.2014.03.009
155. Porporato PE, Payen VL, Pérez-Escuredo J, et al. A mitochondrial switch promotes tumor metastasis. *Cell Rep*. 2014. doi:10.1016/j.celrep.2014.06.043
156. Gryshchenko O, Gerasimenko J V., Peng S, Gerasimenko O V., Petersen OH. Calcium signalling in the acinar environment of the exocrine pancreas: physiology and pathophysiology. *J Physiol*. 2018. doi:10.1113/JP275395
157. Rosty C, Ueki T, Argani P, et al. Overexpression of S100A4 in pancreatic ductal adenocarcinomas is associated with poor differentiation and DNA hypomethylation. *Am J Pathol*. 2002;160(1):45-50. doi:10.1016/S0002-9440(10)64347-7
158. Sekine H, Chen N, Sato K, et al. S100A4, frequently overexpressed in various human cancers, accelerates cell motility in pancreatic cancer cells. *Biochem Biophys Res Commun*. 2012;429(3-4):214-219. doi:10.1016/j.bbrc.2012.10.048
159. Tsukamoto N, Egawa S, Akada M, et al. The expression of S100A4 in human pancreatic cancer is associated with invasion. *Pancreas*. 2013. doi:10.1097/MPA.0b013e31828804e7
160. Mahon PC, Baril P, Bhakta V, et al. S100A4 contributes to the suppression of BNIP3 expression, chemoresistance, and inhibition of apoptosis in pancreatic cancer. *Cancer Res*. 2007. doi:10.1158/0008-5472.CAN-07-0440
161. Raffaello A, Mammucari C, Gherardi G, Rizzuto R. Calcium at the Center of Cell Signaling: Interplay between Endoplasmic Reticulum, Mitochondria, and Lysosomes. *Trends Biochem Sci*. 2016. doi:10.1016/j.tibs.2016.09.001
162. Huang Y, Winkler PA, Sun W, Lü W, Du J. Architecture of the TRPM2 channel and its activation mechanism by ADP-ribose and calcium. *Nature*. 2018. doi:10.1038/s41586-018-0558-4
163. Medina DL, Ballabio A. Lysosomal calcium regulates autophagy. *Autophagy*. 2015. doi:10.1080/15548627.2015.1047130

164. Man SM, Kanneganti TD. Regulation of lysosomal dynamics and autophagy by CTSB/cathepsin B. *Autophagy*. 2016. doi:10.1080/15548627.2016.1239679
165. Whiteman HJ, Weeks ME, Dowen SE, et al. The role of S100P in the invasion of pancreatic cancer cells is mediated through cytoskeletal changes and regulation of cathepsin D. *Cancer Res*. 2007;67(18):8633-8642. doi:10.1158/0008-5472.CAN-07-0545
166. Chen D, Fan W, Lu Y, Ding X, Chen S, Zhong Q. A Mammalian Autophagosome Maturation Mechanism Mediated by TECPR1 and the Atg12-Atg5 Conjugate. *Mol Cell*. 2012. doi:10.1016/j.molcel.2011.12.036
167. Bergsbaken T, Fink SL, den Hartigh AB, Loomis WP, Cookson BT. Coordinated Host Responses during Pyroptosis: Caspase-1-Dependent Lysosome Exocytosis and Inflammatory Cytokine Maturation. *J Immunol*. 2011. doi:10.4049/jimmunol.1100477
168. He Y, Xu Y, Zhang C, et al. Identification of a lysosomal pathway that modulates glucocorticoid signaling and the inflammatory response. *Sci Signal*. 2011. doi:10.1126/scisignal.2001450
169. Wörmann SM, Diakopoulos KN, Lesina M, Algül H. The immune network in pancreatic cancer development and progression. *Oncogene*. 2014. doi:10.1038/onc.2013.257
170. Steele CW, Jamieson NB, Evans TRJ, et al. Exploiting inflammation for therapeutic gain in pancreatic cancer. *Br J Cancer*. 2013. doi:10.1038/bjc.2013.24
171. Mantovani A, Sozzani S, Locati M, Allavena P, Sica A. Macrophage polarization: Tumor-associated macrophages as a paradigm for polarized M2 mononuclear phagocytes. *Trends Immunol*. 2002. doi:10.1016/S1471-4906(02)02302-5
172. Van Overmeire E, Stijlemans B, Heymann F, et al. M-CSF and GM-CSF receptor signaling differentially regulate monocyte maturation and macrophage polarization in the tumor microenvironment. *Cancer Res*. 2016. doi:10.1158/0008-5472.CAN-15-0869
173. Liou GY, Döppler H, Necela B, et al. Mutant KRAS–induced expression of ICAM-1 in pancreatic acinar cells causes attraction of macrophages to expedite the formation of precancerous lesions. *Cancer Discov*. 2015. doi:10.1158/2159-8290.CD-14-0474

174. Flint TR, Fearon DT, Janowitz T. Connecting the Metabolic and Immune Responses to Cancer. *Trends Mol Med*. 2017;xx:1-14. doi:10.1016/j.molmed.2017.03.001
175. Andrejeva G, Rathmell JC. Similarities and Distinctions of Cancer and Immune Metabolism in Inflammation and Tumors. *Cell Metab*. 2017. doi:10.1016/j.cmet.2017.06.004
176. Mazzone M, Menga A, Castegna A. Metabolism and TAM functions—it takes two to tango. *FEBS J*. 2018. doi:10.1111/febs.14295
177. Bronte V, Zanovello P. Regulation of immune responses by L-arginine metabolism. *Nat Rev Immunol*. 2005;5(8):641-654. doi:10.1038/nri1668
178. Wolpin BM, Rubinson DA, Wang X, et al. Phase II and Pharmacodynamic Study of Autophagy Inhibition Using Hydroxychloroquine in Patients With Metastatic Pancreatic Adenocarcinoma. *Oncologist*. 2014. doi:10.1634/theoncologist.2014-0086
179. Boone BA, Bahary N, Zureikat AH, et al. Safety and Biologic Response of Pre-operative Autophagy Inhibition in Combination with Gemcitabine in Patients with Pancreatic Adenocarcinoma. *Ann Surg Oncol*. 2015. doi:10.1245/s10434-015-4566-4
180. Mizushima N, Yoshimori T, Levine B. Methods in Mammalian Autophagy Research. *Cell*. 2010. doi:10.1016/j.cell.2010.01.028
181. Sanoff HK, Deal AM, Krishnamurthy J, et al. Effect of cytotoxic chemotherapy on markers of molecular age in patients with breast cancer. *J Natl Cancer Inst*. 2014. doi:10.1093/jnci/dju057
182. Hansen M, Rubinsztein DC. Autophagy as a promoter of longevity: insights from model organisms. *Nat Rev Mol Cell Biol*. 2018. doi:10.1038/s41580-018-0033-y
183. Burgess MR, Hwang E, Mroue R, et al. KRAS Allelic Imbalance Enhances Fitness and Modulates MAP Kinase Dependence in Cancer. *Cell*. 2017. doi:10.1016/j.cell.2017.01.020
184. Bielski CM, Zehir A, Penson A V., et al. Genome doubling shapes the evolution and prognosis of advanced cancers. *Nat Genet*. 2018. doi:10.1038/s41588-018-0165-1

9 ABBREVIATIONS

ADEX	Aberrantly differentiated endocrine exocrine
ADM	Acinar to ductal metaplasia
ADPR	ADP-ribose
AMPK	AMP-activated protein kinase
AP	Acute pancreatitis
ATG	Autophagy related
ATP	Adenosine triphosphate
BrdU	Bromodeoxyuridine
Ca2+	Calcium ions
CMA	Chaperone mediated autophagy
CP	Chronic pancreatitis
CTS	Cathepsin
CXCL	(C-X-C) motif ligand
ECAR	Extracellular acidification rate
ECM	Extracellular matrix
EDTA	Ethylenediaminetetraacetic acid
ER	Endoplasmic reticulum
FCCP	Carbonilcyanide p-triflouromethoxyphenylhydrazone
GLDH	Glutamate dehydrogenase
GM-CSF	Granulocyte-macrophage colony-stimulating factor
GPCR	G protein-coupled receptor
HE	Hematoxylin and eosin
IMM	Inner mitochondrial membrane
IV	Intravenous
LC3	Microtubule-associated protein 1A/1B-light chain 3
LMP	Lysosomal membrane permeabilization
MAPK	Mitogen-activated protein kinase
MMP	Matrix metalloproteinase
mTORC1	Mammalian target of rapamycin complex 1
NEAA	Non-essential amino acid
Nrf1/2	Nuclear respiratory factor 1/Nuclear factor (erythroid-derived 2)-like 2
OCR	Oxygen consumption rate
p62/SQSTM1	Sequestrosome-1
PanIN	Pancreatic intraepithelial neoplasia
PAS	Pre-autophagosomal structure
PBS	Phosphate-buffered saline
PDAC	Pancreatic ductal adenocarcinoma
pM	Distant metastasis
pN	Lymph node
pT	Primary tumor

PtdIns	Phosphatidylinositol
qRT-PCR	Quantitative real time polymerase chain reaction
R	Resection
ROS	Reactive oxygen species
SOD	Superoxide dismutase
TAM	Tumor associated macrophages
TCA cycle	Tricarboxylic acid cycle
TECPR1	Tectonin beta-propeller repeat containing 1
TNF-a	Tumor necrosis factor - alpha
TRPM2	Transient Receptor Potential Cation Channel Subfamily M Member 2
ULK	Unc-51 like autophagy activating kinase
UPR	Unfolded protein response
Xbp1	X-box binding protein 1

10 ACKNOWLEDGEMENTS

First and foremost, I would like to thank Prof. Dr. med. Hana Algül for giving me a opportunity in his research group as a graduate student. I am sincerely thankful for this chance he gave me and believed in me to perform research with my own ideas in one of the most renowned center about pancreatic cancer in the world. Professor Algül supported me great supervision during my projects via stimulative discussions and important clinically relevant questions. Before anything else, he approached to me like his family member as he does to each member of our laboratory. I am also very thankful with my all respect to Dr. Marina Lesina who supported me all the time during my research period with all aspects of research and life by her gracious and indulgent approaches. She always took us under her wings and supported us all the time with full steam ahead about everything. Furthermore, I appreciate Univ.-Prof. Dr. med. Roland M. Schmid and Prof. Dr. Stephan Herzig who supported my enthusiasm and research during my committee meetings with their deep knowledge and enlightening ideas.

I would like to state my appreciativeness to Dr. Kalliope N. Diakopoulos for her endless support during my doctoral research period. Her understanding and continuous guidance without limits helped me to progress quickly in my project. Addition to scientific life, she was a great role-model for me with her ideas, work discipline, and interaction with the people. Separately, I would like to thank to all of the members of my laboratory including Jiaoyu, Derya and Ezgi, Angelika, Dietrich, Katrin, Alexandra, Marlena, Nan. I call them as my sisters and brothers, because they made the atmosphere of our lab as my family. Without them, finishing my doctoral research period was impossible. They supported me by their hearts in every respect. Especially, the helps of Derya, Ezgi and Hande were really noteworthy during writing my thesis.

On the other hand, I would like to state my thankfulness to my previous professors including Prof. Dr. Seda Vatansever, Prof. Dr. Engin Ulukaya, and Assoc. Prof. Dr. Bülent Özpolat who supported me a lot to reach my goals during my medical education. Additionally, I would like to thank to Prof. Dr. Mert Erkan who helped me to build my research career at the beginning and gave me a chance to meet with my current supervisor.

Finally, I want to thank warmly to all of my family and my friends. Above all of my friends, I would like thank to my best friend Caner Kalay for being supportive everyday by making me feel like at home with his calls and brotherhood. Secondly, Aayush Gupta and Jiaoyu Ai gave me their supports wholeheartedly as my brothers as Caner all the time here in Munich. And I would like to thank specially to my friends including Oguzhan, Anil, Soner, Cem, Nurlan, Sercan for being with me all the time. Especially Aksoy family, Sercan and Ezgi, they were always supporting me as my small family with their all efforts by their big hearts.

Lastly, I am deeply indebted to my mother Neriman Görgülü, father Rahmi Görgülü, my brother Gönenc Görgülü, his wife Figen Özsoy Görgülü and his son, my lovely nephew, Görkem Görgülü for their support all the time. They were the ones who enabled me to reach these days by being my lodestars and teaching me how to be e a nice person. Without their support and existence, this life would have not been soulful to live and this research period would have not been possible to finish.